UCGE Reports
Number 20233

Department of Geomatics Engineering

Evaluation and Enhancement of the Wide Area Augmentation System (WAAS)

(URL: http://www.geomatics.ucalgary.ca/research/publications/GradTheses.html)

by

Ruben Yousuf

September 2005

THE UNIVERSITY OF CALGARY

Evaluation and Enhancement of the Wide Area Augmentation System (WAAS)

by

Ruben Yousuf

A THESIS

SUBMITTED TO THE FACULTY OF GRADUATE STUDIES

IN PARTIAL FULFILLMENT OF THE REQUIREMENTS

FOR THE DEGREE OF MASTER OF SCIENCE

DEPARTMENT OF GEOMATICS ENGINEERING

CALGARY, ALBERTA

September 2005

Abstract

The Global Positioning System (GPS) does not satisfy the requirements set by the Federal Aviation Administration (FAA) for aviation applications at this time. This is mainly because GPS integrity is not guaranteed and even when selective availability is off, the vertical accuracy is worse than 10 m (affirmed by the FAA), whereas the aviation requirements are much more stringent due to safety-of-life measures. In order to accommodate these requirements for safety-critical systems such as a fleet of commercial aircraft, the FAA has developed and commissioned the Wide Area Augmentation System (WAAS) on July 10, 2003. WAAS augments the current GPS constellation by providing differential corrections to its users, which satisfies aviation navigation requirements in terms of integrity, availability, accuracy, and continuity. An addition to the current WAAS configuration is being planned, to better service users in Canada; this extension to the core network is named the Canadian WAAS (CWAAS). Basically, four more wide-area reference stations (WRSs) are being planned to be added in Canada, with seamless operation between the two networks (CWAAS and WAAS). In this research, previous works into describing and testing these systems will be revisited and an evaluation of the proposed CWAAS reference stations will also be conducted, with a focus on ionospheric storm events. Thereafter, the WAAS will be envisioned in a more enhanced form, which will entail having significantly more stations in its reference network. In this manner, the ionosphere could be sampled at a higher spatial resolution, therefore improving the accuracy of the ionospheric model. Results show more than 100% improvements in some cases for the enhancement as compared to the current WAAS performance, and the value added by CWAAS is seen through increased accuracy and coverage in Eastern Canada.

Acknowledgements

I wish to express my sincere gratitude to my supervisor, Dr. Susan Skone for her continued supports and understanding. She has encouraged me to challenge new ideas yet advised to rethink when I got too ambitious. She has provided the invaluable advices, opportunities and assistance that greatly enhanced all the researches during my graduate studies.

I would like to thank some of my colleagues: Natalya Nicholson, Victoria Hoyle, Sudhir Man Shrestha, Yongjin Moon, Lance de Groot and my friend David McAllister for their inputs and feedbacks into this thesis. I would also like to acknowledge the continual support of the faculty and staff members into making this department a higher place of learning, which has led to accomplishments such as this one.

My appreciation also goes to Dr. Anthea Coster (*MIT Haystack Observatory*) for providing the ionospheric truth data and helping with the analysis.

Lastly, I would like to extend my sincere appreciation to my family for their extra-curricular support. In particular, my mother Robeda Yousuf for listening and being supporting during hectic times, my father Yousuf Ali for being extra proud of my achievements and encouraging me to excel further, and my dear sister Imona Yousuf for always being there by my side. A special recognition goes to a person who has made contributions that are intangible but invaluable to my career in general.

Table of Contents

List of Tables

List of Figures

Acronyms

3D	Three-Dimension
ANS	Air Navigation Service
BRDC	Broadcast
CDGPS	Canada-wide Differential Global Positioning System
CODE	Center for Orbit Determination in Europe
CONUS	Continental United States
CORS	Continuously Operating Reference Stations
CWAAS	Canadian Wide Area Augmentation System
DGPS	Differential Global Positioning System
DOT	Department of Transportation
DOT	Department of Transportation
ECEF	Earth Centered Earth Fixed
FAA	Federal Aviation Administration
GEO	Geosynchronous Satellite
GIVE	Grid Ionospheric Vertical Error
GNSS	Global Navigation Satellite System
GPS	Global Positioning System
HA	Horizontal Accuracy
HAL	Horizontal Alarm Limit
IGP	Ionospheric Grid Point
IGS	International GPS Service

INMARSAT	International Maritime Satellite Organization
IONEX	Ionosphere Map Exchange
IPP	Ionospheric Pierce Point
ISO	International Standardization Organization
JPL	Jet Propulsion Laboratory
LAAS	Local Area Augmentation System
LOS	Line-of-Sight
LPV	Localizer Performance with Vertical guidance
LSE	Least Squares Estimation
MPC	Modulated Precision Clock
NAS	National Airspace System
NPA	Non-Precision Approach
PA	Precision Approach
PRC	Pseudorange Correction
PRN	Pseudo Random Noise
RAIM	Receiver Autonomous Integrity Monitoring
RMS	Root Mean Square
RMSE	Root Mean Square Error
RTCA	Radio Technical Commission for Aviation Services
SA	Selective Availability
SA	Selective Availability
SBAS	Satellite Based Augmentation Systems
SED	Storm Enhanced Density

SP3	Standard Product 3
SPIM	Standard Plasmasphere-Ionosphere Model
SPS	Standard Positioning Service
STEC	Slant Total Electron Content
SV	Space Vehicle
TEC	Total Electron Content
TECU	Total Electron Content Unit
UDRE	User Differential Range Error
UIVE	User Ionospheric Vertical Error
UofC	University of Calgary
US	United States
UT	Universal Time
VA	Vertical Accuracy
VAL	Vertical Alarm Limit
VTEC	Vertical Total Electron Content
WAAS	Wide Area Augmentation System
WRS	Wide-Area Reference Station

Chapter 1

Introduction

1.1 Background

GPS is a space-based radio-navigation system, as shown in Figure 1.1. A minimum of 24 satellites orbit the Earth, in a nearly circular path, at altitudes of more than 20,000 km. These space vehicles (SVs) provide accurate position, velocity and time information derived from range measurements. It was originally developed by the United States (US) Department of Defense (DOD) for military navigation and positioning purposes [*Parkinson and Spilker*, 1996]. Since then, the system has emerged into the civilian community offering a wide-range of applications. This service is available anytime,

anywhere in the world and in all weather conditions. The system consists of three segments: the Space Segment, the Control Segment, and the User Segment. Each of these segments has specific functions that as a whole provide the users with positioning and navigation capabilities [*Misra and Enge*, 2001].

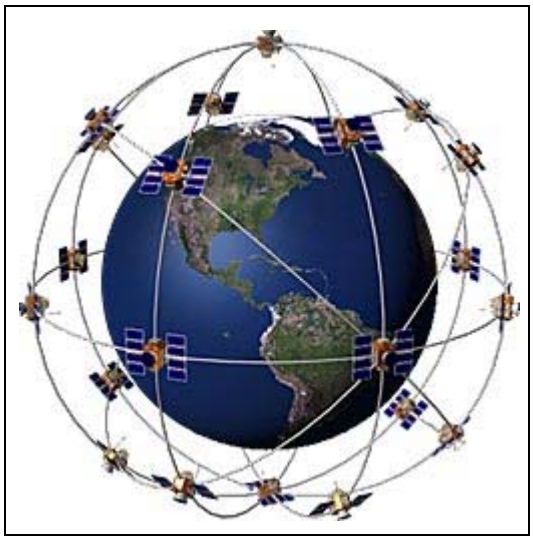

Figure 1.1: GPS Constellation [*NDGPS*, 2003]

The positioning information is extracted by estimating geometric range between the GPS receiver and the tracked satellites – a method known as Trilateration. As in any estimation process, errors are inherent by nature. Thus, GPS has to deal with an error budget that includes various sources of error, both systematic and stochastic. These errors directly impact the positioning accuracies offered by the system [*Kaplan*, 1996]. With the increasing use of GPS for navigation purposes, the dependability expected from this system is being taken to new heights (especially by navigation users). For instance, there is a substantial growth of the use of GPS technology in commercial aviation. However, standalone GPS will not provide the level of navigation-aid required by the aviation

industry. One of the reasons is that GPS integrity is not guaranteed. In aviation, the vertical component of positioning is the most important. The accuracy offered by GPS in the vertical is worse than 10 m, while the requirements set by air-traffic regulation agencies are much more strict. To alleviate the shortcomings of GPS for the purposes of navigating commercial and private aircrafts, the Federal Aviation Administration (FAA) has developed and commissioned the Wide Area Augmentation System (WAAS) (Figure 1.2) on July 10, 2003. WAAS is a safety-critical and software-intensive system that augments the satellite-based GPS constellation to provide users with airborne positions of adequate integrity, availability, accuracy, and continuity during different phases of flight. WAAS positioning is achieved by applying the system-provided differential corrections to the available positioning solution [*Hanlon and Sandhoo*, 1997].

Relating to WAAS accuracy, it generates a vector of corrections using its ground reference stations and sends it to users having WAAS compliant receivers. This vector contains ionospheric, clock and ephemeris corrections that are sent down to the users via geostationary satellites. Currently, WAAS covers the CONUS area, and Calgary is at the edge of this coverage. WAAS testing done over the CONUS region in September 2002 produced accuracy performance of 1–2 m horizontal and 2–3 m vertical 95% of the time [*Altshuler et al.*, 2002].

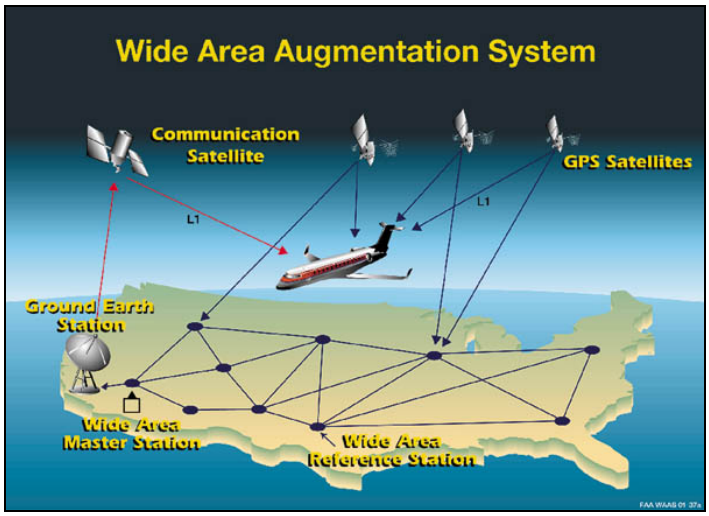

Figure 1.2: WAAS Overview [*FAA*, 2005]

Even after applying the WAAS corrections, the dispersive ionosphere still remains the major contributor in the GPS error budget. The ionosphere consists of ionized gases having free electrons that delay the signals coming from space. In the past 50 years, many different methods have been devised to model the ionosphere. Each model is application specific and thus possesses various attributes. One of such model is the Standard Plasmasphere-Ionosphere Model (SPIM), which is under development for the International Standardization Organization (ISO). This model entails taking empirically derived total electron content (TEC) data and fitting an electron density profile on to the measurements. It is interesting to note that in this model, GPS observations are used as one of the inputs to this model [*Krankowski et al.*, 2005].

In satellite navigation, only the ionospheric delay is modelled (because the incoming signal experiences this delay) and not the full characteristics of the ionosphere. In the GPS community, this modelling is often simply referred to as ionospheric modelling. As

such, from this point onward ionospheric delay modelling will be referred to as ionospheric modelling.

The ionospheric delay is modeled by estimating the TEC in a column of atmosphere through which the signal travels, and by removing the elevation angle dependence the delay is modeled as a standard parameter, which is the vertical TEC (VTEC) [*Liu and Gao*, 2004]. In theory, VTEC is derived by integrating the electron density in a vertical column along the signal path, and this quantity varies diurnally, as a function of altitude and as a function of TEC, as depicted in Figures 1.3a and 1.3b. Estimation of VTEC at standard ionospheric grid points (IGPs) with 5°x5° spacing and interpolation of these estimates at desired user locations form the basis of the WAAS augmentation scheme for ionospheric scheme [*Cormier et al.*, 2005]. Localized scalar differential GPS (DGPS) corrections (ionospheric, clock and orbit), decoded from WAAS messages, can be combined and post-processed to be applied to the user station. It was found in several studies that the final wide area DGPS solution fell well within the WAAS performance specifications [*Cannon et al.*, 2002].

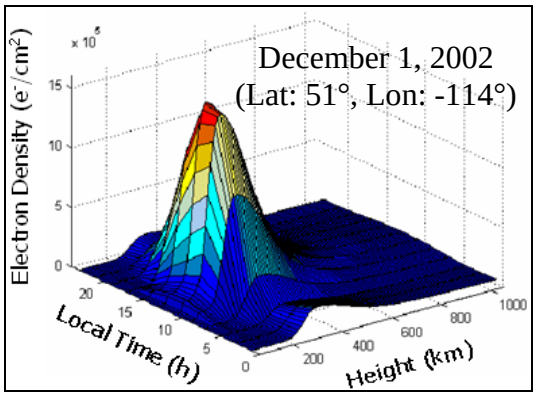

Figure 1.3a: Electron Density Variation

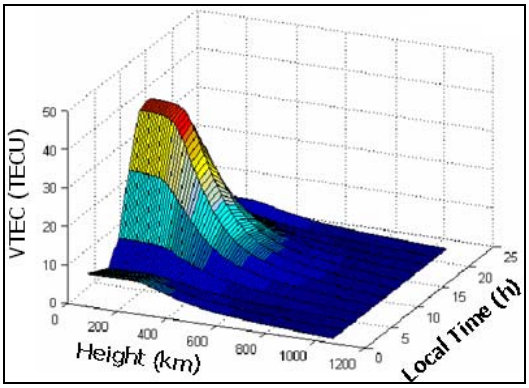

Figure 1.3b: VTEC Variation [*IRI*, 2003]

In Canada, WAAS has definite potential for being used for various navigation applications. However, its main purpose during inception was to service the CONUS region, and since there are a few reference stations in Alaska, WAAS coverage is present in some parts of Western Canada but almost non-existing in the eastern part of the country [*Loh et al.*, 1995]. Therefore, some of the Canadian wide-area systems may offer better performance and coverage here in Canada, because their focus is to provide DGPS services to Canadian users. One of these is the CDGPS Service, which provides reliable wide-area DGPS (WADGPS) corrections to Canadian users for various applications [*NAV CANADA*, 2005]. As well, the original plan to expand the current WAAS network into Canada is being realized, and this is named the Canadian WAAS (CWAAS). Basically, four more wide-area reference stations (WRSs) are being added in Canada, with seamless WAAS operation through the United States into Canada. The coverage in Eastern Canada would be extended, significantly improving availability, accuracy and integrity for that region, as will be shown by the results of this study. The core WAAS network itself is up for improvements. In particular, there are talks by aviation and transportation authorities that more WRSs are in order; the exact details have yet to be disclosed [*Cormier*, 2005].

One of the reasons these improvements are necessary is because of limited capability of the current WAAS to adequately handle challenging ionosphere conditions. In general, the WAAS is only able to capture the low frequency behaviours of the ionosphere, both in the spatial and temporal domains. Thus, it has a tendency to smooth out the high frequency, isolated and localized features. As a result, during geomagnetic storms this

smoothing effect deteriorates the accuracy of the ionospheric corrections and ultimately causes major degradation in positioning accuracies. There is also a tendency of the WAAS to underestimate the ionospheric delay, which is of no surprise since smoothing is actually failing to capture the large values. Consequently, this constant underestimation is causing a bias in the WAAS data. Scenarios of this shortcoming for WAAS will be shown and quantified in later chapters of this thesis.

1.2 Objectives

In a previous study done by *Yousuf et al.* [2005], it has been shown that WAAS horizontal positioning errors reached up to 25 m and vertical errors sometimes surpassed the 30 m mark during severly disturbed ionospheric times. This suggests that WAAS infrastructure/algorithms do not effectively model the ionosphere during such conditions. In light of this, ways to reduce the errors due to ionospheric delay should be sought. Therefore, the intended research will include the following three major objectives:

1. To evaluate the accuracy of the current WAAS satellite clock, orbit and ionosphere corrections for a variety of ionospheric conditions.
2. To quantify the current level of positioning accuracy offered by WAAS in the US and Canada using the standard WAAS ionosphere model for various ionospheric conditions.

3. To investigate the improvements obtainable if the current WAAS network is augmented with additional reference stations. This will involve modelling the ionosphere with a greater spatial resolution over North America using additional stations in Canada and in the US. In addition, this will serve to study the benefits that would be gained in Canada as a result of adding the proposed CWAAS reference.

1.3 Thesis Outline

Chapter Two provides an overview of the WAAS. It outlines the major elements that make up this augmentation system and how these elements viably support the whole system. This chapter goes into describing the different WAAS messages and how the correction information is extracted from them. A section discusses the WAAS localization scheme developed for this study. The discussion is then extended to the CWAAS, which is an extension of the WAAS network in Canada. It includes a review of the proposed CWAAS network, a study of the potential merger of the two networks (WAAS and CWAAS), an analysis of the expected benefits, a discussion on how to evaluate their performances, and a proposal for a denser reference network to better model the ionosphere, which would improve the current WAAS performance.

Chapter 3 presents an analysis of the WAAS corrections in the correction domain. There are four major parts to the analysis: the truth data and three individual error sources (ionosphere, clock and orbit) for which the corrections are generated. Since the ionospheric error is the most significant and the most difficult to model, a greater focus is put towards understanding the methodology behind its modelling.

Chapter 4 is dedicated to evaluating the current WAAS in the positioning domain under various ionospheric conditions. Specific case studies are included; three major storm events from the past decade are studied, and results are described from various perspectives such as: spatial, temporal, statistical, and conditional. Important findings will be extracted from the results to be used as a frame of reference for the enhancements discussed in the next chapter.

Chapter 5 describes the core methodologies behind the research presented herein. It presents the methods involved in WAAS enhancements and CWAAS network simulation. The overall results obtained from conducting this comprehensive evaluation of WAAS/CWAAS positioning accuracies and of the proposed refinements are also described in detail. Essentially, it provides extensive statistical information and discussion on the processed results. Observing interesting features and phenomena within the data, identifying special relationships between parameters, analyzing characteristics, and discussing specific enhancement issues will also be a part of this section.

Finally, Chapter 6 presents the important conclusions drawn from this research and provides some recommendations towards making further progress into the study of this research topic.

Chapter 2

The WAAS

2.1 Ionospheric Effects

The ionosphere is a complex part of the atmosphere, existing from about 60 km of altitude up to several hundreds of kilometres, as shown in Figure 2.1. The ionising radiations of the sun and energetic particles transported by the solar wind produce concentration of free electrons especially in the 250-400 km high layer known as the F-region. This phenomenon results in changes in the refractive index of the medium. Radio waves over 100 MHz that cross the ionosphere are then refracted and delayed. In the L-

band, which corresponds to the GPS frequencies, the delay may reach several tens of metres [*Dai et al.*, 2003].

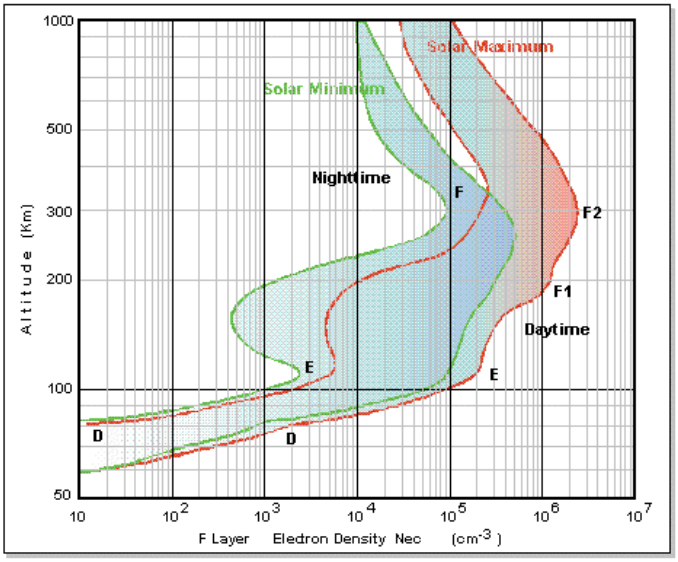

Figure 2.1: Ionospheric Electron Density Profile [*SPARG*, 2003]

Ionospheric effects on satellite-based navigation systems such as GPS are a major concern and interest of experts of the field across the world. The atmospheric effect of interest for this study is the ionosphere, its impacts on WADGPS positioning, and viable mitigation techniques. There are several ionospheric phenomena that have adverse effects on WADGPS in general; of major concerns are 1) phase and amplitude scintillations causing loss of lock and navigation capabilities and 2) large gradients (both spatial and temporal) in electron content. Scintillation mostly affects GPS carrier phase measurements, which are differentially corrected in LAAS. On the other hand, TEC gradients affect differential methods, which is the basis for the WAAS correction model. Therefore, the discussion to follow will focus on TEC gradients [*Skone et al.*, 2003].

Large gradients in TEC are characteristic of an event called storm enhanced density (SED). This is caused by enhanced ionospheric electric fields that are present near the mid- to high-latitudes during geomagnetically disturbed periods, which can lead to depletions and enhancements of electron density in this region. These large gradients (>70 ppm) in TEC can cause large differential ionospheric range errors. This phenomenon initially develops in the lower latitudes during the afternoon (local time). This is also associated with geomagnetic storms in the phase of the solar cycle from a few years ago (Figure 2.2). SED was originally recognized in the early 1990's with the Millstone incoherent scatter (IS) radar [*Foster et al.*, 2002; *Foster and Vo*, 2002] and has been studied in detail with data from the DMSP and IMAGE satellites, and with TEC data collected from multiple GPS receivers located across the US and Canada [*Coster et al.*, 2003a; *Coster et al.*, 2003b].

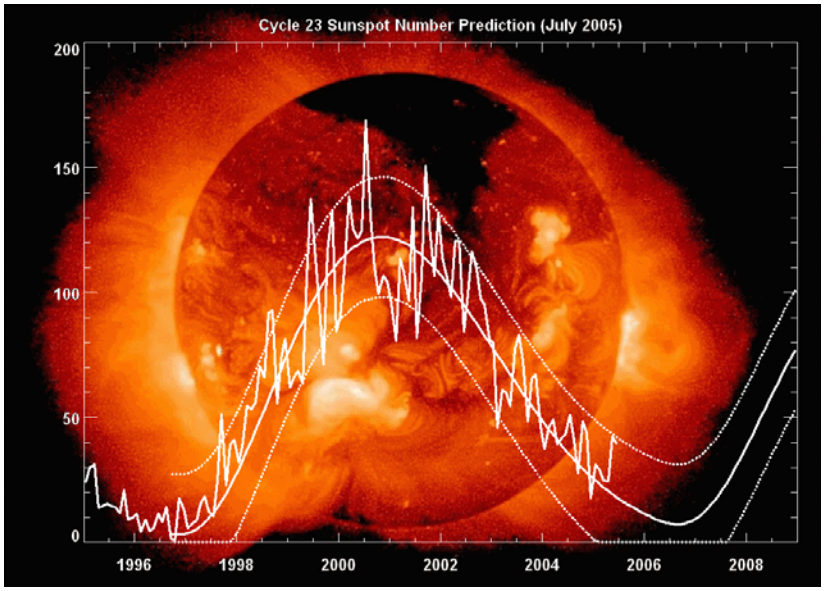

Figure 2.2 Cycle 23 Sunspot Number Prediction (July 2005) [*NOAA*, 2005]

Analysis of the GPS TEC data shows that during geomagnetic disturbances, ionospheric electrons are transported from lower latitudes to higher latitudes, redistributing TEC across latitude and local time (Figure 2.3). Gradients as large as 70 ppm have been observed at geographic latitudes of 45°-50° in North America by the MIT Haystack Observatory. SED effects can persist for several hours in this region, and this is a significant issue for North American DGPS services. As such, for the purpose of this investigation, processing data will include SED occurrences. Namely, during the past few years this has been observed in October and November 2003 and to a lesser extent in November 2004. Later sections of this chapter will discuss the actual processing methodology for this task [*Skone et al.*, 2003].

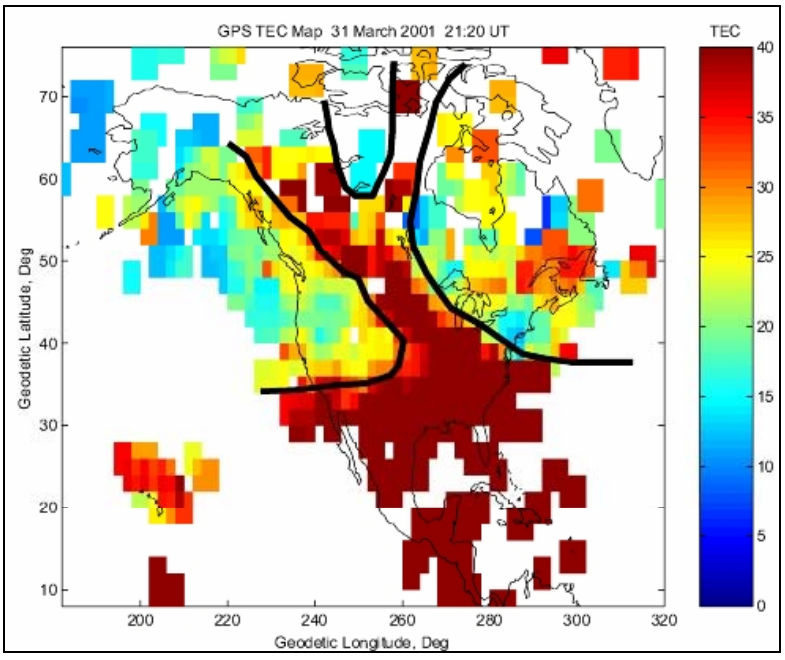

Figure 2.3 Example of Storm Enhanced Density over North America during a Geomagnetic Storm Event (March 31, 2001) [*Skone et al.*, 2003]

2.2 Augmenting GPS

As discussed earlier, GPS positioning is based on range measurements from the space-borne satellites to the receiver. These measurements are made by estimating the travel-time of the signal coming from each satellite to the receiver. During this transmission, the signal passes through many different mediums that delay and modify the signal, therefore corrupting the time interval between transmission and reception of the signal. Of major importance for satellite positioning are the delays caused by the troposphere and the ionosphere. The tropospheric delays are reduced using empirically derived models (e.g. the Hopfield Model) and are relatively stable in terms of magnitude [*Hopfield*, 1969]. The ionosphere (an important element of this research), on the other hand, is much more difficult to model, especially during geomagnetic storms. As such, it impacts the GPS error budget very severely [*Rodrigues et al.*, 2004].

The first line of defense against this positioning impedance is applying differential corrections, which is the basis for DGPS methods. However, sometimes this is not enough to adequately capture the ionospheric features, and so a more robust method of ionospheric modelling technique is usually employed; this is known as WADGPS. These and other topics relating to the augmentation of GPS will be discussed in the following subsections [*Zhang and Bartone*, 2004].

2.2.1 Standard Positioning Service

A typical GPS user would rely on standard positioning service (SPS), which offers a horizontal positioning accuracy at the 95th percentile of 22.5 m (assumes average ionosphere) [*Conley*, 1998]. This is the guaranteed level of horizontal accuracy offered by the system at the moment, but prior to May 1, 2000 the accuracy was intentionally degraded by the US DOD to have greater military control over the system. This was done by introducing controlled errors (clock dithering) to reduce the precision of SPS. Such errors could be removed by DOD-authorized users, enabling them to have selective levels of service; hence, the feature was called Selective Availability (SA) [*Misra and Enge*, 2001].

The SPS positioning solution is based on the broadcast parameters. These are the clock, orbital and ionospheric error models that are broadcast through GPS navigation messages, and the troposphere could be modelled through formulations dependent on meteorological data. These tropospheric model parameters are derived from previously made observation of the GPS constellation and the physical surroundings near the receiver; thus, it is an estimate of the actual occurrences. Post-processing could be done to further improve the positioning solution, but in that case the real-time element would be lost. It is to be noted that SPS does not offer the full potential of the service [*Parkinson and Spilker*, 1996]. Further mitigation of the errors using various methods and techniques form the basis of the next few subsections.

2.2.2 GPS Error Sources and Corrections

GPS errors basically have three different origins: satellite-based errors, propagation errors, and receiver-based errors. Of relevance to this research are clock/orbital errors (satellite-based errors) and ionospheric error (propagation error). The intention herein is to study and present methods, using which these errors are better modelled and/or mitigated.

Two main characteristics of any error are magnitude and variability. In Global Navigation Satellite Systems (GNSS), error variability could depend on temporal and/or spatial correlation. For instance, clock errors are not strongly correlated, spatially; they are only dependent on time. On the other hand, the ionospheric error is both spatially and temporally correlated but very erratic and possesses very localized features. As discussed above, one way to reduce these errors is to apply the broadcast correction models provided in the navigation message, but this only removes 50% of the errors. To have a significant positive impact on the error budget, differential methods should be employed. In DGPS mode, the corrections for these errors are applied in the positioning domain [*Rodrigues et al.*, 2004]. The conceptual details on DGPS are given in Subsection 2.2.4.

Atmospheric effects are generally reasonably reduced in DGPS mode. During severe weather conditions (in case of troposphere) or high levels of ionospheric disturbance, however, the errors could be significant. The ionospheric range error is a function of the signal frequency and the electron density along the signal path:

$$I = \pm 40.3 \frac{TEC}{f^2} \text{ (in meters)} \quad (2.1)$$

where TEC denotes the total electron content integrated along the signal path (in el/m^2), f is the signal frequency (in Hz), and + (-) denotes the group delay (phase advance). The ionospheric range error can dominate the DGPS error budget under high levels of ionospheric activity. Ionospheric range errors can reach up to 25 m in some cases, whereas typical error level is around 7 m [*Lachapelle*, 2003]. Additional effects of ionospheric scintillation can cause degradation of receiver tracking performance and, in extreme cases, loss of navigation capabilities entirely [*Knight et al.*, 1999].

2.2.3 Ionospheric Delay Observable

An ionospheric pierce point (IPP) is defined as the intersection between a given satellite-receiver line-of-sight and the thin ionospheric shell. The height of this virtual shell is nominally taken at 350 km altitude for modelling purposes due to high electron density in the F region, as discussed in Section 2.1. This is approximated as a shell because the majority of the ionospheric electrons affecting the GPS signals are concentrated near 350 km altitude. Therefore, it is a suitable representation of the overall ionosphere and, to minimize the computational burden, only one fixed height is used. Figure 2.4 shows a schematic of how vertical delay, slant delay, and IPP are related in this thin-shell approximation.

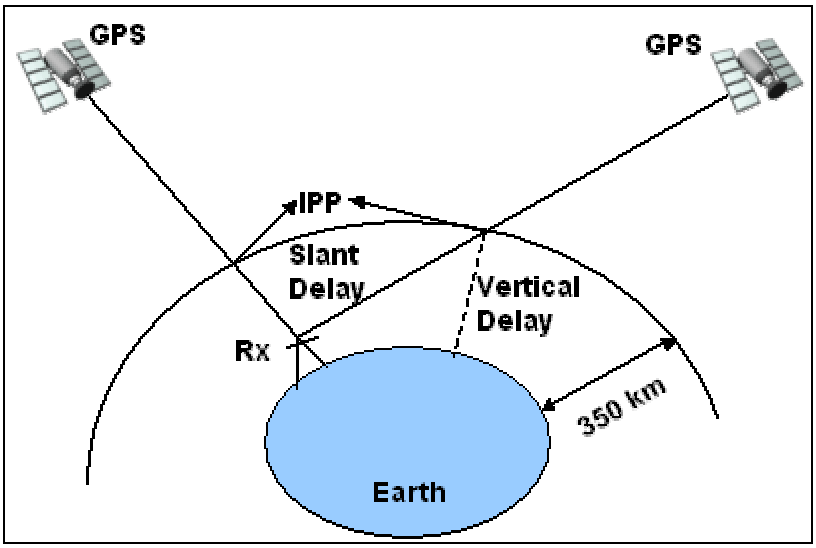

Figure 2.4 Ionospheric Pierce Point Geometry

The actual GPS observations are made in the slant; thus, these have to be mapped to the vertical. In order to do that, a mapping function is used, which is essentially a factor that is a function of the elevation angle. Therefore, slant TEC measurements along the observation line-of-sight can be mapped to the vertical simply by dividing it by this factor. The inverse of this factor would be used to go from the vertical to slant. The expression that describes this mapping function is given in Equation 2.2, and the geometry behind the derivation of this equation is shown in Figure 2.5.

$$M(E) = \sin E' = \left\{ 1 - \left(\frac{R_E}{R_E + h_{IPP}} \right)^2 \cos^2 E \right\}^{-\frac{1}{2}} \tag{2.2}$$

where E is the satellite elevation angle, R_E is the Earth radius, and h_{IPP} is height of the ionospheric shell.

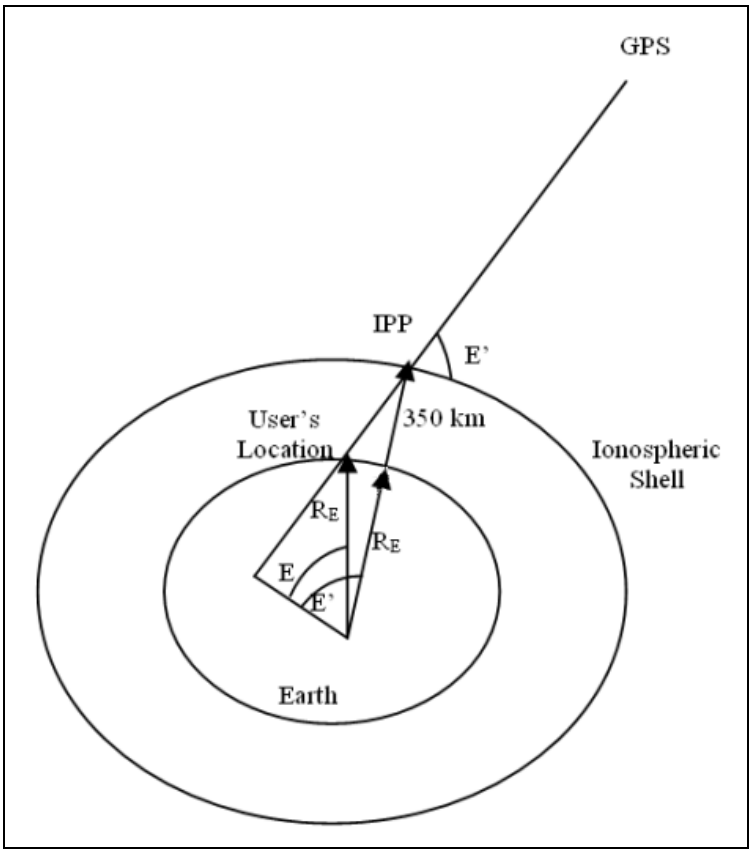

Figure 2.5: Geometry Involved in Deriving the Mapping Function

2.2.4 DGPS Concepts

DGPS involves calculating range errors at a reference station (RS) with its coordinates known and relaying the error information to remote users within the region of coverage, as depicted in Figure 2.6. In this manner, orbital and atmospheric errors are reduced, satellite clock error is eliminated, but receiver noise and Multipath (which is a systematic error produced by the reflected signals contaminating the direct one) still remain. Various multipath mitigation techniques exist consisting of proper selection of antenna, receiver firmware and hardware [*Van Dierendonck et al.*, 1992]. However, solutions could be as simple as placing the antenna far away from reflective surfaces. Noise, on the other hand,

is an inherent error that cannot be eliminated nor reduced, but it can be stochastically modelled [*Zhang and Bartone*, 2004].

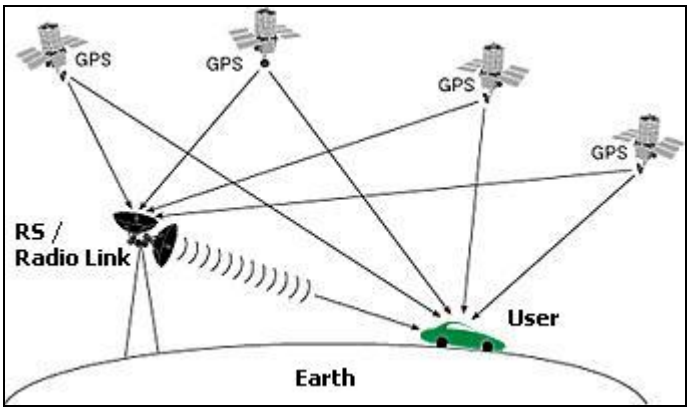

Figure 2.6: Depiction of DGPS basics [*NDGPS*, 2003]

2.2.5 WADGPS and SBAS

In wide area differential DGPS (WADGPS), GPS observations from a sparse network of reference stations are used to model correlated error sources over an extended region. WADGPS services allow specified minimum levels of positioning accuracy to be achieved at all locations within the coverage area. With a growing demand for accurate and reliable DGPS positioning worldwide, several WADGPS services have been developed in recent years [*Cannon and Lachapelle*, 1992]. Current operational WADGPS systems include the WAAS, and commercial WADGPS systems include the OmniSTAR service.

A space-based augmentation system (SBAS) employs a network of reference stations to continually collect Global Navigation Satellite System (GNSS) signals coming from the

satellites. These reference stations assimilate the dataset and pass it onto the master station, which in turn processes the incoming raw data and generates the correction and integrity information for the system. This correction is then fed to the ground uplink station, which uploads it to the geostationary satellites. Finally, the geostationary satellites broadcast the correction, integrity, and ranging messages to the users for navigation augmentation. The schematic in Figure 2.7 depicts the flow of information in a typical SBAS [*NAV CANADA*, 2005].

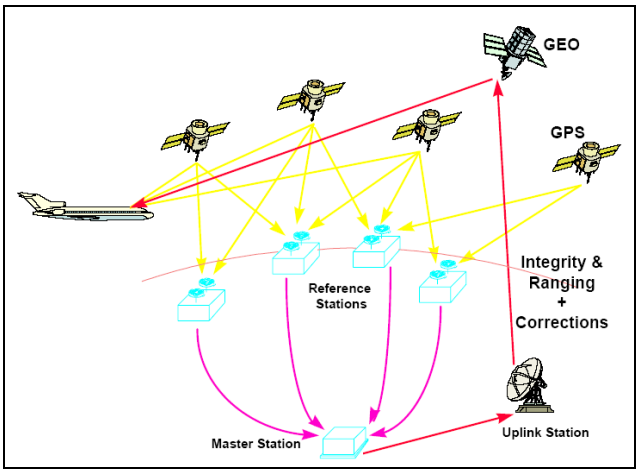

Figure 2.7: SBAS Overview [*NAV CANADA*, 2005]

2.3 The FAA

The FAA is responsible for the civil aviation in the US. It was originally created under the name Federal Aviation Agency upon the establishment of the Federal Aviation Act of 1958. Thereafter, it gained its present name (Federal Aviation Administration) when it

became a part of the Department of Transportation (DOT) in 1967. FAA's roles include regulating civil aviation to promote safety, participating in new aviation and aeronautics technologies, managing air traffic control, conducting research and development of the National Airspace System (NAS), and monitoring environmental effects of civil aviation [*FAA,* 2005].

FAA's major activities are as follows [*FAA*, 2005]:

- Safety Regulation
- Air Space and Air Traffic Management
- Air Navigation Facilities
- Civil Aviation Abroad
- Commercial Space Transportation
- Research, Engineering, and Development
- Organization
- Other Affiliate Programs

As such, FAA overlooks all airspace operations in the US, and throughout the lifespan of the WAAS, it has definitely added value to FAA's overall navigation strategies. Since FAA is the developer and the day-to-day manager of the WAAS, it played an essential role for this study. Its importance for this research is twofold. Firstly, most of the WAAS related data used in the processing have been obtained from the FAA, along with standards and guidelines to follow for proper use of those data products. Secondly, FAA has been a vital source of information for all the background research on WAAS,

provided a frame of reference for the WAAS assessment process and served to establish the theoretical backbone behind the enhancement.

2.4 Technical Overview

GPS has been put to work for various positioning applications. Nowadays, it is increasingly being used for navigation purposes. This push to devise more precise and reliable navigation aids has initiated new research ventures and applications. One of the major areas of interest for users around the world is aircraft navigation using GPS. This is mainly because GPS integrity is not guaranteed and even with SA off, the vertical accuracy is better than 10 m, whereas the aviation requirements are as follows [extracts from *Walter*, 2003]:

- *Accuracy:*
    - Less than 7.6 m 95% horizontal and vertical
- *Integrity:*
    - Less than 10^{-7} probability of true error larger than confidence bound
    - 6 second time-to-alarm
- *Continuity:*
    - Less than 10^{-5} chance of aborting a procedure once it is installed
- *Availability:*

- Horizontal alarm limit (HAL) less than 40 m and vertical alarm limit (VAL) less than 50 m 95% of the time to 95% of Continental USA (CONUS), where HAL and VAL are error limits beyond which service is denied.

In order to accommodate these requirements for safety-critical, the FAA has developed and commissioned the WAAS (Figure 2.8) on July 10, 2003. The WAAS level of coverage over the CONUS region is depicted in Figure 2.9 (the percentile values on the right-hand side represent the coverage level). It consists of [*Bunce*, 2003]:

- 25 WRSs
- 2 WAAS Master Stations (WMSs)
- 2 Geosynchronous Satellites (GEOs)
- 3 Ground Uplink Stations (GUSs)

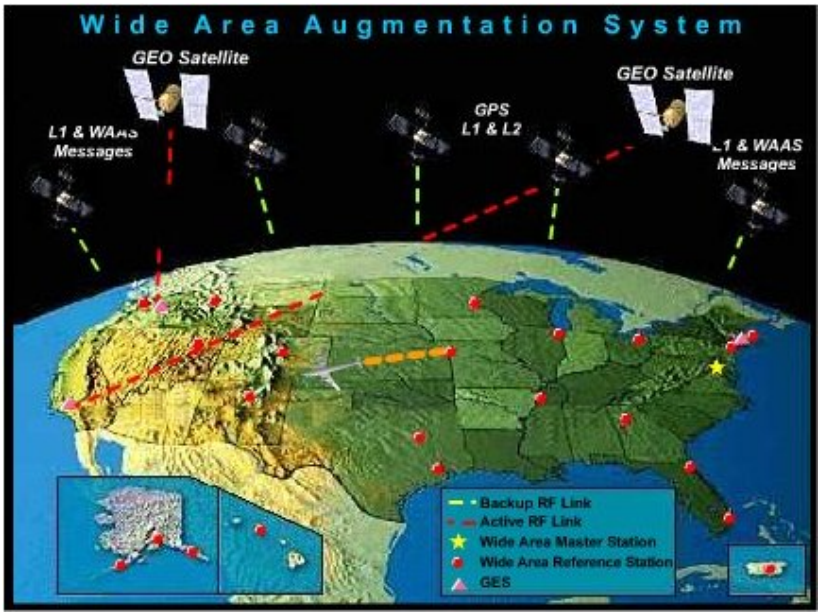

Figure 2.8: WAAS Overview [*FAA*, 2003]

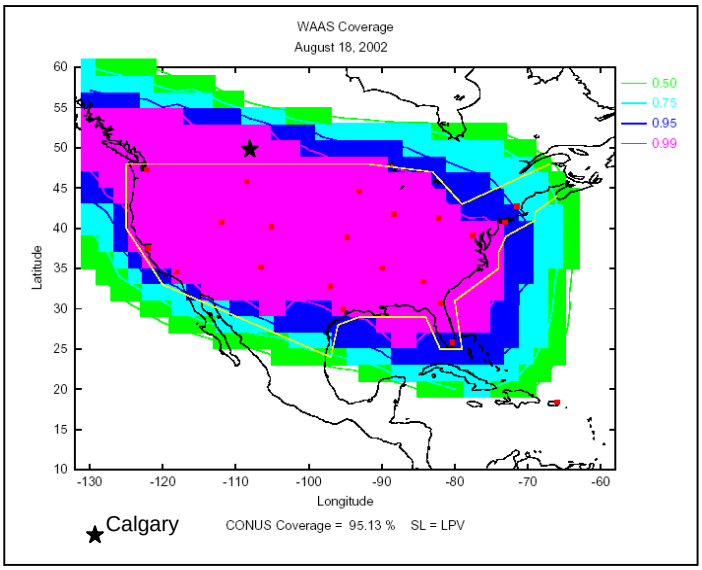

Figure 2.9: WAAS Coverage over the CONUS Region [*FAA*, 2003]

WAAS testing done over the CONUS region in September 2002 produced accuracy performance of 1–2 m horizontal and 2–3 m vertical [*FAA*, 2005] 95% of the time, which meets all phases of Category I (Cat I) precision approach. WAAS currently achieves Cat I approach guaranteed for domestic enroute navigation. The requirements for Cat I are as follows:

- Vertical positioning accuracy should be 4 m
- Integrity should be guaranteed to 4^{-8}/approach
- Time-to-alarm should be 6 seconds
- VAL should be 12 m
- Continuity should be guaranteed to 1^{-5}/approach

As a result of all the abovementioned upgrades, WAAS current and conceivable benefits include [extracts from *Walter*, 2003]:

- Primary means of navigation
- More direct routes
- Precision approach capability
- Simplified equipment on-board the aircraft
- Decommission of older and expensive ground equipment
- Improved accuracy and integrity

2.5 WAAS Components

WAAS is comprised of two different segments: the ground segment and the space segment. The ground segment has three sub-elements: WRS, WMS and GUS. Signals from GPS satellites are received by the WRSs (Figure 2.10). Each of these precisely surveyed reference stations receive the signals and determine if errors exist. Each WRS in the network relays the data to the WMS where correction information is computed. The WMS calculates correction algorithms and assesses the integrity of the system. A correction message is prepared and uplinked to a GEOSAT via a ground uplink system (GUS). The message is then broadcast from the satellite on the same frequency as GPS (L1, 1575.42 MHz) to receivers onboard aircraft (or any other WAAS capable receiver), which are within the broadcast coverage area of the WAAS [*US DOT*, 1999].

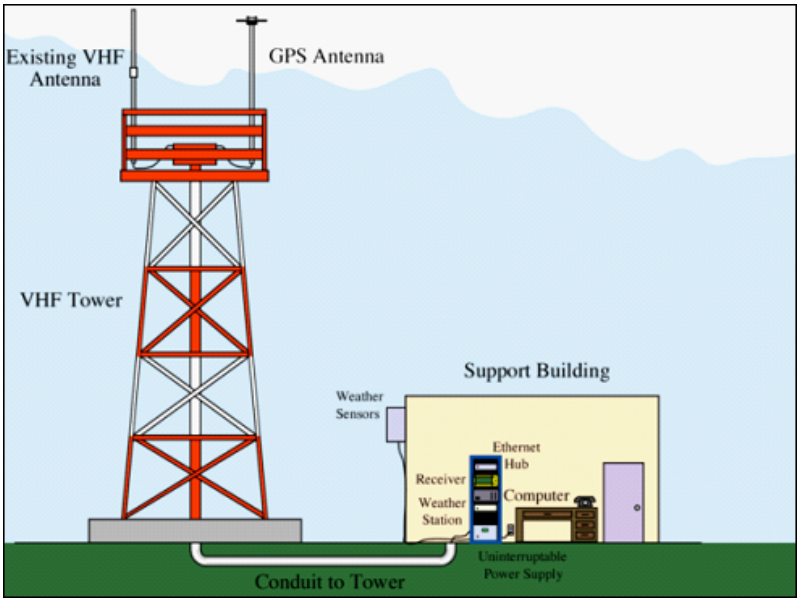

Figure 2.10: Typical WRS Setup in the WAAS Network [*Bunce*, 2003]

The space segment consists of two GEOs (there are more to come in 2005) that remain approximately at a fixed position above the earth. These satellites are the vital links between the system and the end user. These two International Maritime Satellite Organization (INMARSAT) communications-relay satellites (called bent-pipes) provide integrity and ranging corrections [*Walter*, 2003]. These GEOs have poor ranging accuracy and vulnerable uplinks. If one of them fails, about half of CONUS will currently lose coverage until service is restored. Presently, the two satellites serving the WAAS area are called POR (Pacific Ocean Region) and AOR-W (Atlantic Ocean Region-West) (Figure 2.11) [*FAA*, 2005].

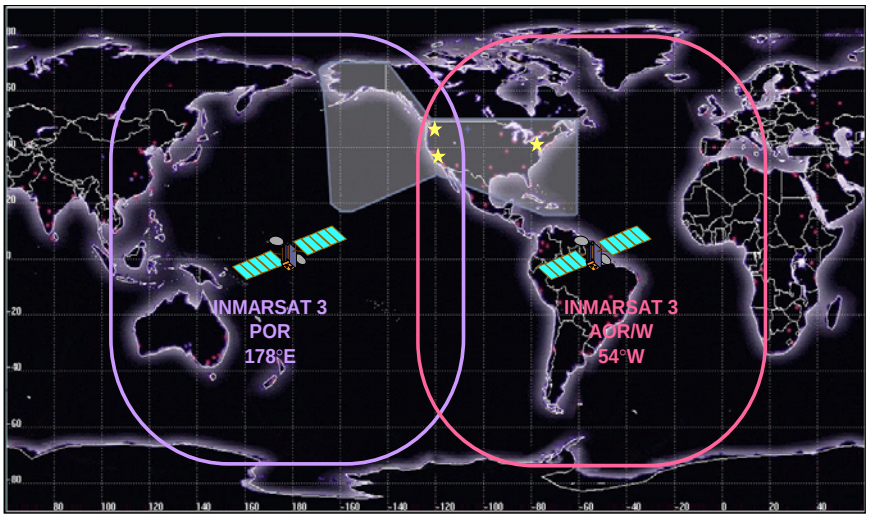

Figure 2.11: INMARSAT Coverage [*FAA*, 2005]

2.6 WAAS Messages

The navigation information generated and compiled by the WAAS network is relayed to the user via various messages in Radio Technical Commission for Aviation Services (RTCA) format. They are received as blocks of data in the form of a bit sequence, as shown in Figure 2.12. These have specific format, purpose and name. The full set of WAAS messages are listed in Table 2.1. Basically, the correction information is given through the message types 2-5, 18, 24 and 25. These and other supporting messages will be described in detail in later sections, where the WAAS correction models will be discussed. The remainder of the messages provide various masks, reliability figures, GEO navigation/almanac data, and status information [*US DOT*, 1999].

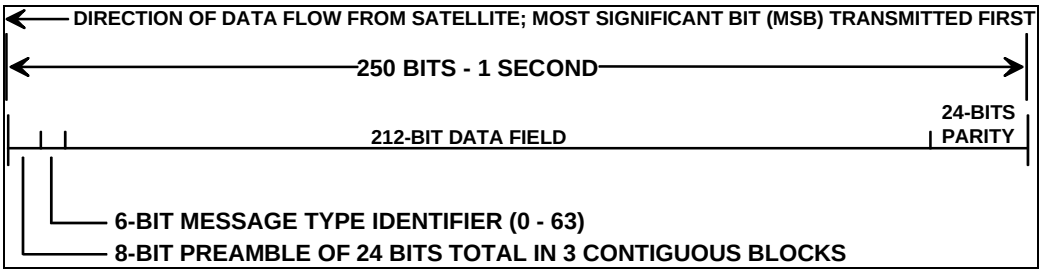

Figure 2.12: Data Block Format [*US DOT*, 1999]

Table 2.1: WAAS Message Types [*US DOT*, 1999]

Type	Contents
0	Don't use this GEO for anything (for WAAS testing)
1	PRN Mask assignments, set up to 51 of 210 bits
2-5	Fast corrections
6	Integrity information
7	Fast Correction Degradation factor
8	Estimated RMS Error message
9	GEO navigation message (*X*, *Y*, *Z*, time, etc.)
10	Degradation Parameters
11	Reserved for future messages
12	WAAS Network Time/UTC offset parameters
13-16	Reserved for future messages
17	GEO almanacs message
18	Ionospheric grid point masks
19-23	Reserved for future messages
24	Mixed fast corrections/long term satellite error corrections
25	Long term satellite error corrections
26	Ionospheric delay corrections
27	Reserved (WAAS Service Message)
28-61	Reserved for future messages
62	Reserved (Internal Test Message)
63	Null Message

2.7 Services Offered and Applications

WAAS was conceptualized by FAA to service the civil aviation community by augmenting various aspects of navigation service for GPS SPS. Its primary objective is to provide a navigation system for all phases of flight through precision approach. In order to meet the designated performance requirements, WAAS includes these eight primary functions [extracts from *US DOT*, 1999]:

(1) Collect data;

(2) Determine ionospheric corrections;

(3) Determine satellite orbits;

(4) Determine satellite clock corrections;

(5) Determine satellite integrity;

(6) Provide independent data verification;

(7) Provide WAAS message broadcast and ranging; and

(8) Provide system operations and maintenance.

In addition to providing GPS corrections, WAAS supplements the SPS satellite constellation by GEO ranging. Although the GEO measurement is rather poor due to limited bandwidth (2 MHz) and use of wide correlator (noisier), overall accuracy does improve by resorting to these satellites (Figures 2.13a and 2.13b) because more ranging satellites means more observations are available, and therefore redundant observations provide a better positioning estimate.

For this study, GEO range observations were not used to conduct positioning. The reason being that positioning solution was computed in post-mission using archived data from the network of Continuously Operating Reference Stations (CORS), and these observation data do not include GEO range measurements because CORS receivers are not WAAS-enabled. Therefore, WAAS corrections were applied independently in the measurement domain.

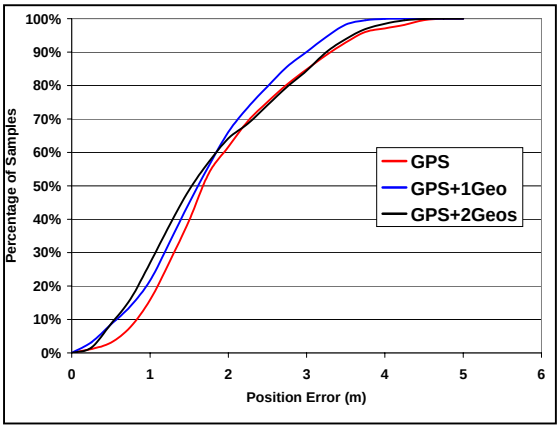

Figure 2.13a: GPS+GEO 2D Accuracy Histogram

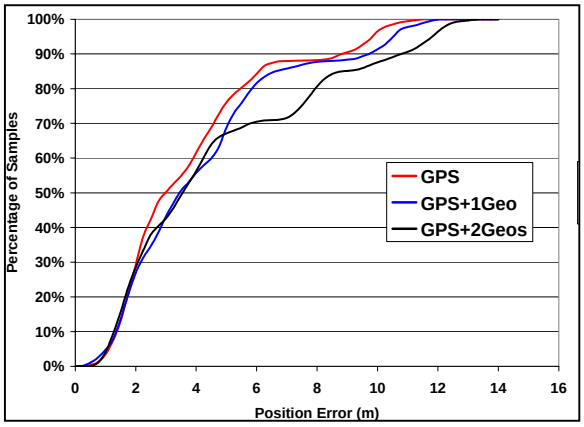

Figure 2.13b: GPS+GEO 3D Accuracy Histogram [*Alud*, Private Comm.]

Since its successful commission in July of 2003, the range of WAAS applications has grown drastically, from automotive and marine applications to farming and construction usage. In fact, it is now possible to procure handheld GPS units that support WAAS positioning, thus offering enhanced accuracy and reliability.

2.7.1 WAAS Aviation Applications

The original intent in developing the WAAS, during its inception phase, was to serve the aviation industry by providing a safe, secure and efficient en-route approach. Since then its applications have ventured into new horizons. Nonetheless, the focus for FAA authorities in regulating the WAAS still remains supporting the fleet of commercial aircrafts. Their continual efforts to support this safety-critical application have shown the way for other countries (such as Japan, China, India and European countries) to adopt SBAS methods for augmenting GPS to aid in air-traffic navigation.

There is a major push from the aviation community to allow sole use of GPS for all phases of flight through Category I precision approach. Clearly, "GPS+" technologies will need to be incorporated into modern avionic equipment. Some of these technologies include (but are not limited to) WAAS, GPS with Receiver Autonomous Integrity Monitoring (RAIM), Local Area Augmentation System (LAAS), and GPS-assisted inertial systems. A summary of these positioning methods and their corresponding phases of flight is listed in Table 2.2. Obviously the WAAS plays a big role in all types of non-precision approaches, as most of the guidance for in-flight operations is provided by WAAS. The most crucial aspect for WAAS-guided avionic navigation is vertical positioning, and WAAS is very sensitive about vertical integrity of the system [*Shively and Hsiao*, 2004]. In particular, FAA is very swift at denying service to all aviation users if they sense any indication of deficiencies in integrity. This research attempts to provide ways to improve these conditions by studying the weaknesses in the current system.

Table 2.2: GPS Augmented Technologies for Aviation [*Hanlon and Sandhoo*, 1997]

Phase of Flight		Integrity	Availability	Accuracy
En Route	Oceanic	GPS with RAIM		
	Domestic	WAAS		
Approach & Landing	Non-precision Approaches			
	Category I Precision Approach	WAAS and LAAS		
	Category II/III Precision Approach	LAAS		
Surface	Ground Movement			

2.7.2 WAAS Non-Aviation Applications

The two major non-aviation applications are navigation on marine and land areas, which only deal with 2D positioning methods. Figure 2.14 shows a Furuno GP32 GPS/WAAS receiver (FUGP32) that is used in leisure or fishing boats for marine navigation. Thus, these types of applications require less stringent integrity and do not involve safety-of-life circumstances. Users worldwide rely on DGPS and WADGPS systems for a variety of marine and land applications. These include hydrographic surveying applications, and exploration/exploitation of marine resources, assistance to vessel traffic management services, search and rescue operations, environmental assessment and clean-up, and underwater mine detection and disposal in the marine side. As for land applications, DGPS and WADGPS systems are being employed in the automotive industry, at construction sites, for farming needs, and even for recreational purposes. Due to the diverse nature of these applications, land accuracy requirements are not that regulated and are very specific to the usage [*Yousuf et al.*, 2005].

Figure 2.14: Furuno GP32 GPS/WAAS receiver (FUGP32) [*The GPS Store*, 2005]

The research conducted herein will also focus on WAAS horizontal positioning, which pertains to land and marine applications. As well, the proposed Canadian WAAS project will be investigated, which holds major improvement potentials for marine applications near the eastern coastlines. In fact the Canadian Coast Guard (CCG) is conducting feasibility studies on integrating WAAS/CWAAS resources into their own DGPS services and providing their marine users with WAAS corrections via CCG radiobeacons [*CCG*, 2005]. Thus, the research investigations will include an analysis of what the WAAS has to offer for Canadian marine users and how the CWAAS would further enhance their horizontal positioning capabilities.

2.8 NAV CANADA

NAV CANADA is a non-profit share capital and private corporation that owns and operates Canada's civil air navigation service (ANS) by fulfilling various functions. It operates coast to coast and provides users with air traffic control, flight information, weather briefings, aeronautical information, airport advisory services and electronic aids to navigation. NAV CANADA co-ordinates and maintains safety and efficiency of aircrafts located in Canadian domestic and international airspace assigned to Canadian control [*NAV CANADA*, 2005].

NAV CANADA's infrastructure of ANS facilities includes the following: [extracts from *NAV CANADA*, 2005]:

- Area Control Centres
- Terminal Control Units
- Air Traffic Control Towers
- Flight Service Stations
- Community Aerodrome Radio Stations
- Remote Communications Outlets and Remote Aerodrome Advisory Services
- Landing and Navigational Aids
- Radio and Navigational Facilities
- NAV CANADA Training Institute
- Technical Systems Centre

In addition, it has over 100 airport control towers and flight service stations. These facilities are complemented by one stand-alone terminal control unit, 78 Flight Service Stations, 42 Control Towers, 41 radar sites, a network of 1,400 enroute and terminal aids to navigation, and landing aids. The provision of safe air navigation services is NAV CANADA's product and its raison d'être.

2.9 The Canadian WAAS

Recent studies of the WAAS program suggest that its services could be available in southern Canada [*MacDonald*, Private Comm.]. The governing body in-charge of this project is NAV CANADA. It is currently exploring the possibilities of such a development. Expansion in WAAS infrastructure is the only viable option to that end. It would consist of fielding additional reference stations strategically located in Canada feeding measurement information to FAA master stations in the US. This service would, thus, be called the Canadian WAAS or CWAAS. NAV CANADA and the FAA have been planning this venture since the mid 1990s. No decision has been made in terms of funding for CWAAS; such a decision depends on the success of WAAS in application mode, the compatibility between WAAS master stations and CWAAS station inputs, and the ability of CWAAS to deliver adequate benefits to aircrafts operating in Canada [*NAV CANADA*, 2005].

2.9.1 Proposed CWAAS Reference Stations

As was shown in Figure 2.9, WAAS coverage is insufficient in Southeast Canada and the Northeast United States. Therefore, the joint venture between the FAA and NAV CANADA is focusing to alleviate this deficiency. NAV CANADA has developed a mathematical model, based on spatial variability, which can determine if WAAS can support service in Southern Canada. The same model is used to select optimum locations for CWAAS reference stations. The model is based on spatial characteristics of the ionosphere over the region of interest [*NAV CANADA*, 2005]. NAV CANADA has also established technical site selection criteria and has evaluated some candidate sites for suitability. Currently the proposed sites are located in Gander, Goose Bay, Iqaluit and Winnipeg (Figure 2.15). The project has been approved and the site development and installation dates are listed in Table 2.3. The station at Gander has been deployed, and tests are being conducted to ensure proper operability. The remaining stations are still scheduled to be deployed at the shown dates. It should be noted that FAA is also planning an expansion of the core WAAS network in the US; the exact details of this expansion are not fully disclosed by FAA as of yet [*MacDonald*, Private Comm.].

Table 2.3: Site Deployment Dates

Station	Deployment Date
Gander	27-May-05
Goose Bay	29-Sep-05
Iqaluit	17-Aug-06
Winnipeg	11-May-06

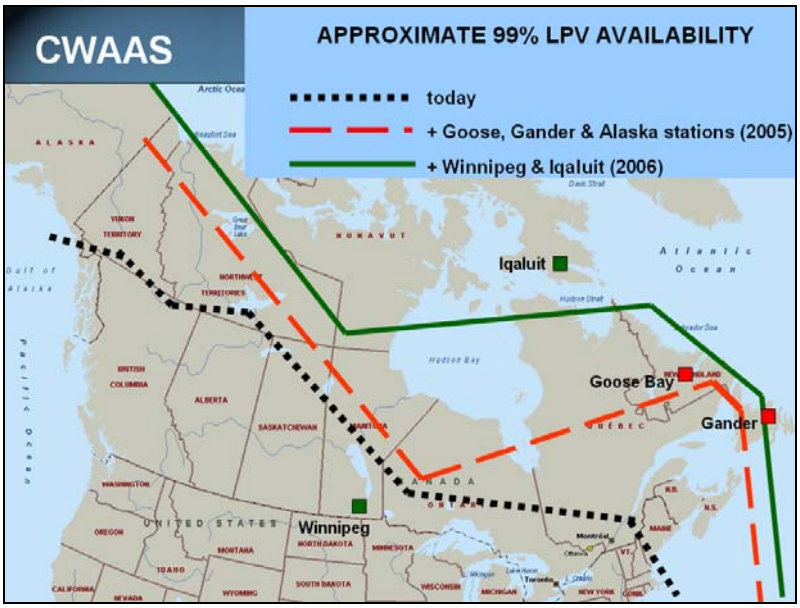

Figure 2.15: Map of Proposed CWAAS Reference Stations [*MacDonald*, Private Comm.]

As can be seen from the figure, improvements attained by adding all or some of the proposed sites to the network is significant. In particular, the 99% availability of localizer performance with vertical guidance (LPV) would be extended farther north once full CWAAS deployment is complete. In terms of coverage, this means that any aircraft flying south of the green line in Figure 2.15 would have effective vertical guidance from the WAAS 99% of the time. Thus, WAAS enroute through non-precision approach coverage would extend to ~65-70°N. As for the regions beyond this coverage, navigation integrity would be supported using other means. For instance, GPS orbits are such that receivers at high latitudes can receive signals from satellites over the other side of the Earth, but GPS signals do not go through the Earth because these signals are in the L-band of the wave spectrum, which get attenuated by Earth's surface. Therefore, GPS/RAIM availability is increased for enroute non-precision approach operations.

LAAS would be used for precision approach at these latitudes. Aircrafts operating through trans-polar routes will most certainly be equipped with GPS-updated inertial navigation systems that will enable the requirements to be met without CWAAS. The Precision Approach (PA) navigation mode refers to the navigation solution operating with a minimum of four satellites with all WAAS corrections (fast-varying, long term, and ionospheric) available. On the other hand, the Non-Precision Approach (NPA) navigation mode refers to the navigation solution operating with a minimum of four satellites with fast-varying and long term WAAS corrections (no WAAS ionospheric corrections) available [*NAV CANADA*, 2005].

2.9.2 CWAAS Strategies

NAV CANADA's CWAAS strategy is as follows [extracts from *NAV CANADA*, 2005]:

- continue analyzing the potential for WAAS to provide service in Canadian airspace;
- delay a recommendation to proceed with CWAAS until after the FAA's WAAS is proven;
- recommend proceeding with CWAAS only if it will deliver meaningful benefits to customers;
- buy only proven WAAS hardware and software off the shelf;
- specify a system architecture that delivers maximum benefits at minimum cost and that is easily adaptable to providing good service with dual-frequency GPS satellites.

2.9.3 Expected Benefits

The foremost benefit to be expected is increased accuracy and coverage for southern Canada. This is mainly due to the fact that with the inclusion of actual Canadian reference stations into the WAAS model, the ionospheric spatial features over this region will be characterized using real observations, and not using a mere mathematical extrapolation from U.S. sites. Furthermore, larger network will mean better orbit determination, and therefore, more accurate correction generation for WAAS and CWAAS users. Augmenting to a larger network has an added benefit of having more reliable and stable solutions. In other words, outliers would have a lesser weight in corrupting valid results. The WAAS network supplemented by the envisioned CWAAS stations is given in Figure 2.16 [*NAV CANADA*, 2005].

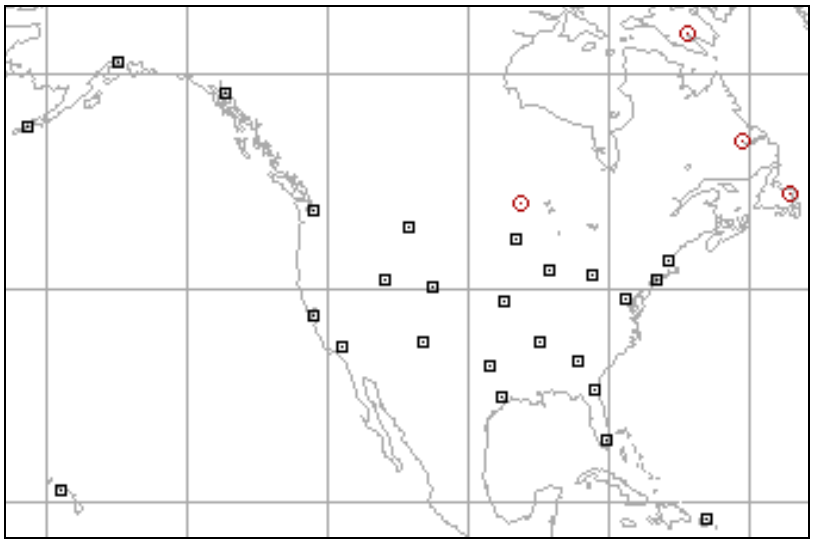

Figure 2.16: CWAAS Stations (circles) Overlaid on the WAAS Network (squares) [*FAA*, 2005]

2.10 WAAS Correction Models

Multipath and receiver noise are specific to equipment and the surrounding environment. The troposphere is modelled by the user applying a tropospheric model in real-time using standard models such as the Hopfield Model, as recommended by WAAS specification [*US DOT*, 1999]. WAAS provides corrections for the remaining errors in the following form: slow clock, slow orbit, fast clock and grid of ionospheric delays. As discussed in Section 2.6, these corrections are provided using various message types. The ones used for this research are shown below with their corresponding error/information [*Enge et al.*, 1996]:

- Type 1: PRN Mask
- Types 2-5: Fast Clock
- Type 18: Ionospheric Grid Point Mask
- Type 24: Mixed Fast/Slow Clock and Orbit
- Type 25: Slow Clock and Orbit and
- Type 26: Ionospheric Delay

Using the above message set, it is possible to derive the appropriate range corrections corresponding to clock, orbital and ionospheric errors. The subsequent subsections will review the models enabling the generation of these range corrections.

2.10.1 Clock Error

This error is due to imperfections in the synchronization between GPS time and amongst the satellite clocks. However, this can be modelled using a higher order polynomial as shown below [*US DOT*, 1999]:

$$\Delta t_{SV}\left(t_k\right) = a_{f0} + a_{f1}\left(t_k - t_0\right) + a_{f2}\left(t_k - t_0\right)^2 \tag{2.3}$$

where $\Delta t_{SV}\left(t_k\right)$ is the total clock correction at time t_k. The a_{f0}, a_{f1} and a_{f2} terms are the zero, first and second order clock coefficients, respectively, and t_0 is an applicable time of day. Note that in Equation 2.3, the total clock correction value is given in seconds. Therefore, it must be multiplied by the speed of light to obtain the actual range correction in metres.

The coefficients are transmitted in the slow clock correction message and are used as inputs to Equation 2.3 to yield the range correction values. In addition, a set of fast clock corrections are also sent, as a separate message, to model the high frequency terms. However, the fast corrections are directly given as scaleable range quantities. The full (slow + fast) range correction obtained from the messages is generally less than 10 μs (3 m) [*Misra and Enge*, 2001].

In practice, the polynomial given in Equation 2.3 is only used up to the second term and sometimes even the second term is omitted depending on the drift rate. A velocity code (1

bit in size) is sent along with the coefficient values. This code dictates whether to use this second term or not. The value of the velocity code is based on a predetermined velocity threshold. It is true (velocity code has a value of 1) when the threshold is surpassed and thus the a_{f1} term is used in the equation, and false (code has a value of 0) when it is not and the a_{f1} term is simply set to 0 [*US DOT*, 1999].

2.10.2 Orbital Error

The orbital error is caused by inaccuracies in the broadcast model parameters defining the satellite orbits, and these errors geometrically translate into an error in range and position. In the WAAS network, the reference and master stations estimate the orbital errors for given satellites in view and this information is sent to users via the different correction messages, as described earlier. Magnitudes of the orbital error are typically in the range of 1-2 m, which could be positive or negative depending on the satellite-receiver geometry [*Lachapelle*, 2003]. Corresponding range errors depend on projection of the orbital error vector along the line-of-sight (LOS) vector from the receiver to the satellite (refer to Figure 2.19 in Subsection 2.11.1). This orbital error vector (in metres) is given in the form of a system of linear equations, as show below [*US DOT*, 1999]:

$$\begin{bmatrix} \delta x_k \\ \delta y_k \\ \delta z_k \end{bmatrix} = \begin{bmatrix} \delta x \\ \delta y \\ \delta z \end{bmatrix} + \begin{bmatrix} \delta \dot{x} \\ \delta \dot{y} \\ \delta \dot{z} \end{bmatrix} \left(t_k - t_0 \right) \tag{2.4}$$

where the orbital error for a given satellite, at time t_k , in the x, y and z directions is equal to the zeroth order error (the most important component of this equation) plus its rate of change multiplied by the difference between t_k and t_0 (an applicable time of day). All the terms present in the right-hand-side of Equation 2.4 are provided through the various WAAS messages and, by solving the equation, the orbital error vector corresponding to an individual satellite is found. However, this vector must then be projected along the appropriate LOS to derive the range error (which is dependent on the location of the receiver) that could be directly applied as a correction to the raw pseudorange observation. The basic principles behind the localization of these errors will be given subsequently in Section 2.11 [*US DOT*, 1999].

2.10.3 Ionospheric Error

The ionosphere is a major contributor in the GPS error budget. Therefore, its mitigation will significantly improve positioning accuracy. WAAS attempts to model the ionospheric delay using dual-frequency GPS measurements from its 25 reference stations and broadcasts values of ionospheric vertical delay at ionospheric grid points (IGPs) over its region of coverage, as pictured in Figure 2.17. IGPs are defined to be virtual points over North America, where the vertical ionospheric delays are estimated by interpolating the measurements made by the WAAS network. A local planar fit is used to estimate the vertical delay at each IGP. It is important to note that a different planar fit is imposed at every IGP using the surrounding local observations [*Altshuler et al.*, 2002].

This fit is derived from all the observations within a given radius (R) in North and East directions. These observations are made by dual-frequency GPS receivers, which enable the isolation of the ionospheric component because of dispersive nature of the ionosphere. R may be varied depending on the density of the surrounding observations, but R is typically 1000 km. If the number of observations within R is less than a preset threshold, R may be increased until this threshold is surpassed [*Altshuler et al.*, 2002].

$$VTEC = a_0 + a_1 d_E + a_2 d_N \tag{2.5}$$

where:

$VTEC$	is vertical total electron content
a_0, a_1, a_2	are the planar fit coefficients
d_E, d_N	are distances from the grid points in the East and North directions, respectively

Using these standard VTEC values, one could compute the ionospheric vertical delay at a location of interest using the surrounding IGP observations [*Altshuler et al.*, 2002]. This requires interpolation of the grid points to derive the WAAS grid prediction for a given user location, which will be discussed in detail in the next section.

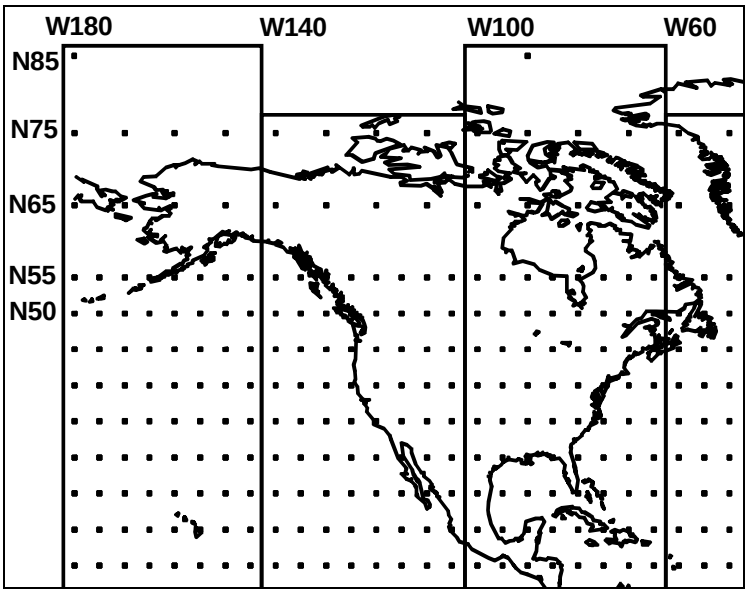

Figure 2.17: WAAS IGP Locations across North America [*US DOT*, 1999]

These ionospheric vertical delay corrections at standard IGPs are provided by WAAS messages. As well, a reliability indicator called grid ionospheric vertical error (GIVE) is also given to inform users about model uncertainty. Because WAAS is a safety-critical system and the ionosphere can be challenging to model, the users are warned about unreliable data using a set of GIVE flags. Using these standard vertical delay values, one could compute the ionospheric vertical delay at a location of interest using the surrounding IGP observations. This requires interpolation between grid points to derive the WAAS prediction for a given user location, which will be discussed later [*US DOT*, 1999].

2.10.4 WAAS Reliability and Integrity

WAAS provides IGP ionospheric vertical delay estimates along with associated reliability indices called the grid ionospheric vertical error (GIVE) values. This is a

measure of the error bound provided at each IGP. GIVE flags, ranging between 0 and 15, are broadcast with associated error and σ^2_{GIVE} values (both given in metres) obtained from a look up table (LUT). The WAAS service provides valid GIVE flags from 0 to 14 (equivalent to a maximum error of 45 m), but when the flag is 15 the service is denied because the ionosphere is not monitored. This 45 m maximum error is used as a threshold to account for reliability in the aviation sector. Therefore, basically a grid of vertical delays and a grid of vertical error bounds are broadcast, which make up the output of the WAAS ionospheric model. Another index is used to quantify reliability of ionospheric vertical delay. Namely, the user ionospheric vertical error (UIVE) bounds the residual (post-correction) pseudorange error and is attributable to the vertical ionospheric delay for a satellite with a probability of 99.9%. It is interpolated from the surrounding GIVEs as follows [*US DOT*, 1999]:

$$UIVE = \sum_{n=1}^{4} W_n \left(x_{pp}, y_{pp} \right) \cdot GIVE_n \tag{2.6}$$

where x_{pp} and y_{pp} are the coordinates of the user's IPP for a given satellite and W_n coefficients are the weight factors, which inversely weigh the distance between the IPP and IGP.

WAAS also publishes other reliability indicators on a regular basis, and these are the HPL and VPL estimates. These ensure that post-correction errors are bounded by error bounds (protection levels) as defined in RTCA/DO-229 Appendix J. Basically, HPL (which has NPA and PA modes) and VPL are computer from degradation factors and parameters

provided in WAAS message Types 7 and 10 [*RTCA*, 2001]. For details on how to compute these error bounds and information on the related equations, please refer to the RTCA document mentioned above.

An example of a published VPL map is given in Figure 2.18. The HPL is the radius of a circle in the horizontal plane (the plane tangent to the WGS-84 ellipsoid), with its center being at the true position, which describes the region that is assured to contain the indicated horizontal position. It is based upon the error estimates provided by WAAS. The VPL is half the length of a segment on the vertical axis (perpendicular to the horizontal plane of WGS-84 ellipsoid), with its center being at the true position, which describes the region that is assured to contain the indicated vertical position. It is based upon the error estimates provided by WAAS. Accordingly, WAAS guarantees that the user receiver will be within the error cylinder defined by the horizontal and vertical protection levels [*FAA*, 2005]. The positioning analyses to be discussed in later chapters will include crosschecks between the results found and the actual HPL/VPL values published by the FAA.

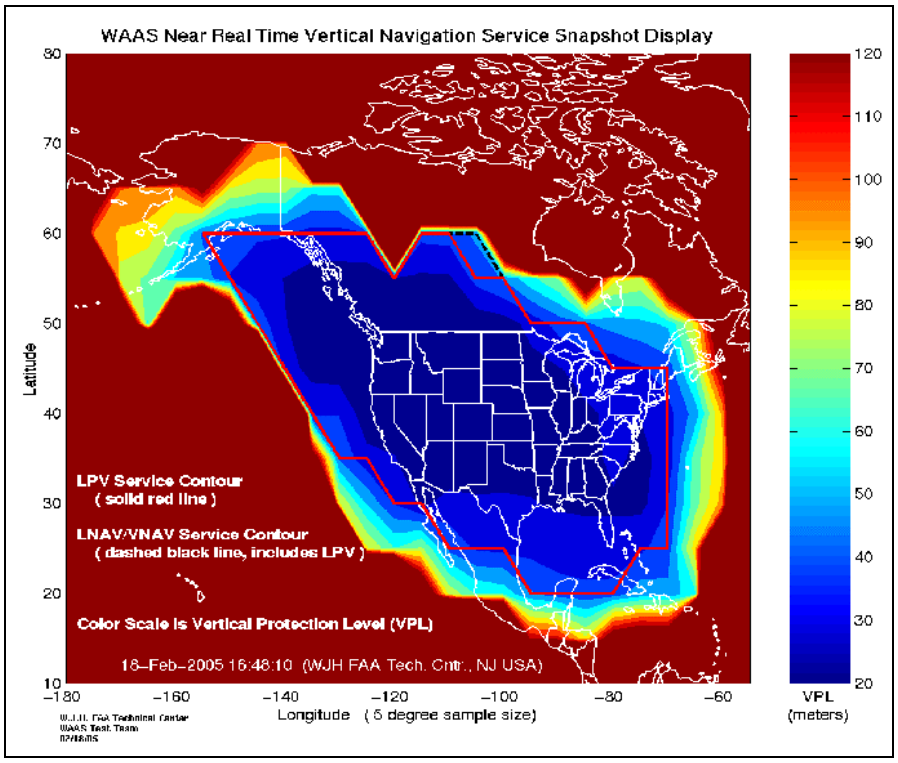

Figure 2.18: FAA Published VPL on February 18, 2005 [*FAA*, 2005]

Since WAAS is used for safety-critical applications, integrity is a very important element of the system. In real-time navigation systems, being informed of failures or being informed late are fatal flaws in system integrity. These issues were closely considered when developing the WAAS. As a result, it is able to offer a less than 10^{-7} probability rate that the true error will be larger than the confidence bound, and the time-to-alarm is assured to be 6 seconds or less. In terms of continuity, there is a less than 10^{-5} chance of aborting a procedure once it is initiated. These along with accuracy and availability specifications, discussed previously, satisfied the aviation requirements Phase I of PA navigation mode. There are also Phase II and III, which are related to airport landings using LAAS and GPS modernization gains. For Phase I, WAAS currently guarantees reliable positioning at less than 8 m in 3D but typical accuracy is 1-3 m [*Walter*, 2003].

2.11 Localization Scheme

A WAAS localization scheme is implemented here to assess the performance offered by the system at various locations in North America. The localization scheme has been tested using such raw data to verify WAAS positioning accuracy at different International GPS Service (IGS) and CORS stations.

The clock error correction requires no spatial localization. It is a scalar quantity specific to the satellite, and computing it simply involves using the appropriate clock coefficients from Equation 2.3. These are provided in the WAAS messages along with the relevant time tags. Therefore, there are two major parts to this localization scheme: 1) localization of orbital errors and 2) interpolation of ionospheric delay values for the user station. In the following subsections, techniques behind the development of the localization scheme will be discussed.

2.11.1 Localization of Orbital Error

The orbital error requires localization that is based purely on geometry and is also specific to a given satellite. Figure 2.19 shows the geometrical relationship between the *LOS*, the orbital correction vector (δ) and the corresponding pseudorange correction (PRC_{orbit}).

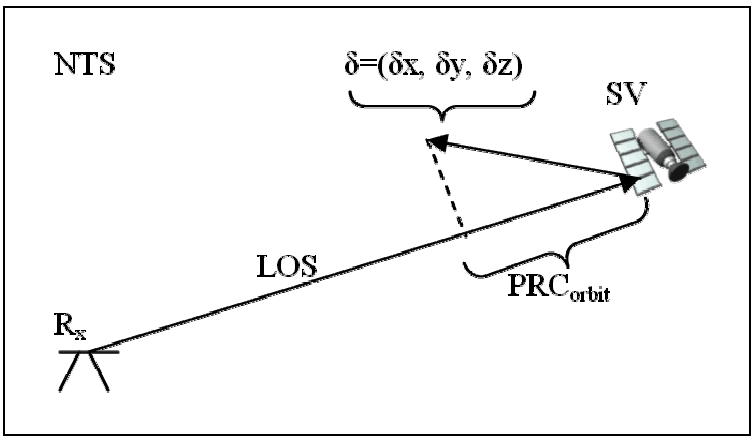

Figure 2.19: Geometry behind the Derivation of the Orbital Error [*Yousuf et al.*, 2005]

This is basically a scalar projection of δ onto *LOS*, which results in producing PRC_{orbit}. The mathematical expression representing this diagram is as follows:

$$PRC_{orbit} = \frac{\underset{\rho}{LOS} \cdot \underset{\rho}{\delta}}{\left|\underset{\rho}{LOS}\right|} \tag{2.7}$$

The right-hand-side of Equation 2.7 is the dot product between the unit vector along *LOS* and δ. This equates to a scalar quantity (in metres) representing the range error and must be subtracted as an error from the raw pseudorange (as per WAAS convention).

2.11.2 Localization of Ionospheric Error

Localizing the ionospheric correction involves slightly more computation than the other two error types. First of all, the WAAS broadcasts an evenly-spaced ionospheric grid

(nominally 5° spacing at latitudes below 55°) over the footprint of its GEOs (two currently in operation: POR and AOR-W). GEO coverage exists for most of the US and the southern parts of Canada, but the WAAS grid actually covers all latitudes across North America. FAA is currently working towards increasing the GEO coverage, as more of the GEO satellites will be launched in the near future. The users must then compute IPPs for each satellite in view and interpolate, from the WAAS grid, their respective ionospheric delay corrections at each IPP. As discussed earlier, this correction is given as vertical delay values at the standardized IGPs. Therefore, the interpolated value must be mapped to the slant path using a mapping function. Three- or four-point interpolation is suggested depending on the grid spacing and IGP band mask, and this interpolation method has been used here for all of the processed results for this research. Further details on the interpolation method and pierce point derivation could be found in *US DOT* [1999].

The full WAAS PRC corresponding to all three error components is, therefore, given by:

$$PRC_{WAAS} = PRC_{orbit} + \Delta t_{SV} \cdot c + PRC_{iono} \tag{2.8}$$

PRC_{WAAS} could now be added to a raw pseudorange value for a given satellite to obtain the differentially corrected pseudorange. All satellites in view will now have this refined observable, thus yielding a more accurate positioning estimate of the user's receiver [*US DOT*, 1999].

Chapter 3

WAAS Correction Assessment

The chapter will focus on WADGPS corrections that the WAAS broadcasts to its users to improve positioning accuracy. As discussed previously, there are three types of corrections: clock, orbit and ionosphere. All these corrections add up to a range quantity, and thus the raw pseudorange values for each satellite get corrected using these corrections. Processing these corrected observations produces the final WAAS positioning solution. Accordingly, the analysis to follow will be conducted in the correction domain. The study will include discussions on correction schemes, data sources and formats, validity checks using truth data, integrity checks, and actual case studies for the correction sets. The ionospheric correction will be studied with great detail,

since it causes the major accuracy problems in GPS positioning during ionspherically disturbed times.

3.1 Truth Data

This section will discuss the sources and methodology behind acquisition and generation of the truth data for the purposes of validating the WAAS ionospheric, clock and orbital corrections. The sources have two different origins: 1) precise clock and orbit products from the IGS website and 2) ionosphere model generated using data from about 400 dual-frequency GPS reference stations across North America. The analysis is conducted by comparing the truth data to different sets of results. This comparison entails having two parts: 1) truth data vs. broadcast data and 2) truth data vs. WAAS data.

3.1.1 Precise Clock and Orbit Data

The data are readily and freely available over the Internet (http://igscb.jpl.nasa.gov/) from IGS, and no restrictions are placed on using these data for research purposes. Both precise clock and orbit values are given in single file, which uses a format called "Standard Product 3" (SP3). A sample file is provided in Figure 3.1. These products are considered to be precise (less than 0.1 ns), since these are derived by post-processing the measurements made by the IGS network, which is distributed worldwide. The post-processing data are sometimes collected over a period of weeks. This extensive spatial

coverage combined with the vast temporal redundancy make the final products very accurate and precise. There are different levels of accuracy for these IGS precise products, depending on the post-processing time allowed after the fact [*JPL*, 2005]. There is a tradeoff between accuracy and latency. As such, IGS also offers rapid products that are available within a day. A list of the different products and levels of accuracy is given in Table 3.1.

Table 3.1: IGS Product List [*JPL*, 2005]

Product	Accuracy
Final GPS orbits, 11 days	5 cm
Final SV clocks	0.5 ns
Rapid GPS orbits, 22h	5 – 10 cm
Rapid SV clocks	0.5 – 1.0 ns
Predicted GPS orbits, 0h	50 – 100 cm
Predicted SV clocks, 0h	80 – 100 ns

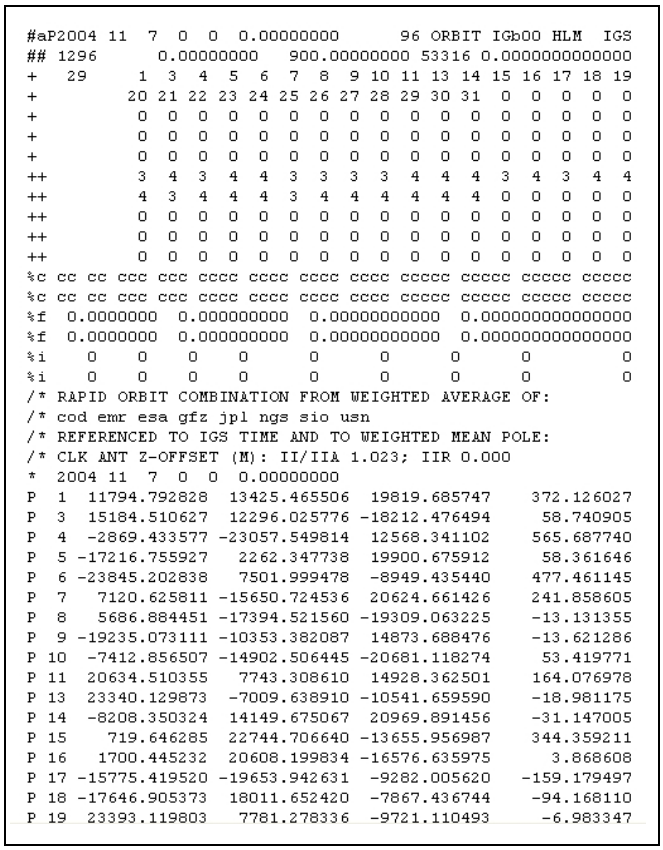

```
#aP2004 11  7  0  0  0.00000000      96 ORBIT IGb00 HLM  IGS
## 1296      0.00000000   900.00000000 53316 0.00000000000000
+   29     1  3  4  5  6  7  8  9 10 11 13 14 15 16 17 18 19
+         20 21 22 23 24 25 26 27 28 29 30 31  0  0  0  0  0
+          0  0  0  0  0  0  0  0  0  0  0  0  0  0  0  0  0
+          0  0  0  0  0  0  0  0  0  0  0  0  0  0  0  0  0
+          0  0  0  0  0  0  0  0  0  0  0  0  0  0  0  0  0
++         3  4  3  4  4  3  3  3  3  4  4  4  3  4  3  4  4
++         4  3  4  4  4  3  4  4  4  4  4  4  0  0  0  0  0
++         0  0  0  0  0  0  0  0  0  0  0  0  0  0  0  0  0
++         0  0  0  0  0  0  0  0  0  0  0  0  0  0  0  0  0
++         0  0  0  0  0  0  0  0  0  0  0  0  0  0  0  0  0
%c cc cc ccc ccc cccc cccc cccc cccc cccc cccc cccc cccc cccc
%c cc cc ccc ccc cccc cccc cccc cccc cccc cccc cccc cccc cccc
%f  0.0000000  0.000000000  0.00000000000  0.000000000000000
%f  0.0000000  0.000000000  0.00000000000  0.000000000000000
%i    0    0    0    0      0      0      0      0         0
%i    0    0    0    0      0      0      0      0         0
/* RAPID ORBIT COMBINATION FROM WEIGHTED AVERAGE OF:
/* cod emr esa gfz jpl ngs sio usn
/* REFERENCED TO IGS TIME AND TO WEIGHTED MEAN POLE:
/* CLK ANT Z-OFFSET (M): II/IIA 1.023; IIR 0.000
*  2004 11  7  0  0  0.00000000
P  1  11794.792828  13425.465506  19819.685747    372.126027
P  3  15184.510627  12296.025776 -18212.476494     58.740905
P  4  -2869.433577 -23057.549814  12568.341102    565.687740
P  5 -17216.755927   2262.347738  19900.675912     58.361646
P  6 -23845.202838   7501.999478  -8949.435440    477.461145
P  7   7120.625811 -15650.724536  20624.661426    241.858605
P  8   5686.884451 -17394.521560 -19309.063225    -13.131355
P  9 -19235.073111 -10353.382087  14873.688476    -13.621286
P 10  -7412.856507 -14902.506445 -20681.118274     53.419771
P 11  20634.510355   7743.308610  14928.362501    164.076978
P 13  23340.129873  -7009.638910 -10541.659590    -18.981175
P 14  -8208.350324  14149.675067  20969.891456    -31.147005
P 15    719.646285  22744.706640 -13655.956987    344.359211
P 16   1700.445232  20608.199834 -16576.635975      3.868608
P 17 -15775.419520 -19653.942631  -9282.005620   -159.179497
P 18 -17646.905373  18011.652420  -7867.436744    -94.168110
P 19  23393.119803   7781.278336  -9721.110493     -6.983347
```

Figure 3.1: Example of an SP3 File

After the header information, data records are given in time sequence. Each record provides a time tag with associated orbit and clock information for a given set of satellite PRN numbers. The true orbits are given as x, y and z coordinates (in km) in the Earth Centered Earth Fixed (ECEF) frame, while the true satellite clock error is given as a quantity of time (in μs) [*JPL*, 2005]. For this study, the selection of the time period is not critical to the analysis. Therefore, no specific criterion was used to select the truth dataset over time; consecutive days of SP3 (truth) data were chosen to conduct a temporal analysis.

3.1.2 Ionospheric Data Derived from Truth Observation

The “truth” observations from a network of stations would closely represent actual ionospheric phenomena. Therefore, the ionospheric truth data were obtained from dual frequency observations made at about 400 reference stations across North America taken from the CORS Network, as show in Figure 3.2 [*Coster et al.*, 2003]. Massachusetts Institute of Technology (MIT) Haystack Observatory provided these absolute slant TEC observations.

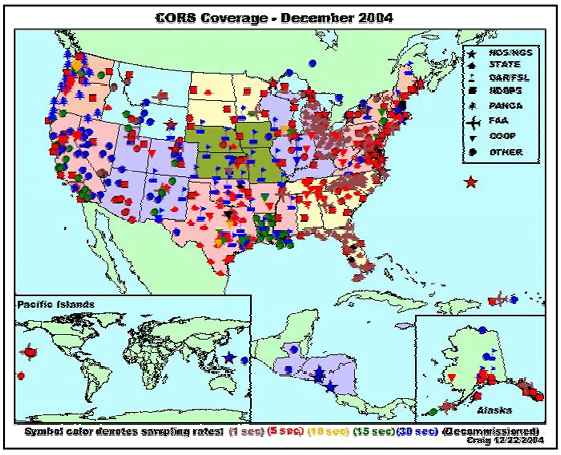

Figure 3.2: The CORS Network [*CORS*, 2005]

To generate the truth estimates, this network of densely spaced stations is used. All satellites in view from each station intersect the ionosphere at IPPs (recall the IPP discussion from Subsection 2.2.3). Each IPP provides a dual-frequency measurement for the station receiver, but these include inter-frequency (L1/L2) receiver and satellite biases. The receiver biases are caused by hardware differences in the GPS receiver that processes the L1 and L2 signals differently, thus yielding an offset in the measurement domain. The satellite biases, on the other hand, arise mainly as a result of the electronics and antenna

on the satellites, which also result in a final measurement offset [*McCaskill et al.*, 2003]. Therefore, it is essential that biases are estimated and removed from the raw observations.

The receiver biases are estimated as part of ionosphere model parameters and are removed from the observations. The satellite biases, on the other hand, are removed using published bias values from JPL [*JPL*, 2005]. An example of a model equation is given by Equation 3.1, showing the use of a second order polynomial to model the spatial data, estimation of the biases (if satellite biases are available, then b_s would be subtracted from the right-hand-side of the equation), and mapping of the slant observations to the vertical. Solving for this type of parametric equation finally produces systematic error-free values, which can be considered as the truth data. These processed results come in files specific to the given reference station. These files contain slant TEC values with corresponding time and PRN tags and other relevant information. As such, the data could be manipulated as needed for comparison with the counterpart data sets [*Coster et al.*, 2003].

$$STEC_{rs}(t_i) = M(E)\{a_0 + a_1(\Delta\phi) + a_2(\Delta\lambda) + a_3(\Delta\phi)^2 + a_4(\Delta\lambda)^2 + a_5(\Delta\phi)(\Delta\lambda)\} + b_s + b_r \quad (3.1)$$

where:

$STEC_{rs}(t_i)$ is the slant *TEC* measurement (for receiver r and satellite s) at time t_i,

$M(E)$ is a mapping function dependent on elevation angle,

$a_0 \ldots a_6$ are unknown coefficients of the model,

the constants b_s and b_r are the satellite and receiver inter-channel biases,

$\Delta\phi$ is difference in latitude between the *IPP* and the model expansion point, and $\Delta\lambda$ is difference in longitude [*Skone*, 2002].

Note: Although this local model was implemented and it produced valid results, this is just an example of how biases can be estimated and was not used to actually derive the biases for processing. Instead, the biases were removed using the values provided by external third parties who estimated the biases conducting a Least-Squares batch solution, as discussed above.

3.2 Broadcast Values

3.2.1 Broadcast Clock

The broadcast satellite clock error is modelled using a time-dependent polynomial. The coefficients of this polynomial are transmitted as part of the satellite navigation message. The computed correlation at time *t* (in seconds) is given by:

$$dt(t) = a_{f0} + a_{f1}\left(t - t_{OC}\right) + a_{f2}\left(t - t_{OC}\right)^2 \tag{3.2}$$

where, $dt(t)$ is the total clock correction at time t. The a_{f0}, a_{f1} and a_{f2} terms are the zero, first and second order clock coefficients, respectively, and t_{OC} is the time of clock

data. Note that in Equation 3.2, the total clock correction value is given in seconds. Therefore, it must be multiplied by the speed of light to obtain the actual range correction in metres.

The coefficients are transmitted as part of the satellite navigation message and are predicted ahead of time. The full range correction obtained from this input data is generally less than 1 ms (300,000 m). It is interesting to note that the observed satellite clock error would be the same for all receivers tracking the same satellites at the same time, and thus can be eliminated by single differencing between receivers [*Misra and Enge*, 2001].

3.2.2 Broadcast Orbit

Similar to clock correction coefficients, the orbital information is provided using a set of parameters that are transmitted as part of the satellite navigation message. Table 3.2 shows a sample ephemeris record containing all the parameters required to compute the satellite coordinates and clock error at a given time. The orbital parameters are input into a set of equations of motion to be solved for the x, y and z coordinates of the satellite (in metres) in the ECEF frame.

Table 3.2: Sample Ephemeris Record [*Lachapelle*, 2003]

Crc (m)	Cos correction to orbital radius	375.843800
Cis (radians)	Sin correction to inclination	-4.097819E-08
Crs (m)	Sin correction to orbital radius	-67.031250
Cuc (radians)	Cos correction to argument of latitude	-3.594905E-06
Cus (radians)	Sin correction to argument of latitude	4.256144E-06
Ω_o (semicircles)	Right ascension at reference time	0.5106722954660654
ω (semicircles)	Argument of perigee	0.7921434477902949
I_o (semicircles)	Inclination at reference time	0.3572512124665082
$\dot{\Omega}$ (rad/s)	Rate of right ascension	-2.092747E-09
$\dot{i}$ (semicircles/s)	Rate of inclination	-6.03677E-11
PRN	Pseudorandom Noise Code	3
GPS Week	Number of GPS week	659
TGD (s)	Total group delay	-4.190952 E-09
IODC	Issue of clock data	48
toc (s)	Time of clock data	262800
af_2 (s/s**2)	Satellite clock coefficient	0.000000
af_1 (s/s)	Satellite clock coefficient	-5.559286E-11
af_0 (s)	Satellite clock coefficient	-5.935552E-04
IODE	Issue of ephemeris data	48
Δn (semicircles/s)	Correction to mean motion	4.358753E-10
M_0 (semicircles)	M_0 at reference time (toe)	0.3418521881103516
e	Orbital eccentricity	0.01301583321765065
$\sqrt{a}(\sqrt{m})$	Square root of semimajor axis	5153.67645835876500
toe (s)	Time of ephemeris	262800
Cic (radians)	Cos correction to inclination	2.030283E-07

3.2.3 Broadcast Ionosphere

It is a known fact that ionospheric activity varies diurnally and has a sinusoidal trend at the lowest frequency term. The diurnal maximum occurs at around 14:00 hours local time. This is why the broadcast ionospheric model was based on the Klobuchar model, which is basically a half-cosine function given by Equation 3.3 [*Klobuchar et al.*, 1995].

$$\tau = DC - A\cos\left(\frac{2\pi(t-\phi)}{P}\right) \tag{3.3}$$

where τ is ionospheric vertical delay (in metres), *DC* is a constant night-time offset (5 ns), *A* is amplitude (in metres) of the sinusoid, ϕ is a constant phase offset (14:00 hours), t (in seconds) is local time, and finally *P* is period. [*Lachapelle*, 2003].

The time-varying coefficients on the right-hand-side of this equation are broadcast in the GPS navigation message. Therefore, ionospheric vertical delay (τ) varies diurnally according to this sinusoid function, which models the ionospheric activity. Figure 3.3 shows an example of this trend seen over a station in North America. From this figure, it could be said that the sinusoid function is not modelling the ionosphere adequately in this intense ionospheric time, as significant local irregularities in the ionosphere are observed. Thus, predicting functions will fall short of resolving spatial features present during these phenomena because a low-order smooth model will never capture the higher order effects. This is especially true for a simple cosine function used in the Klobuchar model, as will be shown in later chapters [*Enge and Van Dierendonck*, 1996].

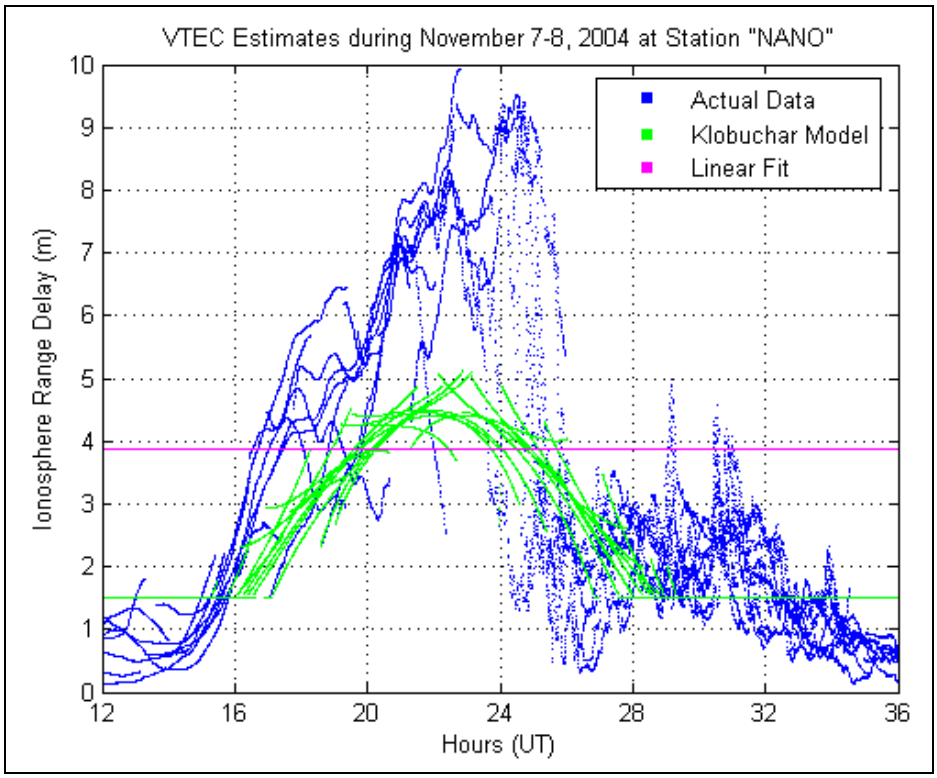

Figure 3.3: Example of Diurnal Ionospheric Variation

3.3 WAAS Correction Accuracy

This section will focus on WAAS assessment conducted in the correction domain. To recap, WAAS correction accuracies were compared to the broadcast ones by subtracting both from a set of truth data. These truth data were based on precise products obtained from IGS. There were three types of corrections per data source: clock, orbit and ionosphere. Since clock and orbital corrections are extracted in a similar manner, these results will be studied concurrently. Whereas the ionospheric corrections were derived separately from an alternate source (dual-frequency observation data from about 400

reference stations provided by MIT Haystack Observatory), thus this analysis will be done independently using data from a variety of ionospheric conditions, including ionospherically disturbed periods.

3.3.1 Methodology Behind the Retrieval of WAAS Corrections

In order to possess the ability to conduct WAAS positioning anywhere in North America, 250-bit raw WAAS frames, that contain all the necessary corrections, for the period of interest had to be obtained. Thus, these data were procured directly from FAA archives. This dataset included the relevant messages pertaining to WAAS clock, orbital and ionospheric error. Thereafter, the 250-bit binary data frames had to be decoded for proper use. The outputs of the decoder were typical and manageable WAAS messages separated into the standard WAAS message types (e.g. Type1, Type2, etc.).

At this point, correction information had an ASCII format, and thus was easily readable by people and software routines. These routines involved retrieving the proper correction information and then passing on to the localization program (see Section 2.11 to review algorithmic details). The clock corrections required no localization but orbital and ionospheric ones did. Orbital localization consisted of a projection on to a vector, and the ionospheric one involved a bi-linear interpolation using the surrounding three or four data points across a spatial grid. Obviously, for each satellite in view the primary inputs to the localization scheme were the coordinates of the “user” location and of the satellite in question, which determined the magnitude of the interpolated correction value.

The above steps ultimately produced the WAAS corrections required for the study, and the other part of the analysis consisted of the corresponding datasets for precise and broadcast corrections, so that WAAS vs. truth and broadcast vs. truth comparisons can be conducted. Once the datasets overlapped, it was a matter of time and PRN matching to find the two sets of accuracies. To recall how truth and broadcast data were acquired and processed, revisit the previous sections of this chapter. The clock and orbital errors don't have any particular significance when it comes to the "user" location. The ionosphere, on the other hand, offers a great deal of insight into its physical process depending on the "user" location, especially if the location is right beneath SEDs. As such, for the ionospheric correction analysis, this criterion was used to make the selections of the sites to be studied. A flowchart summarizing this methodology is given in Figure 3.4.

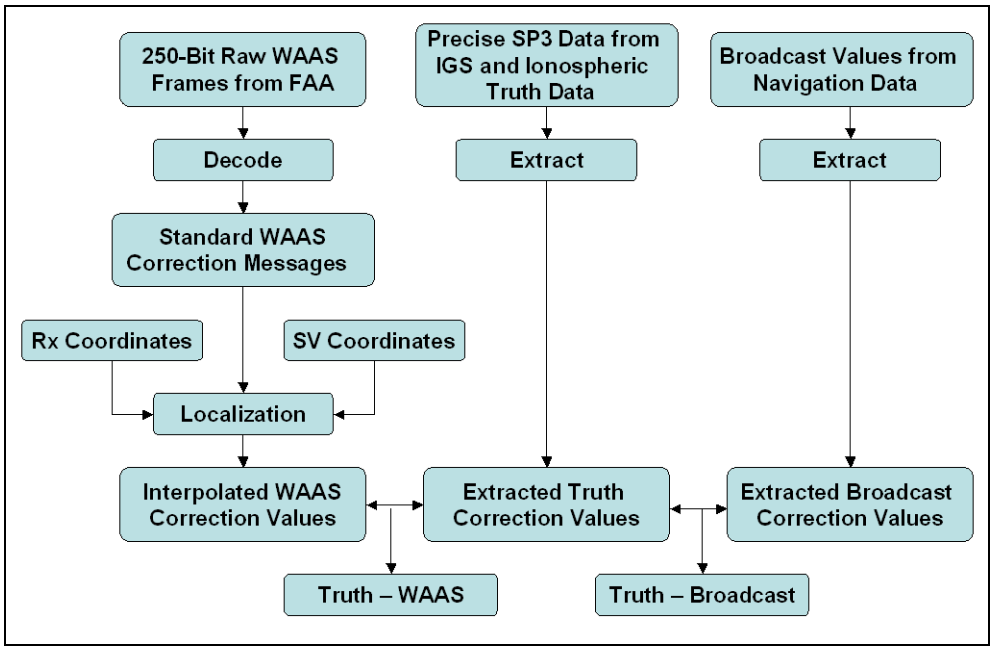

Figure 3.4: Flowchart of Methodology to Derive WADGPS Corrections

3.3.2 Clock and Orbital Accuracy Results

These corrections are usually broadcast together in a single message. The exception to this is WAAS clock, which is given in two different messages: one component is long term (slow) and the other component is fast. On the other hand, clock and orbital corrections of type broadcast and precise are extracted from their respective single data records, as discussed earlier in this chapter.

This analysis will entail looking at the big picture then narrowing down to specific elements of interest. As such, the first thing to observe is the overall time series for the whole study period. Figure 3.5 shows the clock errors (in metres) for broadcast and WAAS during November 7-10, 2004. Similarly, Figure 3.6 shows the three-dimension (3D) orbital error (in metres) for the same period. These were computed using the methods discussed in Subsection 2.11.1. Although this is an ionospheric storm event, in terms of clock and orbital errors it could be considered as typical condition, as ionospheric activity does not affect those errors.

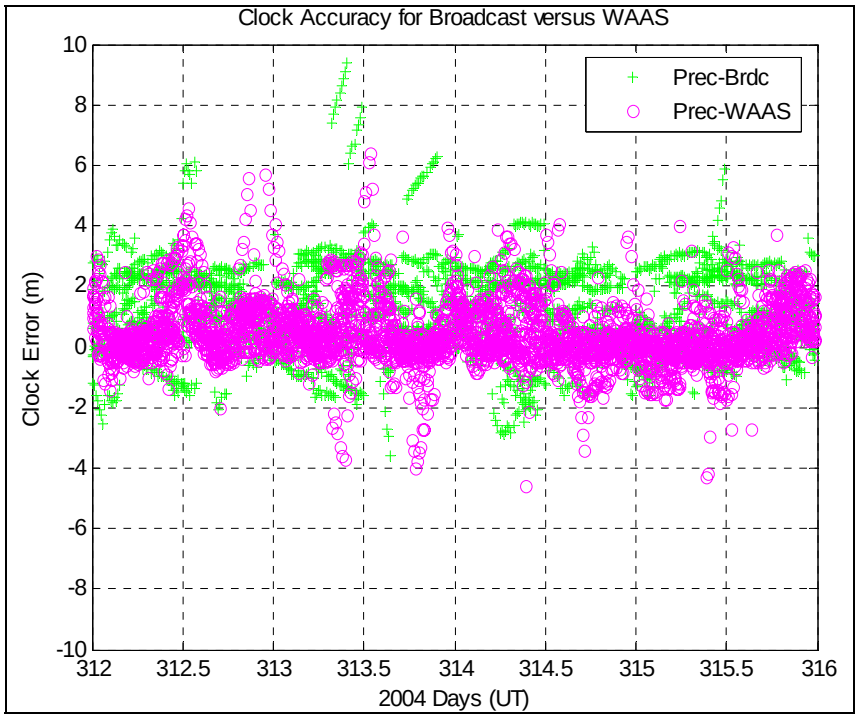

Figure 3.5: Clock Accuracy for Broadcast versus WAAS

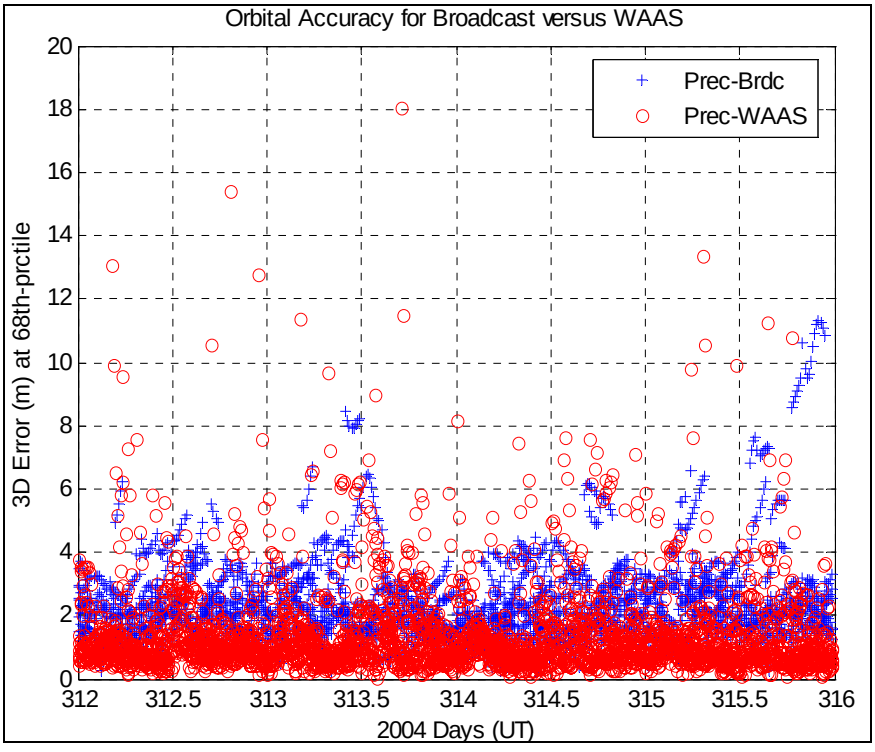

Figure 3.6: Orbital Accuracy for Broadcast versus WAAS

As can be seen from these plots, WAAS is definitely more accurate than broadcast for both clock and orbital cases, in general. However, WAAS has some extreme values (up to 10 m for clock and up to 18 m for orbit) that are of concern. The statistics representing the above datasets are summarized in Table 3.3, where again the maxima and minima appear to be unusual. These instances of large range errors were compared to the corresponding positioning solutions. It was observed that positioning errors for those epochs having satellites with outliers were degraded to 5 m as compared to 2 m for typical WAAS positioning. Therefore, these large inaccuracies were genuinely a product of the WAAS network.

Table 3.3: Clock and Orbital Accuracies for Broadcast versus WAAS

		7-Nov-04		8-Nov-04		9-Nov-04		10-Nov-04	
		BRDC	WAAS	BRDC	WAAS	BRDC	WAAS	BRDC	WAAS
Clock (m)	STD	0.72	0.69	0.85	0.47	0.46	0.40	0.53	0.27
	RMS	1.83	1.26	2.22	1.24	1.75	1.06	1.67	1.00
	MAX	6.12	5.72	9.37	6.42	4.14	4.07	5.87	3.98
	MIN	-2.53	-2.00	-3.60	-4.01	-2.88	-4.60	-1.63	-4.28
Orbit (m)	MEAN	2.16	1.44	2.18	1.47	2.17	1.33	2.56	1.32
	RMS	2.34	2.03	2.48	2.07	2.40	1.80	3.03	1.98
	MAX	6.20	15.54	8.42	18.06	6.18	8.13	11.31	18.47
	MIN	0.27	0.13	0.20	0.03	0.22	0.10	0.29	0.09

It was found that if the age of the corrections is significantly large (several minutes) and if the satellite just came into view of the WAAS network, which would only affect the orbit prediction, large outliers would exist in the results. In contrast, precise orbits have

the advantage of a global IGS network that does not lose sight of the satellites. Nonetheless, the provided user differential range error (UDRE), which indicates the 99.9% combined fast and slow clock/orbital error for the corrections, should bound the combined clock and orbital error [*Cormier*, 2005]. According to these justifications, the mentioned issues were verified; it was found that the age of correction for the outlying cases were up to seven minutes, even for the satellites in view; some of the affected satellites were newly visible by the WAAS network and the corresponding UDREs were up to 50 m for those cases. Therefore, these outliers are justifiable in terms of circumstantial occurrences caused by system limitations. A couple of final comments to be made about the above plots are 1) the fact that no timely trend could be identified, because clock and orbital errors have no time drifts, and 2) there exists a bias in the clock correction accuracy (more significant for the broadcast), which is also seen in other studies done on the topic [*Misra and Enge*, 2001]. Although, the origin of the biases were not explicitly discussed in those studies.

The second part of this analysis will focus on observing the range errors for individual satellites. Specific PRNs were chosen to study both the clock and orbital errors. Shown in Figures 3.7 and 3.8 are the clock and orbital errors for the given satellites on November 7, 2004. Note that the time interval between two successive data points is 15 minutes because the precise data were available at that rate. These plots show exact clock and orbital behaviors over time for the given satellites. As seen in the overall plot and statistics, the broadcast clock error has a positive bias and the WAAS clock error is usually non-biased. Although there are occasions, as in the case of PRN 23 in Figure 3.7,

where WAAS clock error is significant (up to 5 m) and larger than the broadcast clock error.

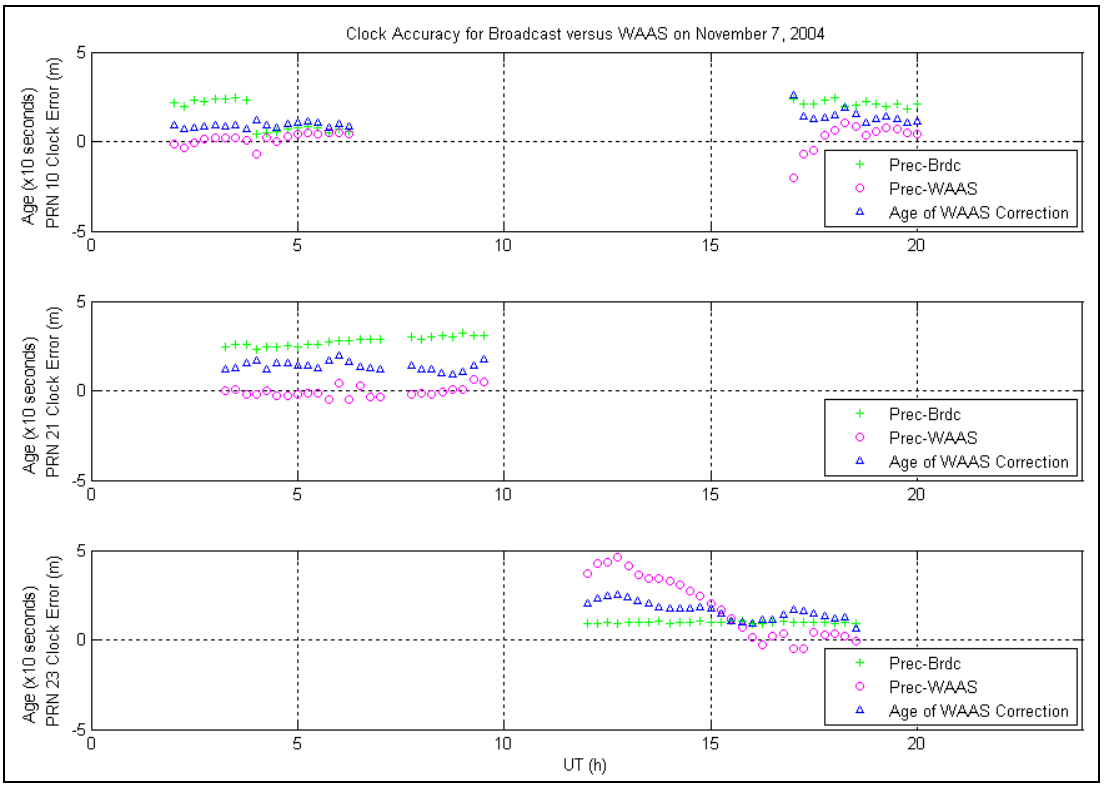

Figure 3.7: Clock Accuracy for Broadcast versus WAAS on November 7, 2004

For the orbital case, WAAS values are generally better except for outliers (seen in PRNs 19 and 22 in Figure 3.8), as discussed above. For the most part, both sets of data have a parallel error pattern but are vertically offset by some value. In some cases, the two sets are almost coincident; for instance, the broadcast errors in PRN 28 are very close to the ones for WAAS. The ionosphere on that day was moderately active, but this should not affect the orbital corrections. The biases are likely caused by calibration differences between the source networks.

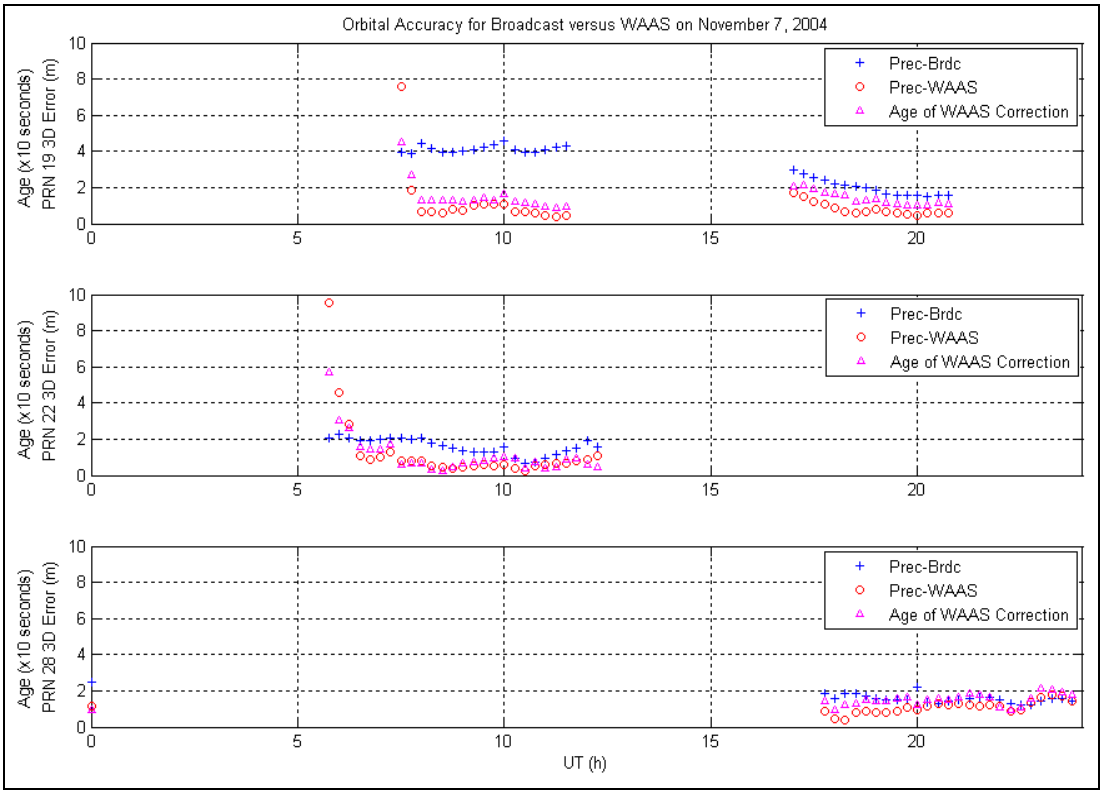

Figure 3.8: Orbital Accuracy for Broadcast versus WAAS on November 7, 2004

In addition to accuracy, reliability is an important aspect of a correction set. As such, it was necessary to verify if in fact WAAS corrections are bounded reliably, for a given period of time. For this purpose, the November 7-10 2004 dataset was taken once again to observe the WAAS UDRE estimates for the whole period for each satellite. This validation simply involved taking the difference between UDRE and the corresponding WAAS error, as shown in Figure 3.9. As can be seen, the difference values in this plot are all positive, which indicates that for this time period the errors in WAAS corrections were bounded by UDRE at all times. In many instances, extremely large values (100 – 150 m) were observed; it was seen that these usually indicate that satellites have just

come into view of the WAAS network. Although, it could be said that WAAS is somewhat conservative in predicting the UDRE, as the difference values have a minimum buffer of 15 m and in some cases exceed 200 m.

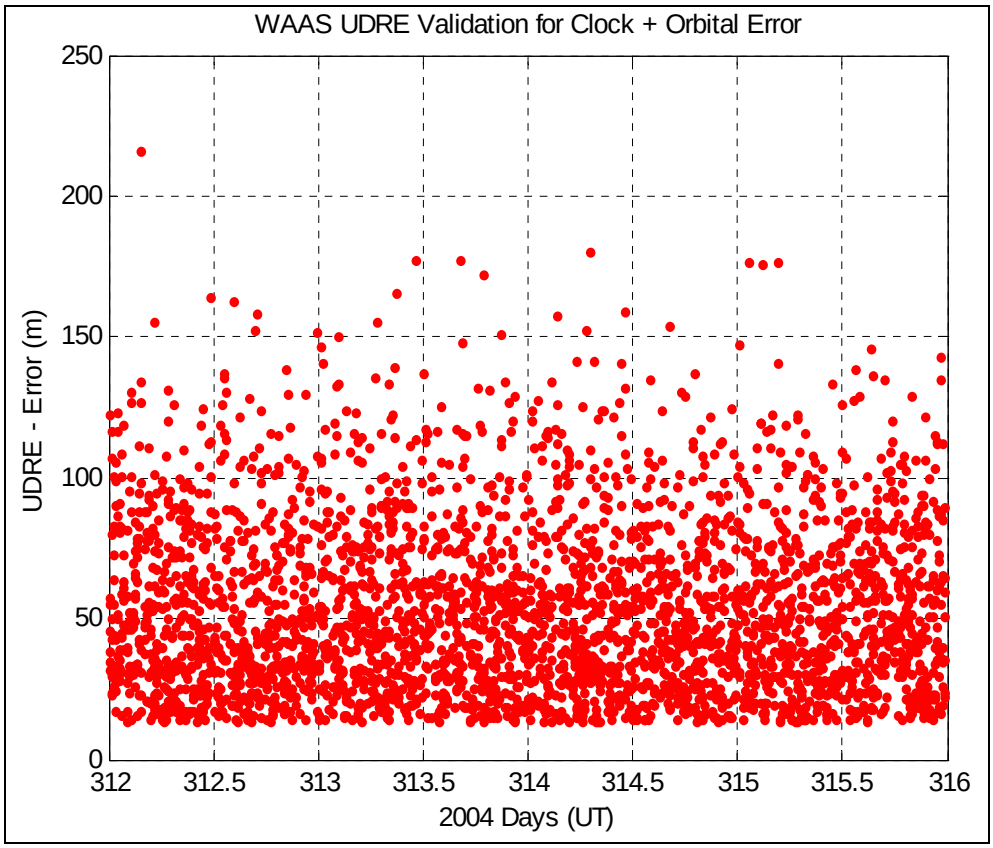

Figure 3.9: WAAS UDRE Validation for Clock/Orbital Error

One last aspect of interest in the study of clock/orbital correction is correlation between accuracy and age of correction. Therefore, WAAS clock/orbital corrections for a given day (November 9, 2004) were chosen, differenced from the truth, and plotted versus the correction age in seconds. Figure 3.10 presents the results from this study. There is a definite correlation between the two elements of interest. As the age of the corrections becomes larger; thus, a direct relationship in the temporal domain exists for the two

quantities. This makes sense because older corrections are less valid at present time than the more recent ones.

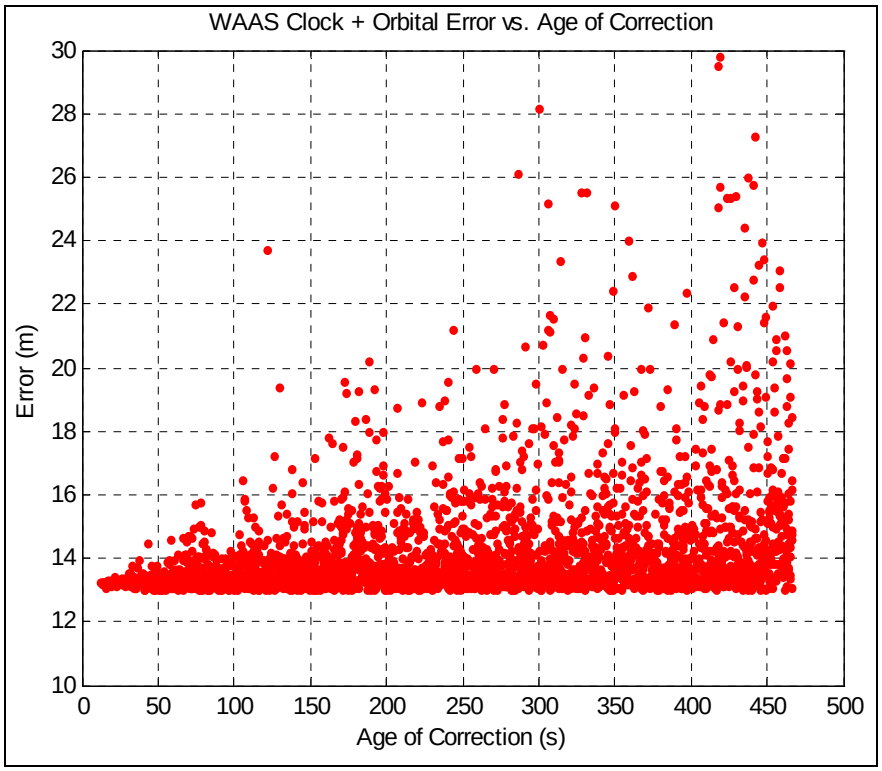

Figure 3.10: WAAS Clock/Orbital Error versus Age of Correction

3.3.3 Ionospheric Accuracy Results

The true model of the ionosphere providing the truth data has been generated from a network about 400 reference stations across North America (station locations shown in Figure 3.11). The full dataset used to accomplish this task was obtained from MIT Haystack Observatory. Dual-frequency observations are made by each reference station to accurately determine the ionospheric delay (slant TEC) to each satellite in view. Thereafter, the slant observations are mapped to the vertical using a mapping function

(refer to Section 2.2) to derive the VTEC values, which are then processed further to smooth the observations using carrier phase data. Note that the smoothing of the data was done by the data provider before these were delivered. The receiver and satellite biases were also removed. Finally, the smooth non-bias VTEC can be considered to be the ionospheric truth data. There were approximately 612 observations made within the network per epoch at a sample rate of 90 sec.

The date selection for this study was crucial for the analysis, as the goal is to verify how the WAAS model performs under various ionospheric conditions. Therefore, specific ionospheric storm events were chosen to conduct the evaluation. Namely, the October 29-31, 2003, November 20, 2003 and November 7-10, 2004 events were chosen, where significant disturbances were observed towards the afternoon (local time). As a result, the effects of an ionosphere that is quiet versus disturbed could be studied by observing the diurnal dependence, as well as ability of the WAAS to handle this transition.

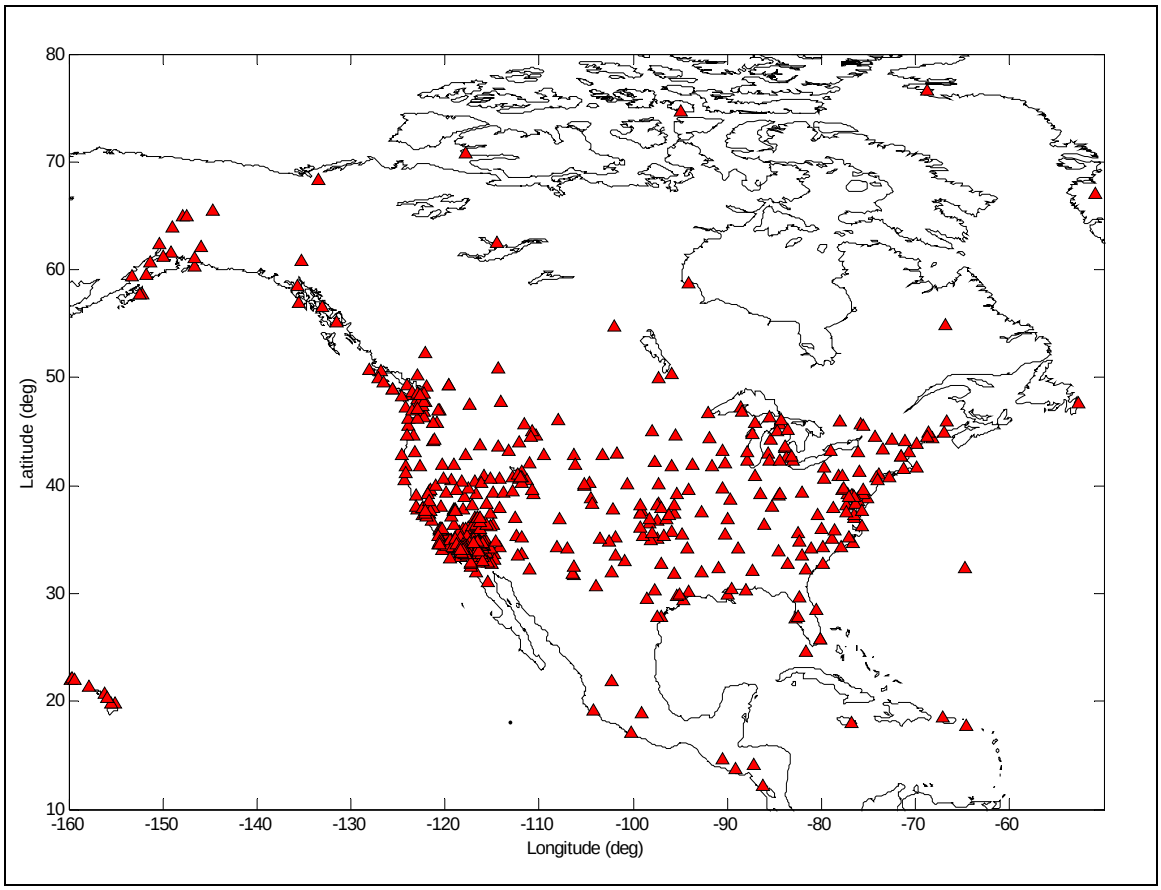

Figure 3.11: Map of Reference Stations used to Generate Ionospheric Truth Data

October 29-31, 2003 Storm

One of the highest intensity storms of the past 15 years occurred in late October 2003. A major solar flare developed at approximately 1100 UT on October 28. A severe geomagnetic storm commenced in the Earth's environment at 0600 UT on October 29. Activity continued for several days, with further coronal mass ejections at approximately 2100 UT October 29 and 1600 UT October 30.

The level of global ionospheric activity during this event is quantified using the conventional space weather index Kp. This index is based on observations of magnetic

field fluctuations at ground-based magnetometer stations (periods of enhanced ionospheric activity being characterized by strong electric currents which are observed as magnetic field perturbations at the Earth's surface). This is a valid method of monitoring ionospheric activity because strong electric currents signify high electron content, which drives the ionospheric activity. The planetary Kp index is derived from measurements of magnetic field variations at thirteen global stations at (approximately) equally spaced longitudes. This index is derived at three-hourly intervals and values range from 0 (quiet) to 9 (extreme). Such indices provide an approximate measure of global ionospheric activity at higher latitudes.

Figure 3.12 shows the Kp index for the full storm period. Kp values of 9 were observed on October 29 and 30. Figure 3.13 shows the TEC time series for the same period at the user station "AMC2" (latitude: 38.8031° and longitude: -104.5246°). As can be seen, the Kp value peaks line up with TEC peaks, which suggests enhancement of ionospheric TEC during the storm periods, and this indicates severe storm events for extended periods on both days. Typical diurnal behaviour caused by the ionosphere is could be seen through the minor peaks in Figure 3.13, where at around mid-day the TEC values peak to about 5 m. Communications were disrupted for commercial aircraft operating in polar regions, and satellite instruments were shut down to mitigate the impact of enhanced radiation in the space environment. Aurora were observed at mid-latitudes – in both Europe and the United States. Development of strong SED was observed in North America.

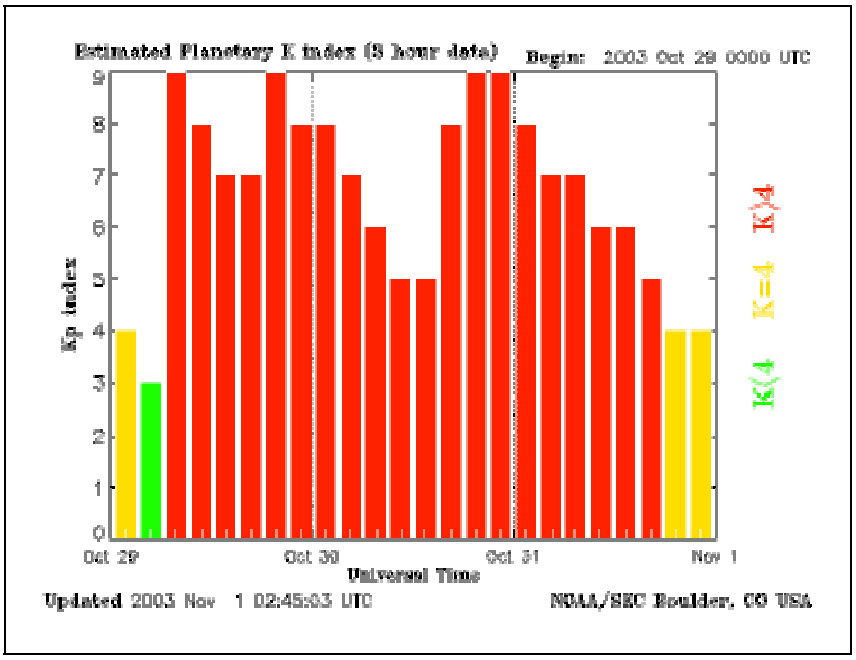

Figure 3.12: Kp Values for October 29-31, 2003 (NOAA SEC)

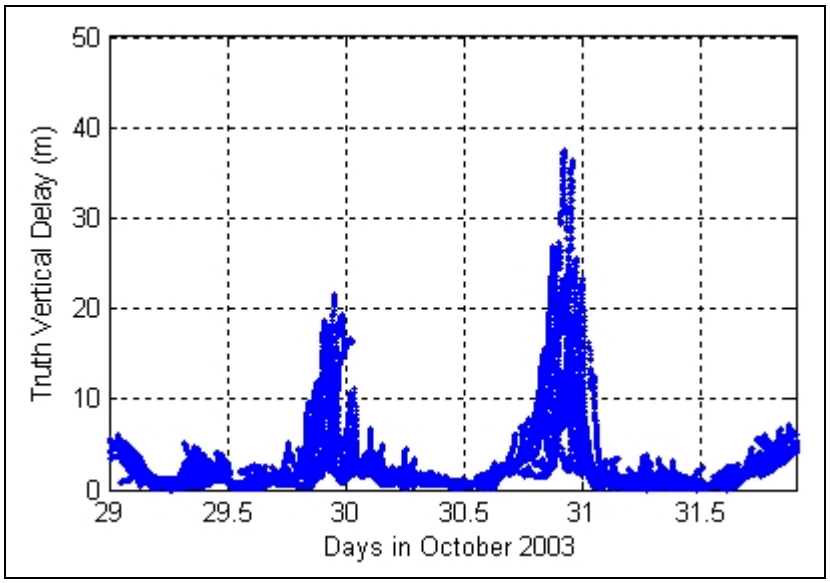

Figure 3.13: Time Series Plot of VTEC Truth during October 29-31, 2003 at User Station "AMC2"

The gradients associated with SED were extremely large during this event. The spatial distribution of SED over North America is shown in Figure 3.14a for October 29, 2003, which is also representing the truth data for the given time period. Figure 3.14b is providing the vertical delay values (in metres, converted using Equation 2.1) corresponding to the WAAS ionosphere corrections during the same time.

Spatial maps were created to conduct the analysis over North America. These maps spatially represent the vertical delay distribution for a given time period. These are derived by taking all the spatial data points for a half-hour batch solution and binning them into a 2.5° x 2.5° grid-cell; thus, the final cell value for the batch solution is plotted over the corresponding area. The spatial map in Figure 3.14c shows the difference in VTEC between the two previous figures; the difference map is simply the subtracted (WAAS – Truth) image of the two. Figure 3.14d provides the WAAS estimated error bound for that time frame through its spatially distributed GIVE values. This specific half-hour interval was chosen for analysis because on October 29 TEC values peak near the end of the day, and so an interval had to be selected that optimally depicted the ionospheric intensity during that time.

As can be seen from the truth map, SED is moving across North America. The spatial series plots in Appendix A shows the SED behaviour. The duration of this phenomenon was about three hours and caused severe degradation in positioning accuracy and reliability, as will be shown in later sections. From the WAAS map, it is clear that WAAS under-estimates TEC values in southern US; this is where the SED effects

(featuring steep TEC gradients, fast temporal development, large TEC plume heading north) are the most pronounced. As a result, the steep TEC gradients cutting across northwestern US into southwestern Canada are almost not present in the WAAS estimates, and significant smoothing effect has taken place. This deficiency is best noticeable in the VTEC difference (WAAS – truth) map. Thus, subtracting the truth image from WAAS would yield the remaining errors. Clearly, the larger errors (up to 25 m) are located where the SED is most prominent, and these errors are mostly negative, which again suggests the under-estimation done by the WAAS. Nonetheless, the difference map is in general non-biased overall for this event. Accordingly, WAAS fails to fully characterize the ionospheric event pictured in the figures below. The WAAS with its coarse spatial resolution tends to smooth out the high frequency trends in the data. Thus, the large valued peaks are modelled by low frequency estimates. This lower bound approximation ultimately sums up to produce the under-estimation effect.

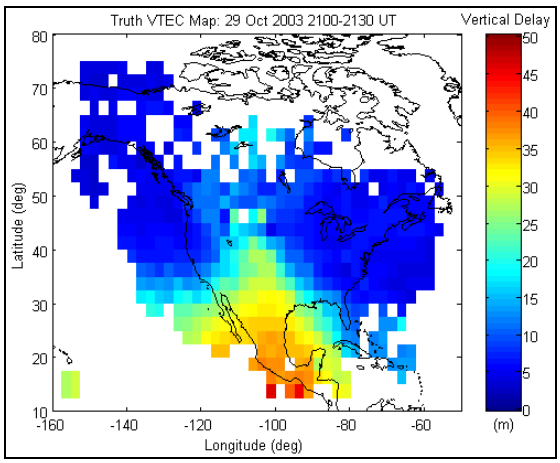

Figure 3.14a: Truth VTEC Map (2100-2130 UT, October 29, 2003)

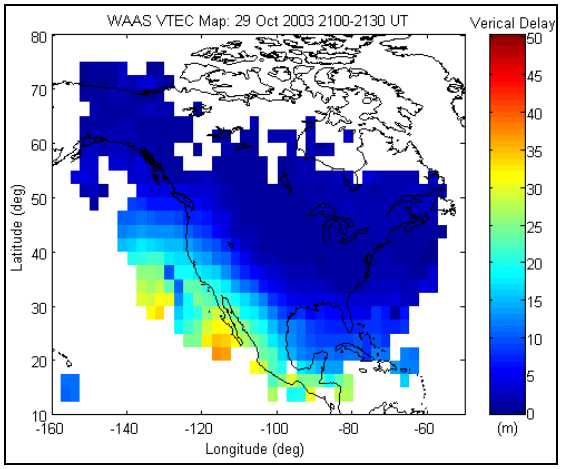

Figure 3.14b: WAAS VTEC Map (2100-2130 UT, October 29, 2003)

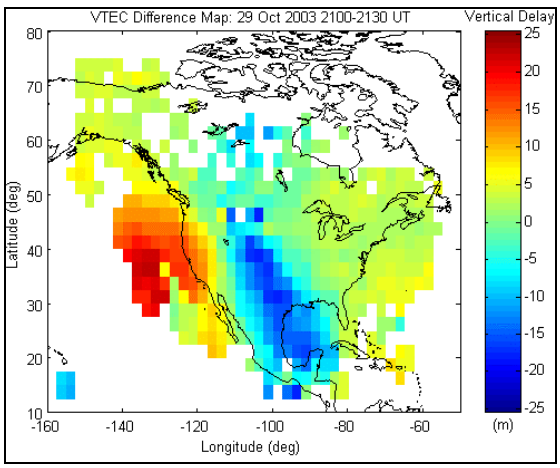

Figure 3.14c: VTEC Difference Map (2100-2130 UT, October 29, 2003)

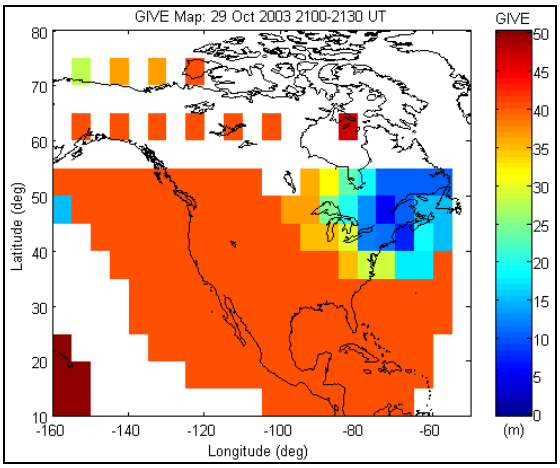

Figure 3.14d: WAAS GIVE Map (2100 UT, October 29, 2003)

As can be noticed from Figure 3.14d (compared with Figure 3.14c), WAAS errors were bounded by the GIVE values because these are larger than absolute error values. The GIVE map also establishes the fact that for most parts of North America, WAAS service was denied for the period above, as GIVE values exceeded the safe threshold of 45 m (which is the case in Figure 3.15d but not in 3.14d). An important point to be noted is that the denial of service only concerns vertical guidance (i.e. aircraft navigation); for WAAS users dealing in the horizontal and using non-safety-critical applications, the service was valid. When WAAS ionospheric model become this unreliable, the positioning solution is then computed using the broadcast model. Thus, WAAS-capable GPS receivers would be able to provide positioning estimates.

SED effects were also observed on October 30 and were very similar to the occurrences of October 29. Full development of the event on the 30th is also shown as spatial series plots in Appendix A. Development of SED persisted during the period 1900-2300 UT.

However, the effects were more significant as compared to the previous day, as shown by Figures 3.15a-d. Unlike in the earlier case, the TEC gradients were steeper and the plume of high TEC values was wider, but the SED events from both days traveled over the same regions and showed similar deficiencies in WAAS capability to fully characterize the phenomenon. TEC values reached up to 30 m for the regions affected by the SED. Once again, the WAAS TEC values are significantly lower than the truth in terms of magnitude of the vertical ionospheric delay, especially for the SED regions. Nonetheless, the errors were once again bounded by WAAS GIVE values.

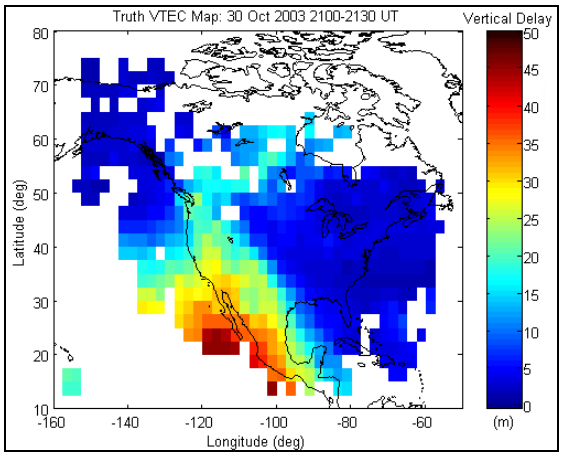

Figure 3.15a: Truth VTEC Map (2100-2130 UT, October 30, 2003)

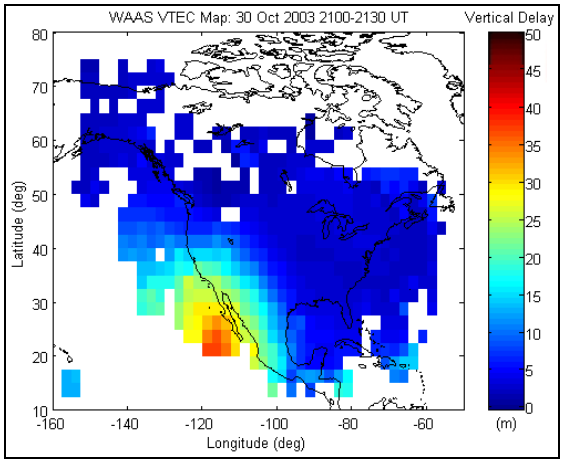

Figure 3.15b: WAAS VTEC Map (2100-2130 UT, October 30, 2003)

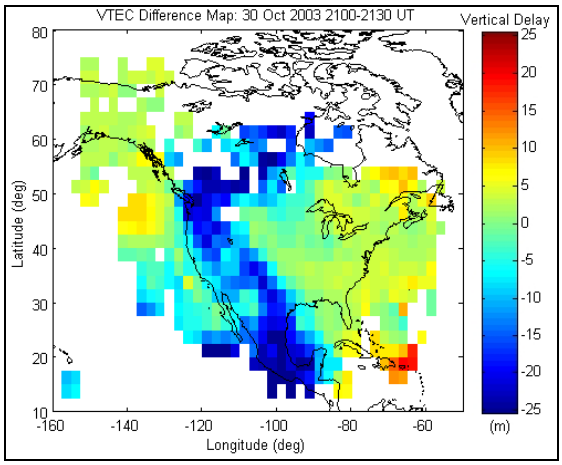

Figure 3.15c: VTEC Difference Map (2100-2130 UT, October 30, 2003)

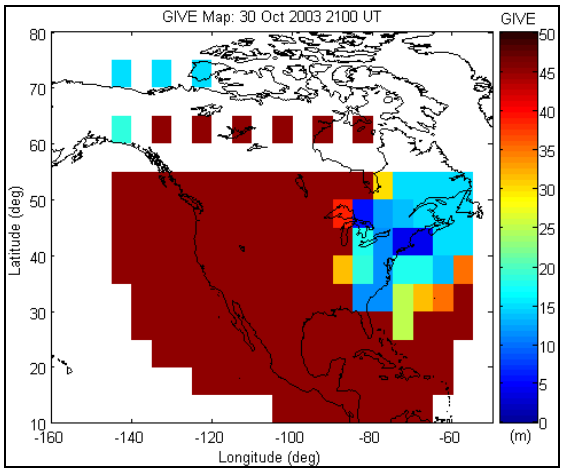

Figure 3.15d: WAAS GIVE Map (2100 UT, October 30, 2003)

It would be interesting to observe how the SED evolved over time on that day. For this purpose a consequent half hour time-interval was processed, and the results are below in Figures 3.16a-3.16d. The main difference between the two intervals, for vertical delay truth, is the fact that VTEC values are slightly larger corresponding to the SED. However, in the WAAS map this temporal development of the SED is practically non-existent. Thus the VTEC errors, as shown in the difference map (Figure 3.16c), are even larger than the previous half hour period for this day.

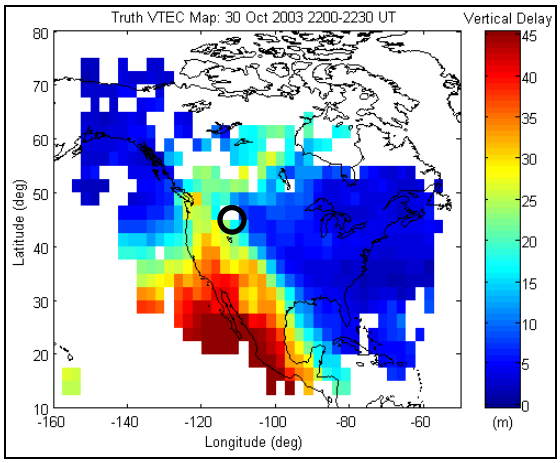

Figure 3.16a: Truth VTEC Map (2200-2230 UT, October 30, 2003)

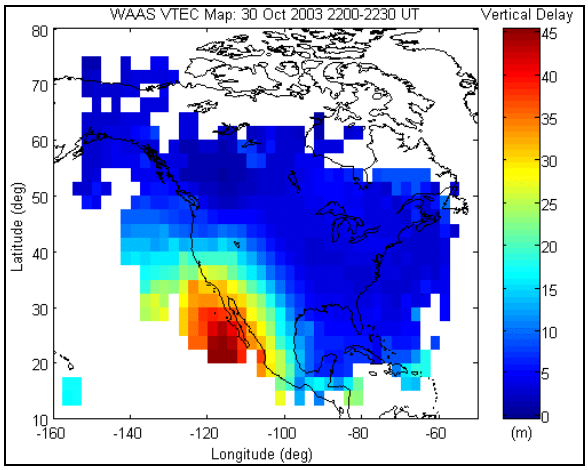

Figure 3.16b: WAAS VTEC Map (2200-2230 UT, October 30, 2003)

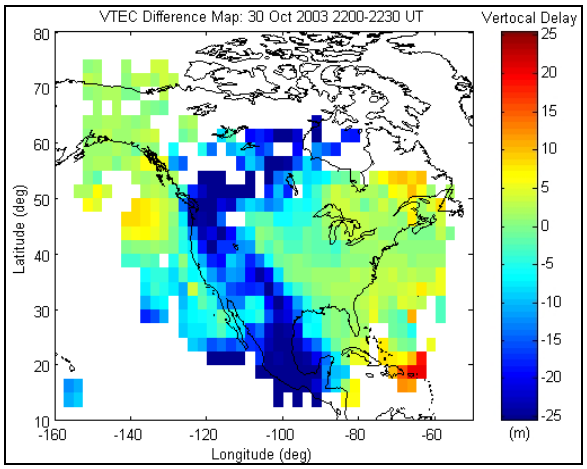

Figure 3.16c: VTEC Difference Map (2200-2230 UT, October 30, 2003)

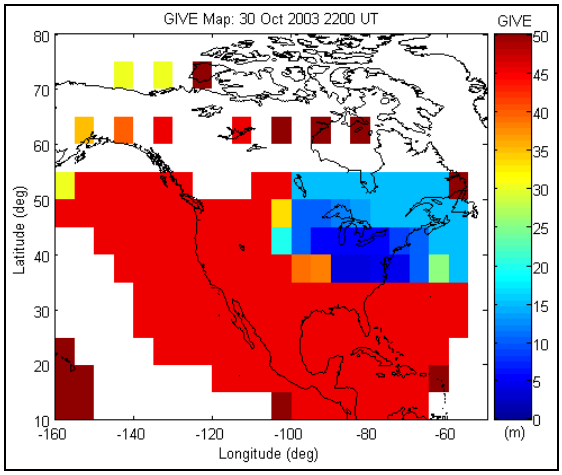

Figure 3.16d: WAAS GIVE Map (2200 UT, October 30, 2003)

A temporal analysis is also conducted. Station "AMC2" (black circle in Figure 3.16a) located directly below the SED was studied closely to observe trends over time. Figure 3.17 presents the results obtained at user station "AMC2". What are shown are VTEC truth, WAAS ionosphere corrections, difference between the two and UIVE values over

the three days. As seen in the spatial plots above (Figures 3.14a, 3.15a and 3.16a), there were two major rises in ionospheric delay during this storm period (associated with the SED), and the two VTEC peaks (on each day) in the figure below indicate those disturbances. These are seen in the WAAS plot, but the peaks are not significant as compared to truth observations, especially for the second day. The difference plot is in support of this fact, in that there is 15 m offset between the maximum errors from the two days, and on the second day the error is greater. Therefore, it could be said that ionospheric disturbance reduce the WAAS ability to spatially model the ionosphere. The last plot in the figure is the UIVE for the period; this is to show that even after interpolating the GIVE, the errors are still bounded. This could be verified by observing a scatter plot showing UIVE versus VTEC error (Figure 3.18). The diagonal line in this plot is separating the Cartesian space into two segments: region where all UIVE values are less than VTEC errors (upper triangle) and region where all UIVE values are greater than VTEC errors (lower triangle). Thus, it can be inferred from this figure that for this dataset UIVE values were always greater than VTEC errors, since all data points lie in the lower triangle.

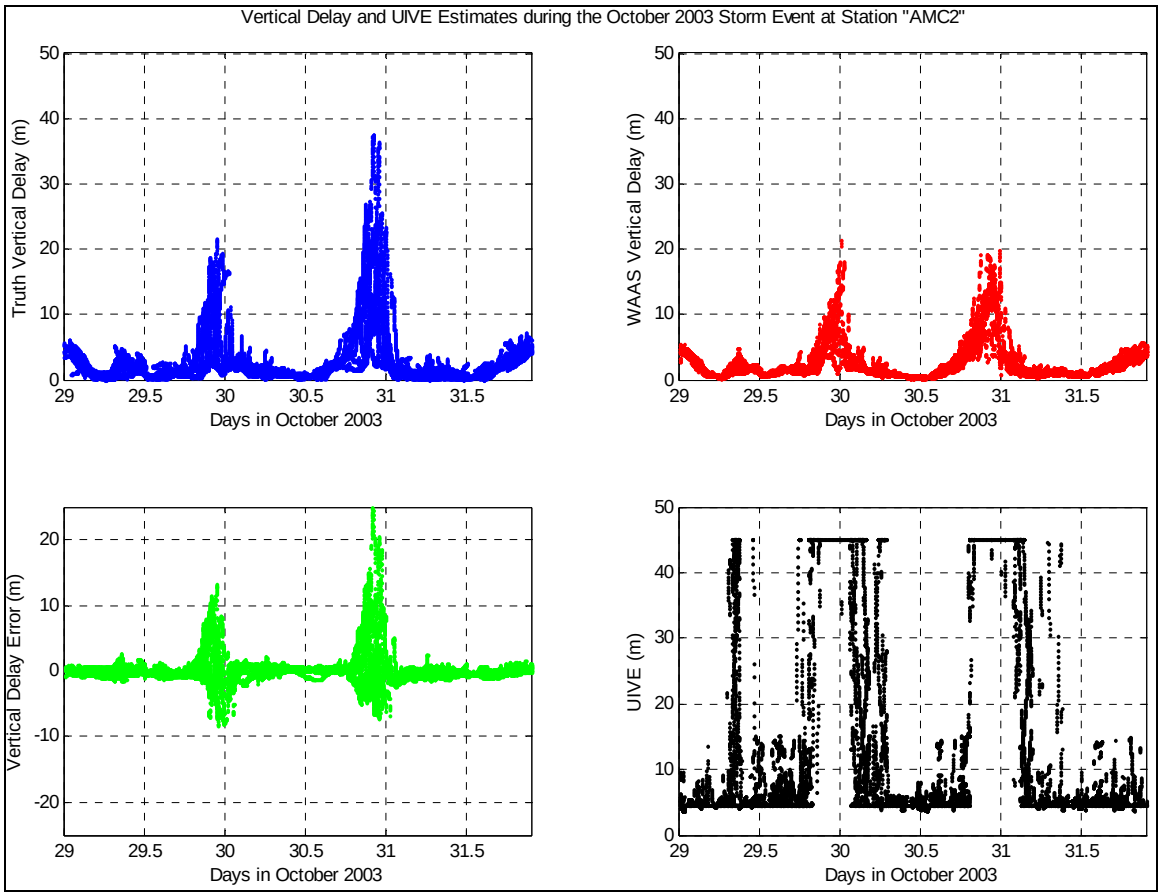

Figure 3.17: Time Series Plots (VTEC Truth, WAAS Ionosphere Model, Error (Truth – WAAS), UIVE) during October 29-31, 2003 at User Station "AMC2"

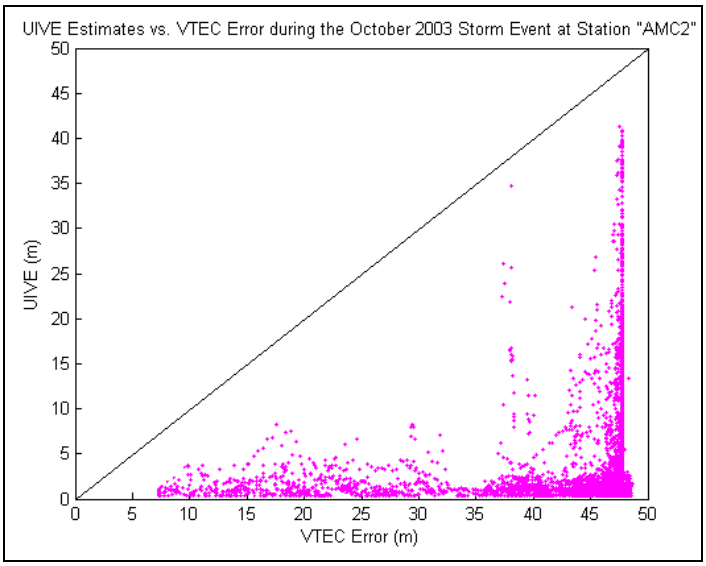

Figure 3.18: UIVE Estimates vs. VTEC Error during the October 2003 Storm Event at Station "AMC2"

A final look at this event was to compute statistics (Table 3.4) of the above dataset, to derive values for the VTEC errors corresponding to each day. Clearly, October 31 appears to be a relatively quiet day in terms of ionospheric activity. Thus, the ionospherically quiet versus active days could be compared quantitatively. The daily variation is clearly seen in the RMS values (computed by taking the root mean square of all the data points lying within the 24-hour UT boundaries), with the larger errors occurring on the second day of the storm event. On Oct. 30 the maximum error in WAAS predicted vertical ionospheric delay climbed to 26 m. Usually, those users relying on the WAAS for vertical guidance would be denied availability because of large GIVE values causing such deficiencies in accuracy. WAAS typical performance bounds were surpassed by a large amount. This is why further refinement of the system is necessary to adequately handle localized events such as the ones seen above.

Table 3.4: WAAS VTEC Error Statistics during October 29-31, 2003 at "AMC2"

		Oct. 29	Oct. 30	Oct. 31
VTEC Error (m)	MEAN	-0.09	0.30	-0.20
	RMS	1.67	2.64	0.67
	MAX	13.24	26.36	5.01
	MIN	-8.27	-7.42	-6.85

November 20, 2003 Storm

Similarly to the October 2003 storm event, this storm evolved over an extended period of time (over six hours) but only endured for a single day (November 20). Figure 3.19 depicts the temporal evolution of this storm event. What is shown are VTEC values obtained from the truth dataset; this shows the temporal evolution of the storm as it was developing over northeastern US during the course of that day. As can be seen, interesting features were starting to emerge near the end of the day. At around 1600 UT, there was a steep increase of the vertical ionospheric delay over the station "UIUC" (latitude: 40.0990° and longitude: -88.2203°), which is located in northeastern US. Unlike the October event, these storm effects were observed in the east. This event in particular is quite unfavorable for users in Eastern Canada, because this area already has poor WAAS coverage and with the added SED effects, positioning degradations are substantial. Further investigation of these positioning degradations will be done by observing this SED from a spatial perspective.

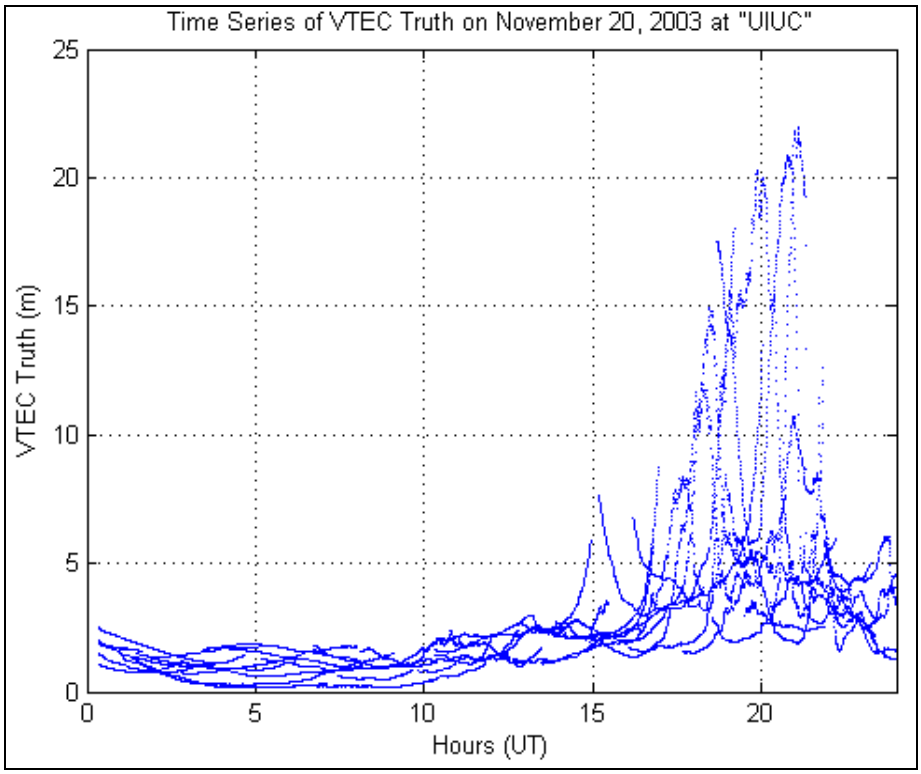

Figure 3.19: Time Series of VTEC Truth on November 20, 2003 at Station "UIUC"

The gradients associated with SED were extremely large during this event. The spatial distribution of SED (truth VTEC map) over North America for November 20, 2003 is shown in Figure 3.20a, and the corresponding VTEC WAAS, VTEC difference (biases removed) and GIVE maps are given by Figures 3.20b, 3.20c and 3.20d, respectively. Note that spatial plots of other time intervals for this event are given in Appendix B. SED is evolving earlier for this event than the October event, with the larger gradients now occurring in the central region; this time it is originating in southeastern US and emerging into southeastern Canada near the Great Lakes area – but similar effects were observed as in October 2003. In the same manner, for this event WAAS fails to completely resolve the SED features. Consequently, the difference plot shows an imprint of the SED feature as large differences in VTEC values, which are still being under-estimated by the WAAS

as the SED differenced values are mostly negative; still the errors are bounded by the GIVE, as can be noticed from Figure 3.20c and then comparing it to Figure 3.20d. Clearly, most of the GIVE values over North America for this period are about 15 m, whereas the error level has a maximum at about 12 m; thus, the upper bound is maintained by the GIVE. Although, a major distinction is that WAAS service was not denied to any capacity because GIVE values were well below the 45 m threshold. Another interesting element to note is the noisy characteristic of WAAS vertical delay estimates in Figure 3.20b. In the previous plots (e.g. from the October 2003 storm event) it was seen that WAAS estimated values are fairly smooth, spatially; but for this event this is not the case. It seems that in southeastern US, WAAS ionospheric data have been corrupted by some kind of random noise or systematic error. Nonetheless, the remainder of the WAAS ionospheric map appears to be valid, with delay values at around 5 metres.

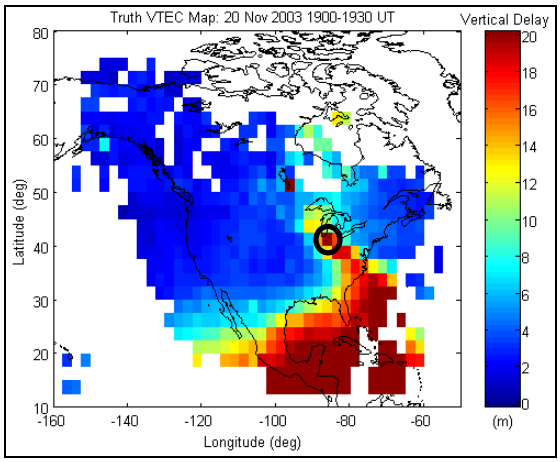

Figure 3.20a: Truth VTEC Map (1900-1930 UT, November 20, 2003)

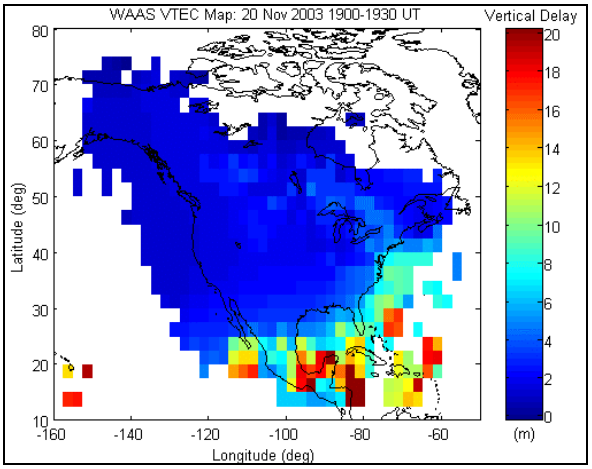

Figure 3.20b: WAAS VTEC Map (1900-1930 UT, November 20, 2003)

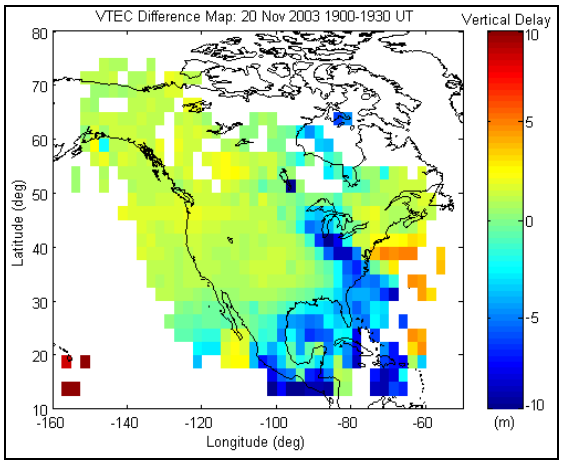

Figure 3.20c: VTEC Difference Map (1900-1930 UT, November 20, 2003)

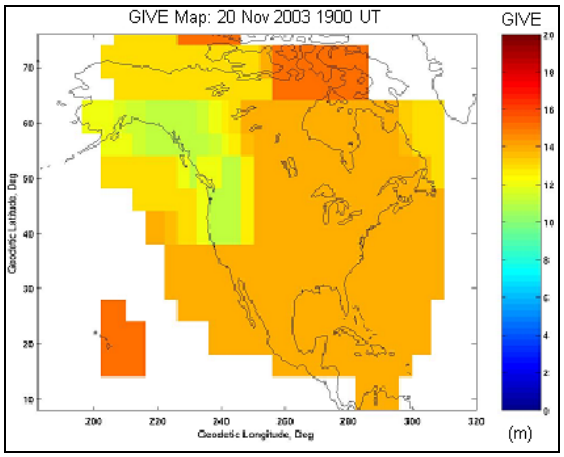

Figure 3.20d: WAAS GIVE Map (1900 UT, November 20, 2003)

Once again, a user station that is directly beneath this SED event was chosen to conduct the VTEC accuracy analysis over time. The station is "UIUC" located near the Great Lakes, as indicated by the black circle in Figure 3.20a. Previously, it was shown (in (Figure 3.19) how the VTEC truth values behaved over time, to get an idea of the temporal trend. Figure 3.21 will present a comparison of the ionospheric delay estimates during November 20th, 2003 for all satellites in view. The WAAS VTEC values have a similar peak to the truth and it occurs around the same time, but the peak is not as prominent as compared to the truth. The major inaccuracies are thus seen in those peak values, and these WAAS errors are negative with a minimum of about 7 m. But, in general the errors for the remaining of the day (quiet ionospheric time) are non-biased. Therefore, it is useful to look at the impact of the SED on WAAS accuracy. As such, statistics were derived for this day and were separated in terms of quiet (0000-1500 UT) versus active (1500-2400 UT) ionospheric times; the boundary between what is quiet and what is active was set by observing the time of day when VTEC values start to pick up

and head towards the diurnal peak. Table 3.5 is providing these results. As expected, the errors are much larger during the active time (RMSE of 4.56 m vs. 0.67 m). Accordingly, the SED has posed major obstructions in WAAS' ability to accurately estimate the ionospheric delay during the timeframe in question. It is noticeable that most of the VTEC error values are biased during the storm. This is due to the fact that WAAS tends to under-estimate the ionospheric delay during storm events. As such, the VTEC errors tend to be biased in most cases where a storm is present.

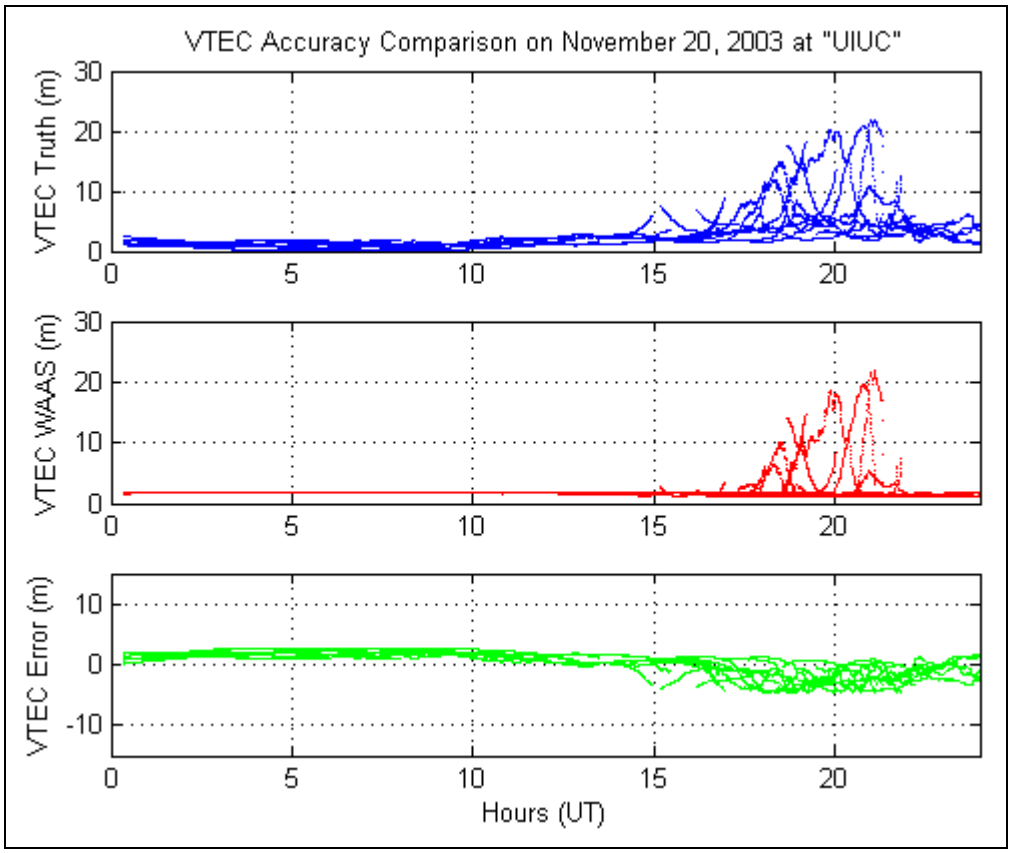

Figure 3.21: VTEC Accuracy Comparison on November 20, 2003 at "UIUC"

Table 3.5: Overall WAAS VTEC Accuracy Statistics for November 20, 2003

		November 20, 2003	
		Ionospherically Quiet Time (1600-2200 UT)	**Ionospherically Active Time (1600-2200 UT)**
VTEC Error (m)	MEAN	0.41	-1.98
	RMS	1.23	4.65
	MAX	2.42	1.08
	MIN	-3.89	-5.06

November 7-10, 2004 Storm

This storm was much less significant than the October and November 2003 storm events, but it showed similar characteristics at a lower scale. Figure 3.22 shows the Kp index for the storm period. Kp values of 9 were observed on November 8 and 10. These were less localized as compared to typical SED phenomena and did not have the usual steep TEC gradients and northerly TEC plume usually associated with SEDs. Thus, this event would not necessarily fall into the SED category. Nevertheless, large ionospheric delays spread across North America were observed. A snapshot of the ionospheric disturbance over North America on November 7, 2004 is pictured in Figure 3.23. This specific half-hour was chosen because the largest TEC gradients of the whole storm period were seen around this time. As can be seen from this plot, the west coast and some central regions are affected, though the vertical ionospheric delay values are much lower than the earlier storm events studied in previous sections, and ionospheric delay values climbed upwards to about 10 m. In this figure, there is a large localized value in central North America. This is an actual true value and appears to be the extremity of a small-scale TEC plume, as a low order TEC gradient leads up to that extreme value.

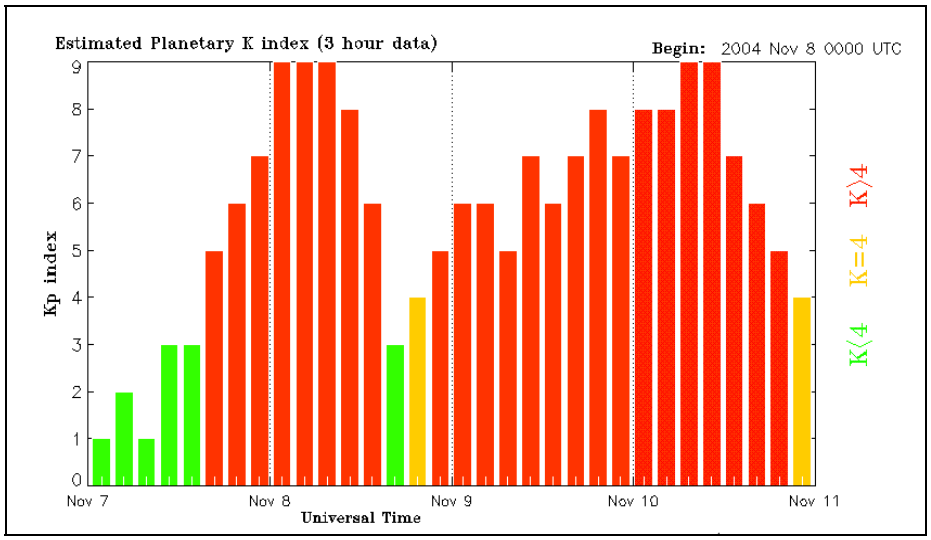

Figure 3.22: Kp Values for November 7-10, 2004 [*NOAA SEC*, 2005]

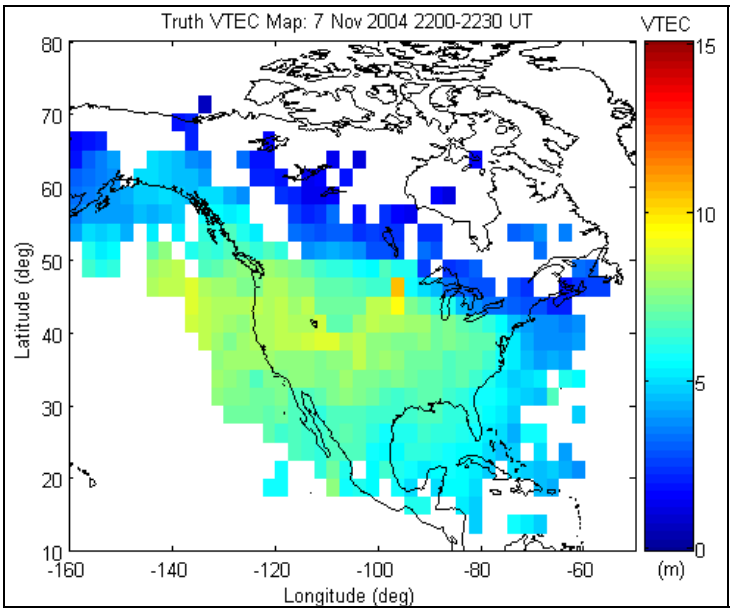

Figure 3.23: GPS TEC Map for 2200-2230 UT, November 7, 2004

Since this event included minor disturbance peaks of moderate magnitudes over time (because maximum VTEC was 10 m for this event), an analysis in the time domain will be conducted. Substorms are generally characterized by short duration lengths, radical

changes in ionospheric activity, separated in time by quiet ionospheric periods and isolated phenomena occurring independent from the major storm event. Hence, observing the effects on a single user station over the storm period will be the focus of the study. In addition to computing the truth and WAAS VTEC values for the given station, the values for the broadcast ionospheric (Klobuchar) model will also be generated. The selection of the test station ("user") is a crucial factor for effective analysis, and so the choice was based on where the impact of this storm was most prevalent. After initial processing of several candidate stations, NANO located in Nanoose Bay (latitude: 49.2948° and longitude: -124.0865°) from the IGS network offered the most representative estimates. As such, the analysis to follow will be based on a simulated user located at this site attempting to estimate the ionospheric delay using the aforesaid three methods (VTEC truth, WAAS and Klobuchar). Shown in Figure 3.24 are the results obtained from each of these methods. Note that the data points in the figure below represent the actual vertical ionospheric delays (in metres) as estimated by the individual methods and that these are NOT VTEC errors. These were presented in this manner so that the exact behaviour of the ionosphere (shown by truth VTEC in blue) during the storm event could be observed.

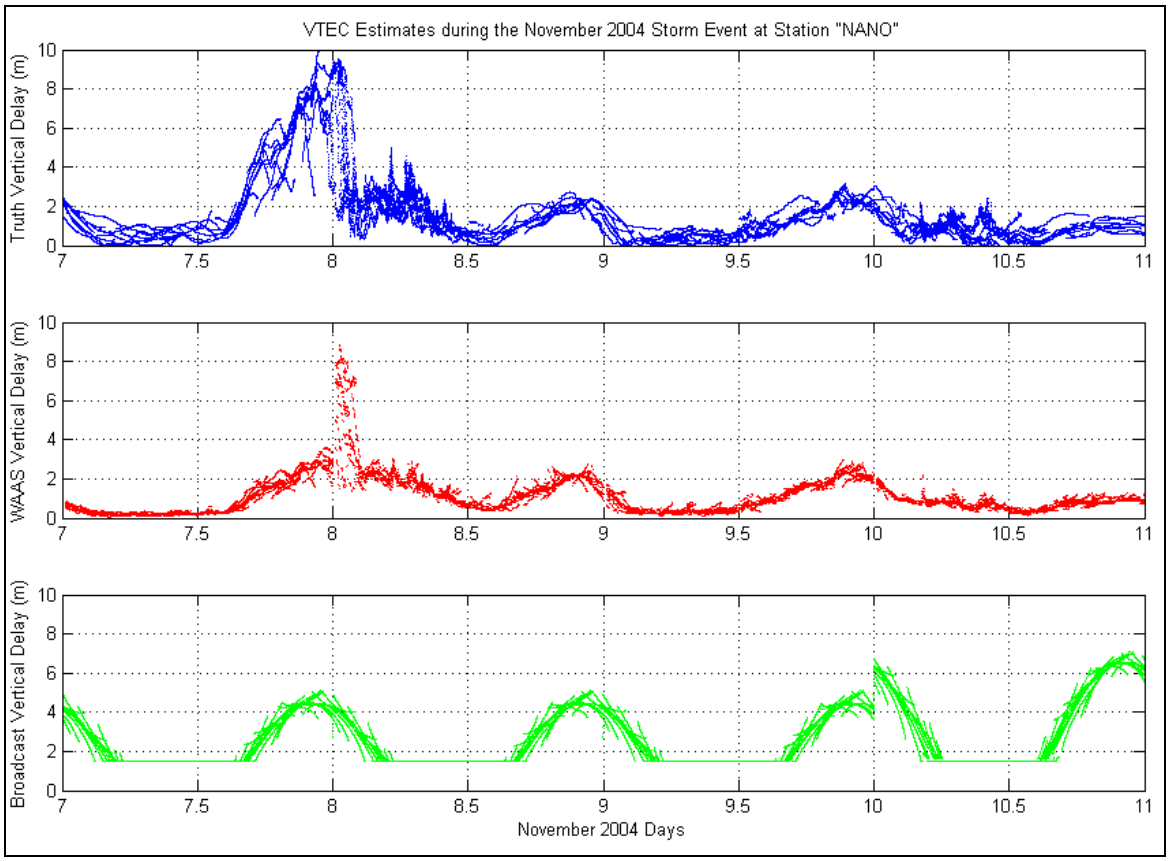

Figure 3.24: VTEC Estimates during the November 7-10, 2004 at "NANO"

The most prominent feature in the plots above is the increased ionospheric disturbance seen in the truth plot during the second half of November 7 (day 312) and continuing into the next day. Vertical ionospheric delay is reaching upwards of 10 m during the affected period. Although a minor disturbance exists later in the week on November 10, this is nothing like the former in terms of magnitude. The WAAS somewhat follows the true temporal trend and is able to detect some of the feature anomalies but fails to fully resolve the temporal features of the ionosphere. In general, significant under-estimation is done by the WAAS, especially during the disturbed times.

Diurnal patterns of the ionosphere are observed in all three of the plots including the Klobuchar model, which is based on the half cosine function. However, the level of ionospheric activity practically has no effect on the model output because it is not based on local parameters. Two VTEC daytime peaks from an ionospherically quiet versus disturbed day are almost identical, as can be seen from the plot above. Even during the nighttime, the model is simplifying the delay estimates. Therefore, if high precision of the ionospheric delay estimates is required, the Klobuchar model should not be used, as it is only guaranteed to remove 50% of the ionosphere effect [*Klobuchar et al.*, 1995]. Similarly, WAAS is not performing well either – the storm spanning over November 7 and 8 (the first major VTEC peak) is poorly characterized by WAAS.

A summary of how the WAAS and Klobuchar models performed is given in Table 3.6, where the model estimates are differenced from the truth-values for the days of interest. The intent here is to present a direct comparison between the two different methods and to observe the daily progression or recession of the storm event. As such, the increases in VTEC errors in Table 3.6 are representative of the peaks seen in Figure 3.24. Note that the statistics in the table below provide VTEC error information for the station “NANO” and not the overall dataset.

Table 3.6: VTEC Accuracies for Broadcast vs. WAAS during November 7-10, 2004 at "NANO"

		7-Nov-04		8-Nov-04		9-Nov-04		10-Nov-04	
		BRDC	WAAS	BRDC	WAAS	BRDC	WAAS	BRDC	WAAS
VTEC (m)	MEAN	3.79	3.32	-0.63	1.29	-0.96	0.87	-2.25	1.63
	RMS	4.95	4.19	2.06	1.80	1.74	1.62	3.59	2.04
	MAX	8.26	9.55	4.26	2.87	1.32	1.50	6.68	1.31
	MIN	-2.81	-2.77	-1.89	-0.88	-2.56	-0.37	-0.97	0.23

The study of this storm event would not be complete without a spatial analysis. As such, spatial maps were also generated for the most disturbed time period. In particular, the ionospheric delays peaked near the end of the day on November 7th, and so the time-period 2200-2230 UT was chosen to depict the spatial picture from this storm. Figures 3.25a-3.25d show VTEC truth, WAAS, difference, and the GIVE map, respectively for that timeframe. Truth and WAAS VTEC values are of similar magnitude (maximum of 10 m), except that WAAS value distribution is smooth, and it fails to detect the fine localized events. Thus in this case, the difference values shown in the map is more precise (maximum/minimum of ± 5 m) than those for the October and November 2003 storm events. WAAS GIVE values are less conservative this time, as the GIVEs marginally bound the VTEC errors (shown in Figure 3.26). This is so because the accuracy degradation is not that severe, and so the error safety margins could be relaxed.

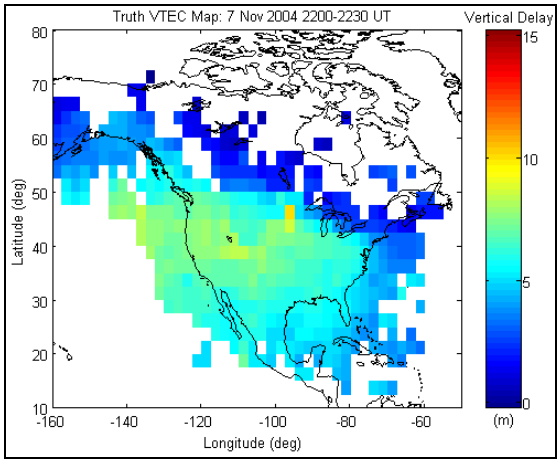

Figure 3.25a: Truth VTEC Map (2200-2230 UT, November 7, 2004)

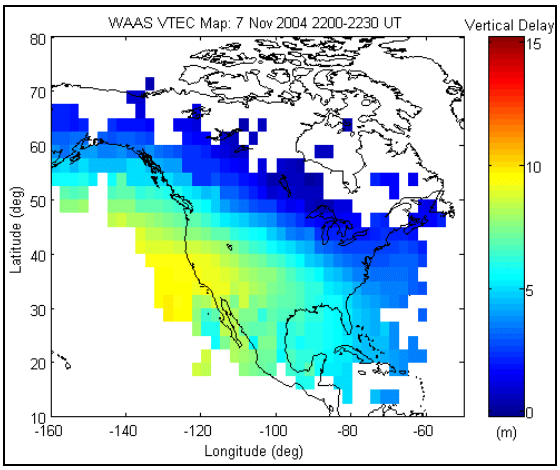

Figure 3.25b: WAAS VTEC Map (2200-2230 UT, November 7, 2004)

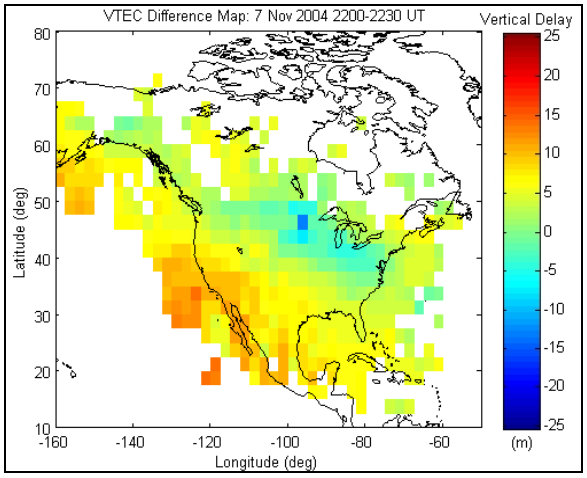

Figure 3.25c: VTEC Difference Map (2200-2230 UT, November 7, 2004)

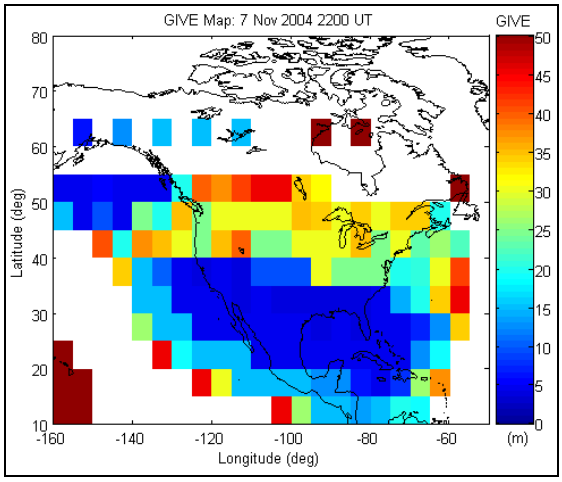

Figure 3.25d: WAAS GIVE Map (2200 UT, November 7, 2004)

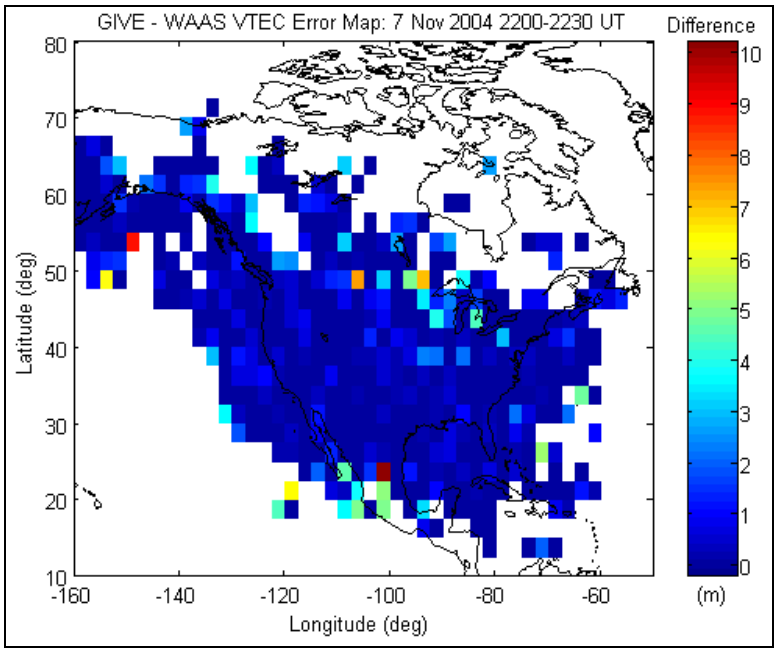

Figure 3.26: Map Showing GIVE minus Differenced WAAS VTEC Error

As discussed previously and seen in the statistics above, the WAAS performed much better than the broadcast model. However, it is not sufficient to only observe the accuracy aspect to judge on performance; it is also important to verify the system's reliability. In case of WAAS, this is done by observing the corresponding UIVE indices for the period of interest, as shown in Figure 3.27. Once again, WAAS UIVE bounds the errors for every epoch at station "NANO", because it is clearly noticeable that every single UIVE value lies above the maximum VTEC error estimate (the cutoff value is shown by the black line in the figure). Thus, reliability is maintained throughout the storm event. One last comment to be made is on the typical accuracy level offered by WAAS for the ionospheric corrections. Previous studies have shown that the ionospheric correction accuracy offered by WAAS is around 2-3 m [*Klobuchar et al.*, 1995]. And, the results from this chapter are consistent with that level of accuracy during quiet ionospheric times,

but SED effects had degraded WAAS performance significantly, as seen through large error peaks.

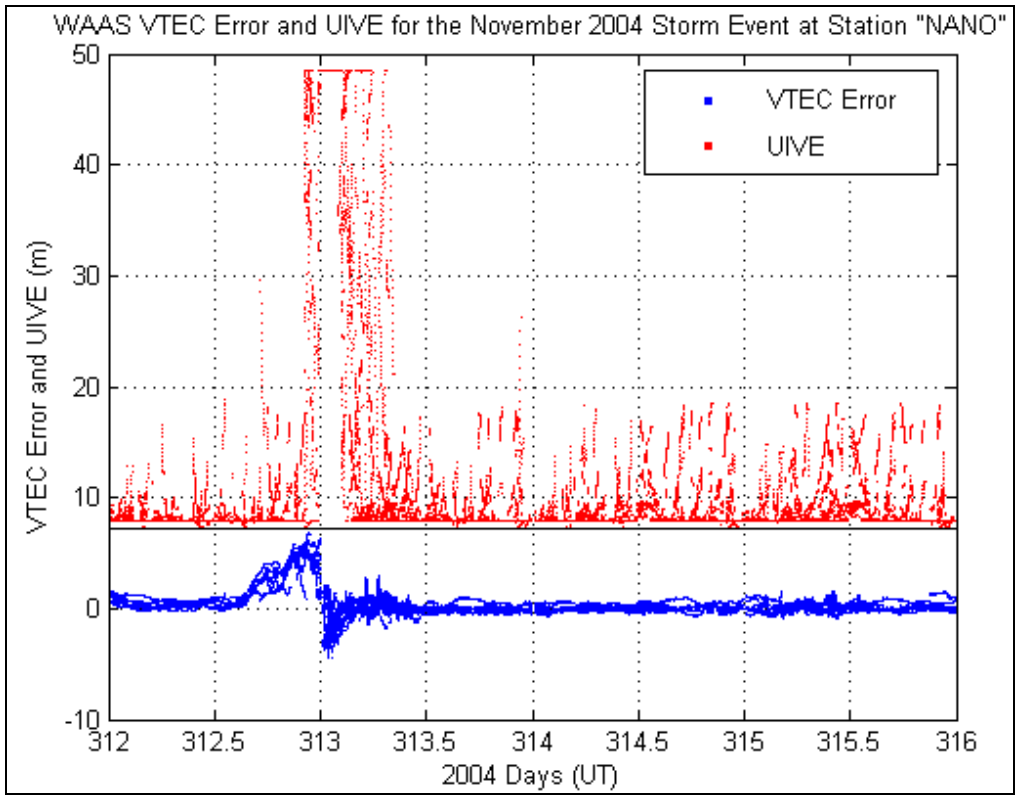

Figure 3.27: UIVE Validation for the November 2004 Storm Event at "NANO"

Chapter 4

Positioning Performance Evaluation of the Current WAAS

This chapter will first describe the methodology behind the WADGPS processing and discuss the input parameters that were used to derive the results. Thereafter, the actual results for three different case-studies will be presented. The importance of these case-studies lies in that these are major ionospheric storm events that were studied in the correction domain in Chapter 3. This time the analysis will be in the positioning domain, to observe the impact of the correction inaccuracies in the positioning domain. For each event, the results will be discussed by focusing on a single station (temporal analysis) and then moving onto observing the accuracy trends spatially across North America.

Inferences will be made on the observed effects, trends and WAAS performance levels under the disturbed ionosphere. Lastly, a validity check of this research will be conducted using an independent study possessing similar experimental conditions to the ones for this study.

4.1 WAAS Positioning across North America under Various Ionospheric Conditions

WAAS overall performance across North America is evaluated here. Estimating the ionospheric delay is a crucial and difficult task for Satellite Based Augmentation Systems (SBASs) such as the WAAS, especially during intensely disturbed ionospheric times. This is due to isolated ionospheric phenomena that require fine spatial modelling and, as discussed in earlier sections, WAAS has a sparse network producing a coarse resolution ionospheric grid – which lacks refinement for proper spatial characterization. Thus, ionospheric activity will play a big role in the assessment of the WAAS network.

4.1.1 WADGPS Processing

Since gathering the proper data is the key to successful analysis, the first step of data processing is to identify the right set of data and then to make sure that the dataset is appropriate for all phases of the processing. Thereafter, the rest of the associated tasks could be performed.

1) Data Retrieval

IGS and CORS data were retrieved by downloading them off the internet from an archive site (*ftp://cddisa.gsfc.nasa.gov/pub/gps/*), and the WAAS data containing clock, orbital and ionospheric correction messages were obtained by request to T. Dehel from FAA.

2) Data Formatting

Data formatting involved decompression of files, conversion of binary observation and ephemeris files to ASCII and RINEX formats, and other custom conversions for compatibility between software routines. Some of the formatting could be done in batch mode but some had to be done manually due to data anomalies.

3) Data Processing

WADGPS processing work was carried out in the manner shown in Figure 4.1. Various forms of inputs went into this processing scheme, and the ultimate output that came out of all this processing was the WAAS positioning estimates. Most of the software required for the processing components shown in these diagrams was developed specifically for this research, with the exceptions of computing final WADGPS positioning estimates and computing the observation IPPs at each station. These were done using a modified version of a software package called C3NAV™ [*Cannon et al.*, 1995] and TECANALYS© [*Skone*, 2002], respectively.

Figure 4.1 provides a summary and workflow diagram of the processing scheme involved in generating the required results. As discussed above, GPS and WAAS data were

acquired from the IGS and FAA, respectively. These were then processed to extract the necessary GPS observation files and the proper WAAS messages containing the corrections clock, orbit and ionosphere. The outputs from this extraction process went into the localization and ionospheric modeling routines as inputs. Thereafter, the three sets of corrections were prepared to be matched in time and PRN and combined to produce scalar range corrections. They were then used to generate DGPS correction files for the WADGPS processing, and finally the resulting output of this process was the computed WAAS positioning solution. Note that the standard model referred to in the figure below implies the ionospheric model that is used by WAAS to generate the WAAS ionosphere grid for North America. This model was discussed earlier in Subsection 2.10.3.

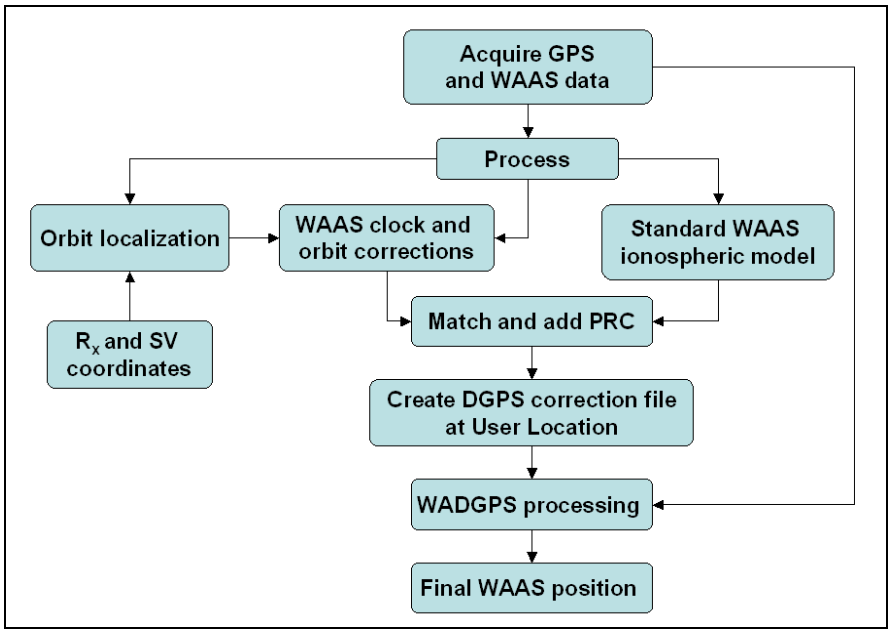

Figure 4.1: WADGPS Processing Flowchart with a Standard Ionospheric Model

4) Data Analysis

In some instances, further refinements of the results were needed to attain compatibility between output files from different categories. For example, to observe how WADGPS positioning solution was affected by the magnitude of ionospheric delay, epoch-matching between two sets of results was needed. For the most part, all repetitions were avoided by automating the processes using batch script files.

4.2 Results of WAAS Positioning across North America

Clock and orbital correction (typical) accuracies are about 2 m. WAAS ionosphere corrections, however, may have large errors during active ionospheric conditions. Such larger errors will lead to degraded WAAS positioning accuracies. In order to quantify the impact on positioning accuracy, discussed in this section are various aspects of WAAS positioning performance across North America. The various storm events that were discussed in Chapter 3 will be revisited but this time with results in the position domain. Horizontal, vertical and 3D accuracies will be quantified spatially for North America, and important conclusions will be drawn about overall WAAS performance.

In this section, WAAS position results are generated for a number of sites across North America. In order to generate WAAS positioning accuracies, processing was done by following the methodologies described above. The input data were the RINEX observation files obtained from each reference station where a user location was

simulated. The locations of CORS reference stations used in the processing are shown as magenta triangles in Figure 4.2. As can be noticed in this figure, every 5° x 5° grid-cell (or bin) contains at least one reference station, which was assumed to represent the WAAS performance attained in that 5° x 5° grid-space. Although some of the stations are close to the edges of the bins (which is not very optimal), this was the best modelling method available, because fully optimal locations for every bin physically don't exist or data were not available for the period of interest. The bin size was chosen to be the same as WAAS ionospheric grid spacing in those latitudes. The spatial plots that will be shown later in this section were derived by binning all computed errors corresponding to the specific cell and by deriving the 95th-percentile value in the given bin for the time interval (nominally half-hour interval).

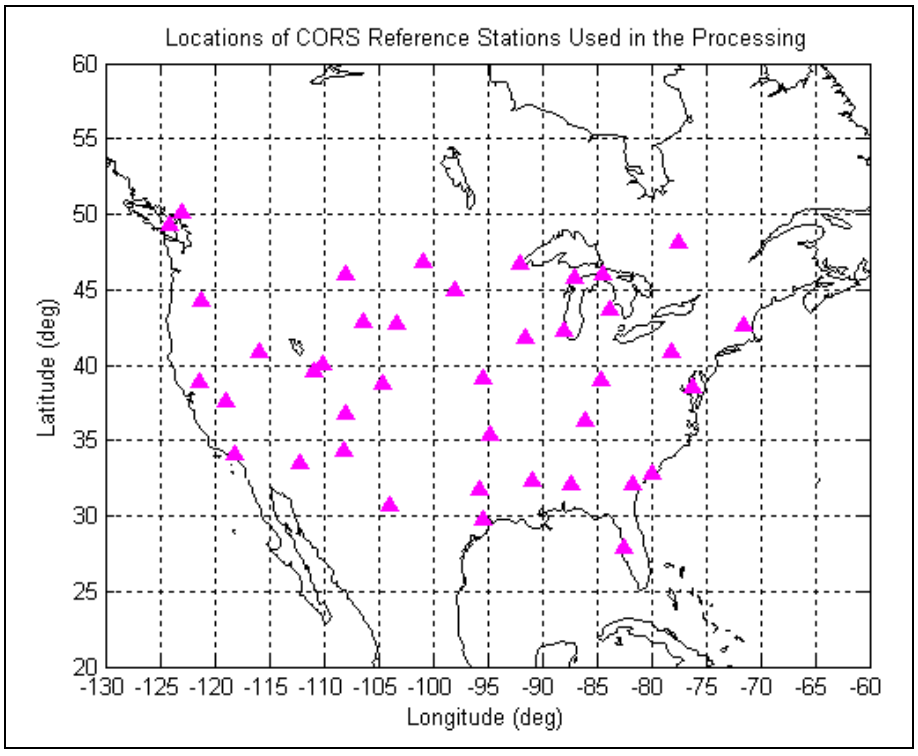

Figure 4.2: Locations of CORS Reference Stations Used for WAAS Positioning

4.2.1 WAAS Horizontal, Vertical and 3D Positioning Accuracies

October 29-31, 2003 Storm

Results shown herein are generated for the entire October 29-31, 2003 storm period. Firstly, positioning accuracy time series plots are presented in Figure 4.3. These plots are generated by computing the 95th-percentile over half hour periods and representing them at the centres of those half hours. This helped in removing some of the noise components in the dataset. Note that all positioning solutions were computed using a mask angle of 10°; HDOP filter was set to 2.3 and PDOP at 3.0. The results presented in the figure below are from a station ("AMC2", latitude: 38.8031° and longitude: -104.5246°) that was directly beneath the SED while it traveled through North America. As can be seen, both vertical and horizontal positioning accuracies (computed by taking the square root of the sum between errors in northing and easting) were poor near the end of October 29 and 30 (UT); the accuracy degradation periods in those instances were over 12 hours in length. However, the HPL and VPL limits indicate that the errors were bounded throughout the storm event for this given station. As can be noticed in the time-series plots below, the 95th-percentile statistic is used to compare the errors to the accuracy protection levels. It is important to note that during the storm events that were studied for this research, no epochs were observed where the errors exceeded HPL or VPL. Later in the chapter, plots will be presented showing the spatial bounds of HPL and VPL. This is a valid statistic to use because most DGPS service providers such as the Coast Guard use this to quote their system's performance levels. Although, the RMSE values could sometimes be useful to quantify distinctive accuracy trends over time.

Therefore, further investigations into the storm event will include a spatial analysis of the North American region. This will entail focusing on those degradation periods and observing the WAAS positioning performance from a spatial perspective during specific time-intervals of interest.

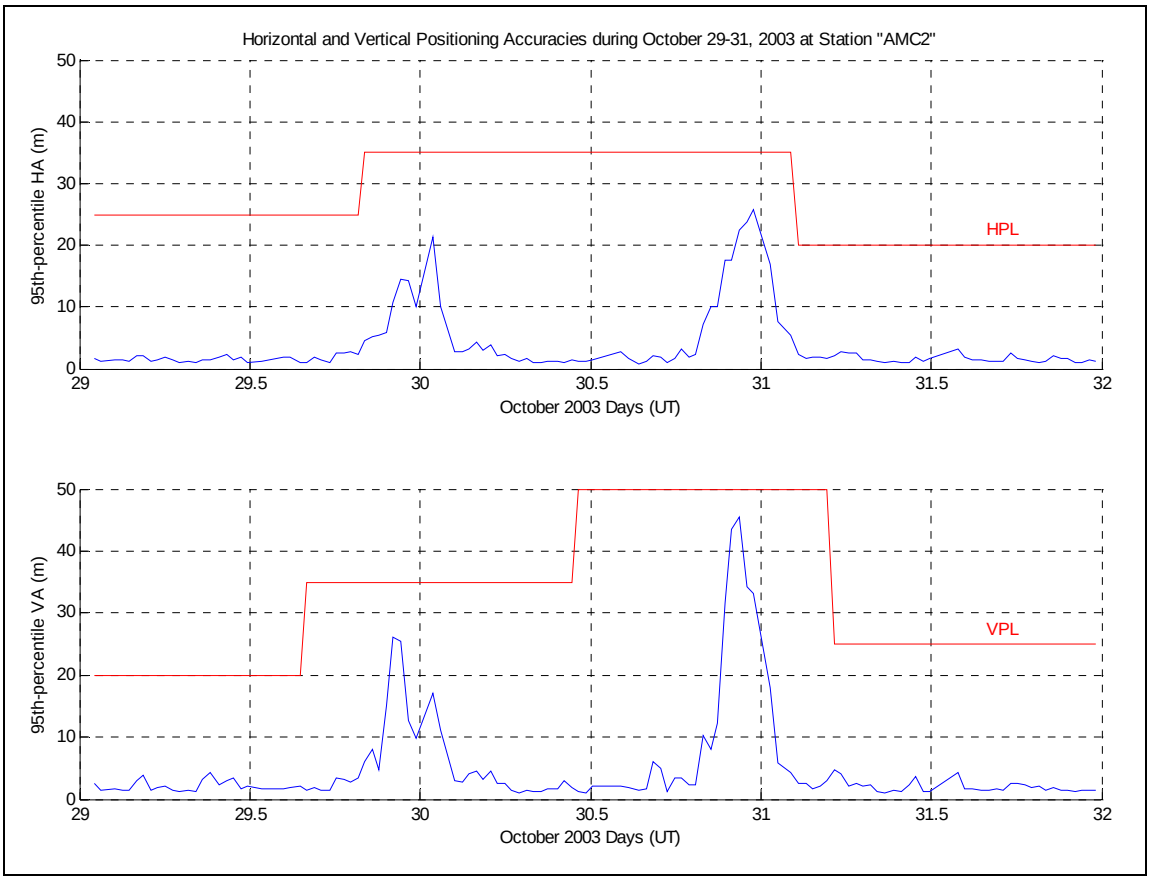

Figure 4.3: WAAS HA and VA during October 29-31, 2003 at Station "AMC2"

Figure 4.4a, 4.4b, 4.4c and 4.4d show WAAS horizontal and vertical positioning accuracies, respectively, derived for all stations in Figure 4.2 (95^{th}-percentile, which is the 95^{th}-percentile value amongst all data points in the given half hour period) for the period 0600-0630 UT on October 29 and 30, 2003, respectively – prior to the

development of SED across North America. The positioning accuracies for these quiet ionospheric conditions are in the range 2-6 m in the horizontal and 3-7 m in the vertical. These accuracies are consistent across the entire United States. In contrast, Figures 4.5a, 4.5b, 4.5c and 4.5d show WAAS horizontal and vertical positioning accuracies (95^{th}-percentile) for the period 2100-2130 UT on October 29 and 30, 2003, respectively. During these periods, severe ionospheric gradients have developed across the western United States, consistent with the SED development. Positioning errors were in the range of 5-15 m in the horizontal and 5-20 in the vertical for the affected areas. Namely, significant degradations in positioning accuracy were seen in the western parts of US. This implies that land or marine users in those areas were not offered the typical WAAS horizontal accuracies (1-2 m); instead, the positioning errors were more than ten times the typical accuracy level. One last remark to be made for this discussion is the accuracy comparison between these two ionospherically active days. As seen in the time series plots, higher error peaks exist on October 30 as compared to the ones from October 29. This is consistent in the spatial maps as well, where the second day error values are larger than the earlier day, in general. Accuracy plots of other time intervals for this event can be found in Appendix C.

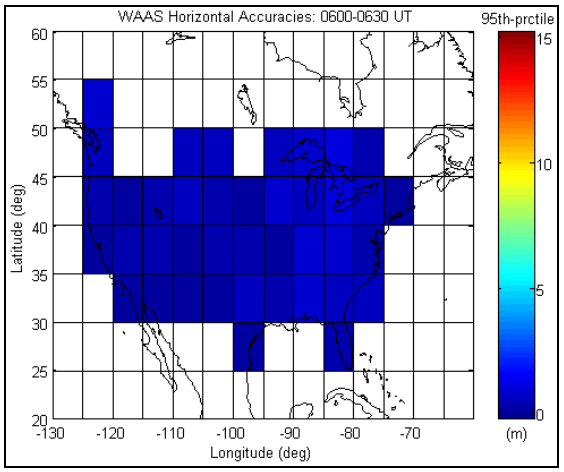

Figure 4.4a: WAAS Horizontal Positioning Accuracies (0600-0630 UT, October 29, 2003)

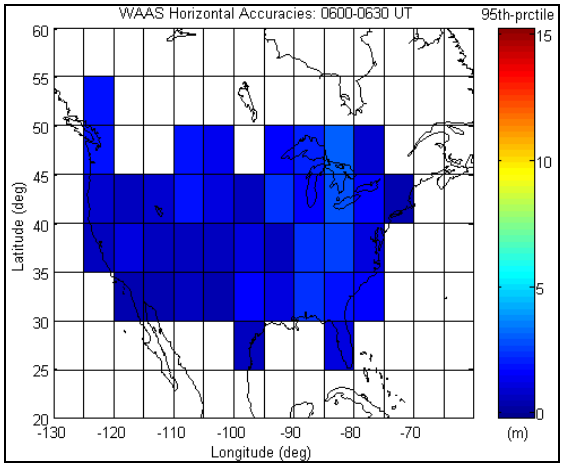

Figure 4.4b: WAAS Horizontal Positioning Accuracies (0600-0630 UT, October 30, 2003)

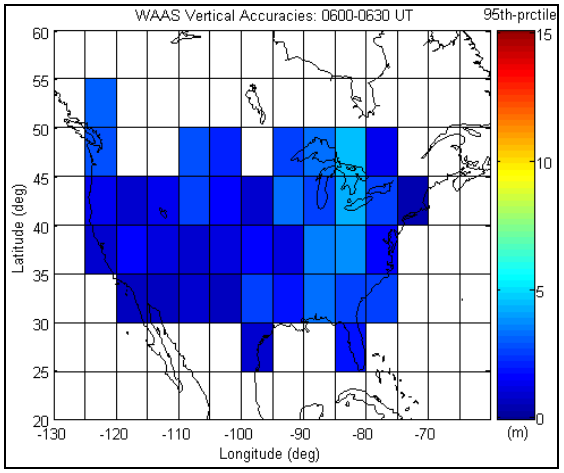

Figure 4.4c: WAAS Vertical Positioning Accuracies (0600-0630 UT, October 29, 2003)

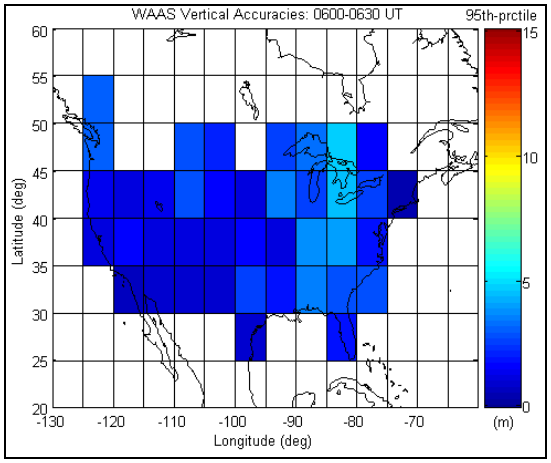

Figure 4.4d: WAAS Vertical Positioning Accuracies (0600-0630 UT, October 30, 2003)

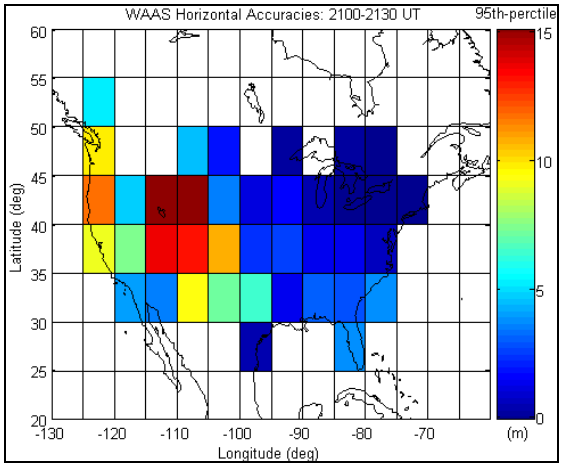

Figure 4.5a: WAAS Horizontal Positioning Accuracies (2100-2130 UT, October 29, 2003)

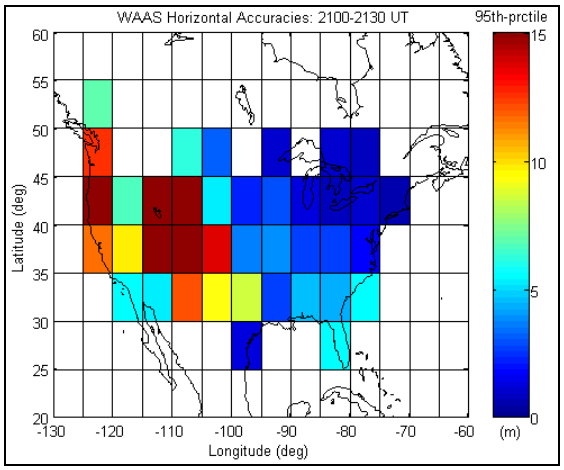

Figure 4.5b: WAAS Horizontal Positioning Accuracies (2100-2130 UT, October 30, 2003)

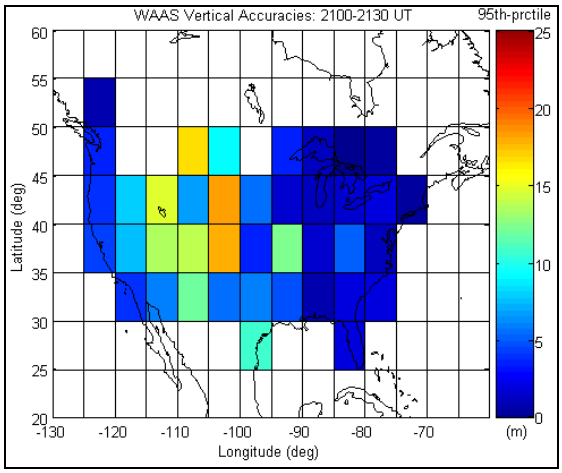

Figure 4.5c: WAAS Vertical Positioning Accuracies (2100-2130 UT, October 29, 2003)

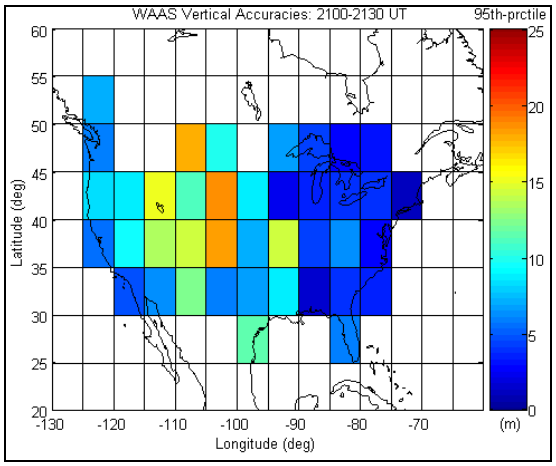

Figure 4.5d: WAAS Vertical Positioning Accuracies (2100-2130 UT, October 30, 2003)

Since WAAS is a system primarily serving to vertically position aircraft, it is essential to study the vertical positioning accuracies also. Thus, results were generated that put this

aspect into context. Typical “quiet” time accuracies for vertical were about 3-4 m. However, ionospherically disturbed conditions showed significantly higher inaccuracies. Pictured in Figures 4.6a and 4.6b are spatial plots during 2100-2130 UT, October 29, 2003 for vertical and 3D accuracies, respectively. 3D accuracies are computed by taking the square root of the sum HA squared and VA squared. Thereafter, Figures 4.7a and 4.7b show spatial plots during 2100-2130 UT, October 30, 2003 for vertical and 3D accuracies, respectively. In satellite positioning vertical accuracy is usually poorer than horizontal, as previously seen in the time series plots (Figure 4.3). This is also clearly apparent in the results below. On both days, the vertical error is driving the 3D positioning error to increase significantly (~25 m in some cases whereas horizontal errors were ~15 m as seen earlier). Once again, the errors are larger on October 30 than on the previous day, and this is true for both height and 3D accuracies. One other point to be noted is the fact that spatial patterns are different for horizontal versus vertical – the larger errors are in different locations for vertical as compared with horizontal. Perhaps this is caused by differences in TEC gradients between the two positioning components, which would affect the accuracies differently. Although this likely the case, it is not possible to infer from the TEC maps presented in Chapter 3 because those maps show gradients in 2D. In order to visualize TEC gradients in the vertical, it would be necessary to have TEC samples at different elevation points to build TEC height profiles, which was outside the scope of this thesis.

From observing these large vertical errors for this storm event, it can be acknowledged that aviation users would have encountered disruptions in WAAS navigation guidance

during this event. By monitoring and detecting this type of degradation of accuracy in real-time, the FAA had denied service to all aviation users in North America during that time for all northwestern and central CONUS locations in plots 4.6 and 4.7, as was seen in Subsection 3.3.3. Under these conditions, typical (non-aviation) applications would have operable 2D navigation and positioning capabilities as services would not be denied and thus it would still be possible to conduct WAAS positioning, but WAAS must also preserve safety-of-life applications. Thus for these types of applications such as aviation, the users would have to switch to alternate navigation methods, given that WAAS transmits “unmonitored” GIVE values. Even if this scenario persists for several hours, this would still be acceptable. The major concern is if the errors are accurately bounded HPL and VPL. In the next subsection, various spatial plots will be shown where these protection levels have bounded the positioning errors, to verify WAAS integrity. The secondary issue is if, for future implementations, WAAS can make improvements to have better accuracies and increase service availability. This is the enhancement part of the study, and eventually this research will present some options to do so.

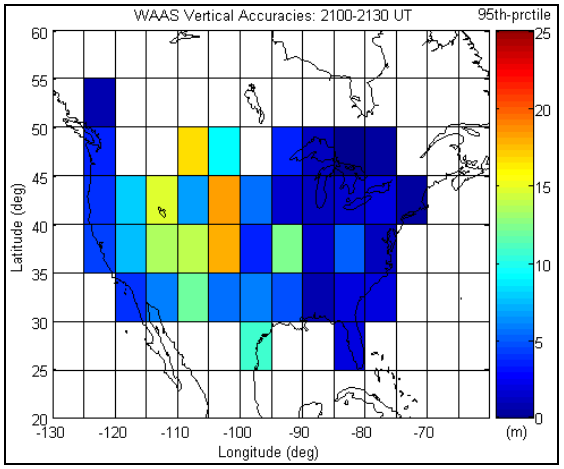

Figure 4.6a: WAAS Vertical Positioning Accuracies (2100-2130 UT, October 29, 2003)

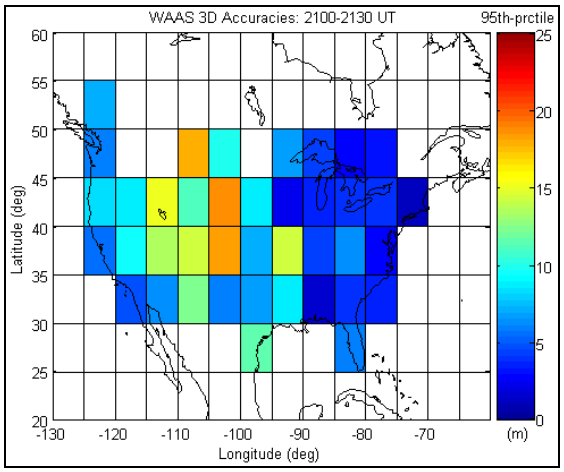

Figure 4.6b: WAAS 3D Positioning Accuracies (2100-2130 UT, October 29, 2003)

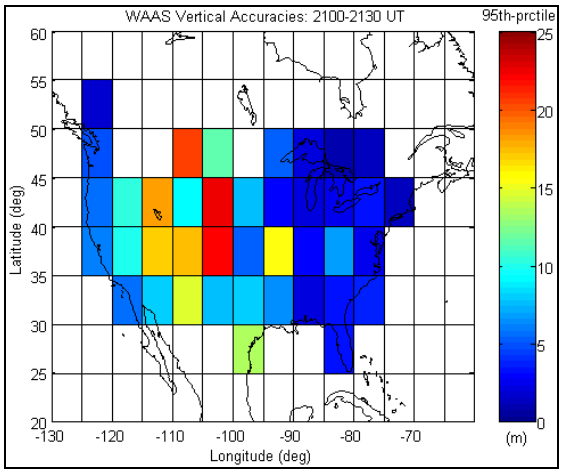

Figure 4.7a: WAAS Vertical Positioning Accuracies (2100-2130 UT, October 30, 2003)

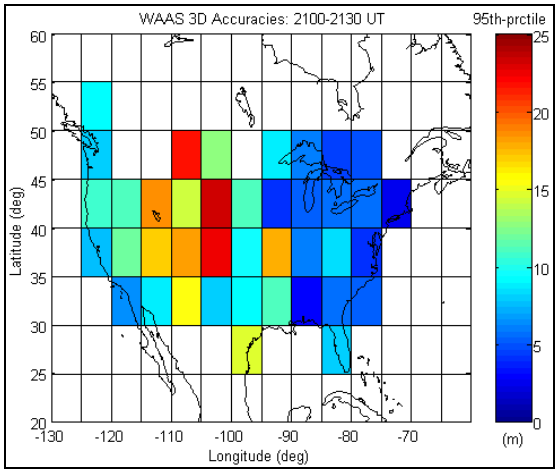

Figure 4.7b: WAAS 3D Positioning Accuracies (2100-2130 UT, October 30, 2003)

November 20, 2003 Storm

This was a single-day event that showed typical SED characteristics, but this time ionospheric disturbance was seen in the east, as will be seen later in the spatial plots. But first, time series plots are presented in Figure 4.8 showing the horizontal and vertical accuracies at the station “VALD” (latitude: 48.80971° and latitude: -77.5642°) in Eastern Canada; this station is located directly beneath the SED, and so the degradation in accuracies are seen near the end of the day in the figure below. Errors surpass the 30 m mark in some instances, thus this was again a major concern for the WAAS users. Once again, HA versus VA trends are very different. In particular, the first major peak in the VA plot is virtually non-existent in HA but the second (minor) peak is aligned. As discussed earlier, these discrepancies between HA and VA trends are caused by TEC gradients, which will have an effect on the horizontal but not necessarily on the vertical.

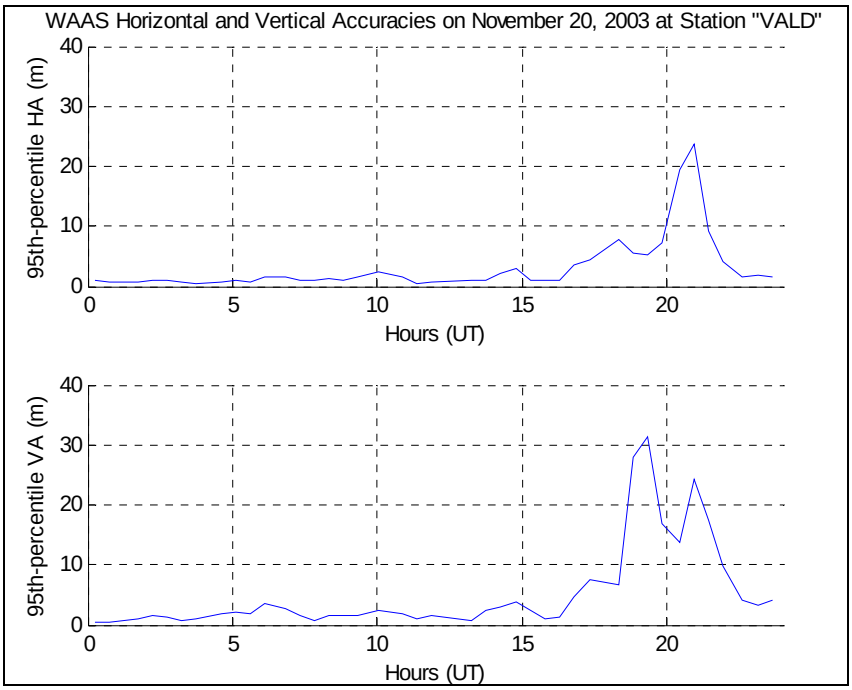

Figure 4.8: WAAS HA and VA on November 20, 2003 at Station "VALD"

As seen in the above time plots, accuracy problems seem to take shape at around 1900 UT for HA and persist until about 2100 UT. Thus, timely snap shots of the phenomenon near those times of interest were taken and are presented in Figures 4.9a and 4.9b (showing horizontal accuracies). Areas not affected by SED, show horizontal accuracies less than 5 m but significant degradation in positioning accuracy is caused by the SED elsewhere in North America. Horizontal errors in Eastern Canada and US were greater than 15 m for some stations.

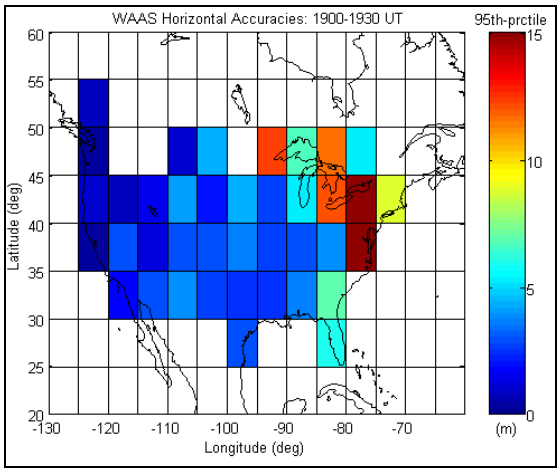

Figure 4.9a: WAAS Horizontal Positioning Accuracies (1900-1930 UT, November 20, 2003)

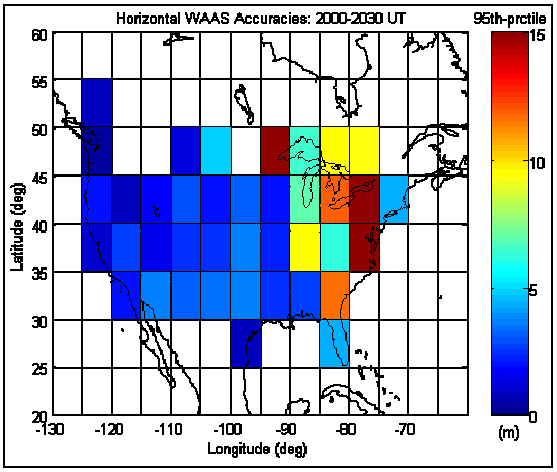

Figure 4.9b: WAAS Horizontal Positioning Accuracies (2000-2030 UT, November 20, 2003)

A similar scenario to the October event is seen here, but this time in the east – the large error pattern is moving northwesterly across the Great Lakes. Vertical and 3D errors for November 20 during 1900-1930 UT and 2000-2030 UT (Figures 4.10a, 4.10b, 4.10c and 4.10d, respectively) are in general greater than the ones in October (over 25 m for several stations). It is not solely due to ionospheric disturbance but also due to the fact that

WAAS network's distribution is spatially weaker in the northeast as compared to the northwest. As a result, relative differences in network coverage between the two regions may be causing the increased degradation in positioning accuracy for this event. For example, Figure 4.11 is showing vertical accuracies for a period of time (0600-0630 UT, October 29, 2003 with Kp Value of 3) when the ionospheric activities are relatively normal. It was found that WAAS accuracy level is 2-3 m better for the western stations as compared to the eastern ones during ionspherically quiet time periods. This is due to not having the same amount of stations in the east versus the west. Although the ionospheric model is computed with east-west persistence, lower network coverage in the east is causing the additional inaccuracies.

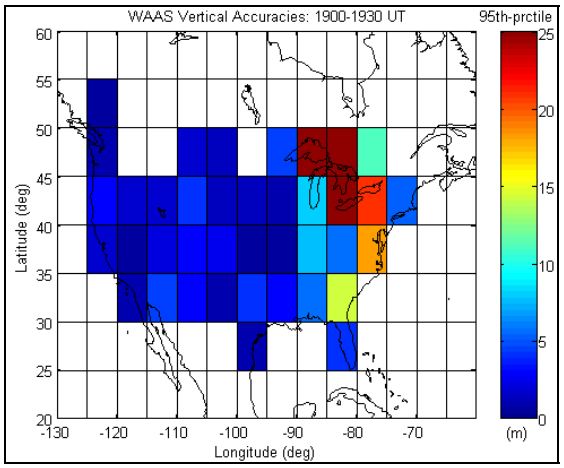

Figure 4.10a: WAAS Vertical Positioning Accuracies (1900-1930 UT, November 20, 2003)

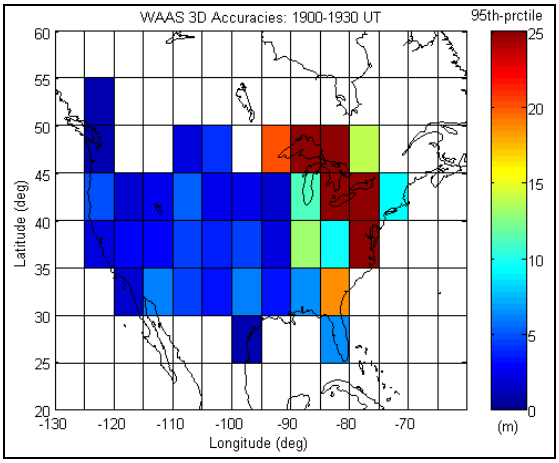

Figure 4.10b: WAAS 3D Positioning Accuracies (1900-1930 UT, November 20, 2003)

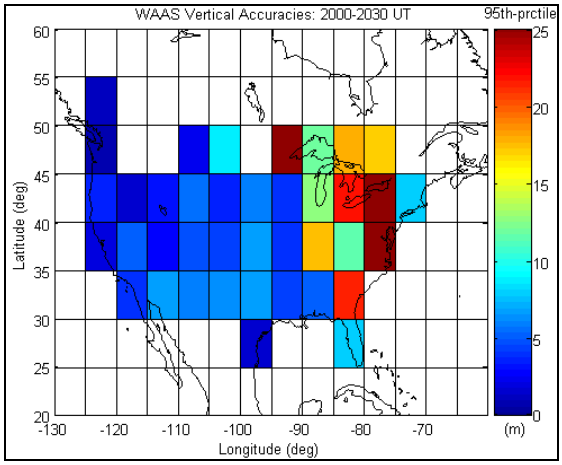

Figure 4.10c: WAAS Vertical Positioning Accuracies (2000-2030 UT, November 20, 2003)

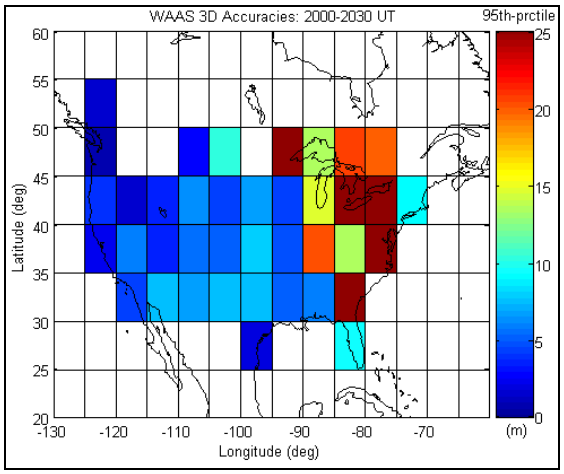

Figure 4.10d: WAAS 3D Positioning Accuracies (2000-2030 UT, November 20, 2003)

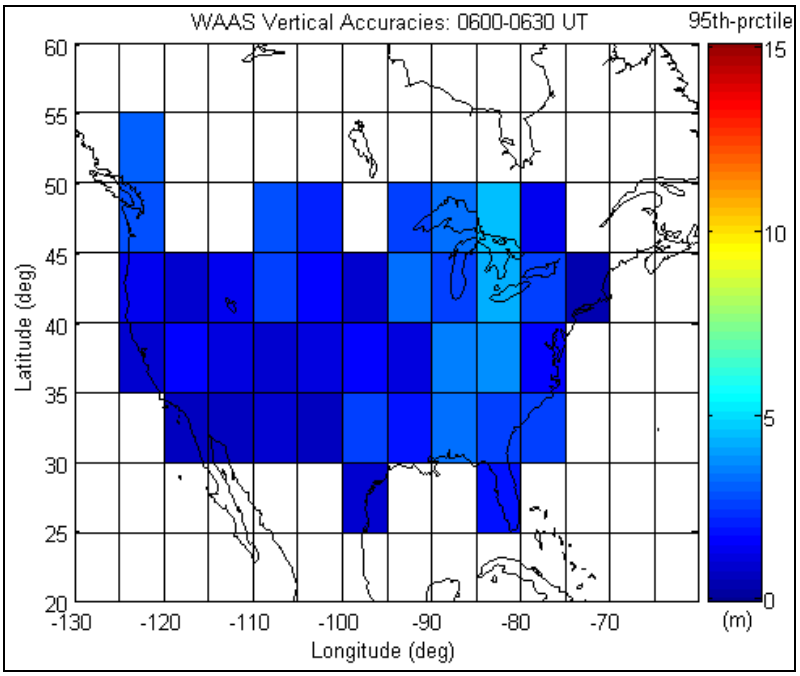

Figure 4.11: WAAS Vertical Positioning Accuracies during Ionospherically Quiet Time (0600-0630 UT, October 29, 2003 with Kp Value of 3)

November 7-10, 2004 Storm

The November 2004 storm was not as significant in terms of the disturbance magnitude as compared to the previous two storm events, but periodic effects were observed for several days. The major characteristics were observed on the four days that will be studied here. Thus, a station was selected in Central US to study the temporal behaviour for this event. Figure 4.12 shows the horizontal and vertical positioning accuracies during the four days at station "AMC2" (latitude: 38.8031° and longitude: -104.5246°). These plots were generated in the same manner as earlier in Figures 4.3 and 4.8. Major accuracy degradations occur on November 7 and continue on to November 8. Thereafter, a second set of increase in error is seen on November 10, but this is not as significant as the first two days. Typical error levels during this period and for this day is about 2 m HA and 3 m VA. But, there are several error spikes in the dataset, especially for the vertical. These error spikes reached about 7 m in the horizontal and 12 m in the vertical, which are correlated with storm effects. Although, there are several significant spikes that are not associated to any storm effects. This is an indication of large TEC gradients over time. The rapid changes in the ionosphere over time is causing the sudden jumps in positioning accuracies because the errors in ionospheric delay seen earlier (Figure 3.24) showed similar variability over time.

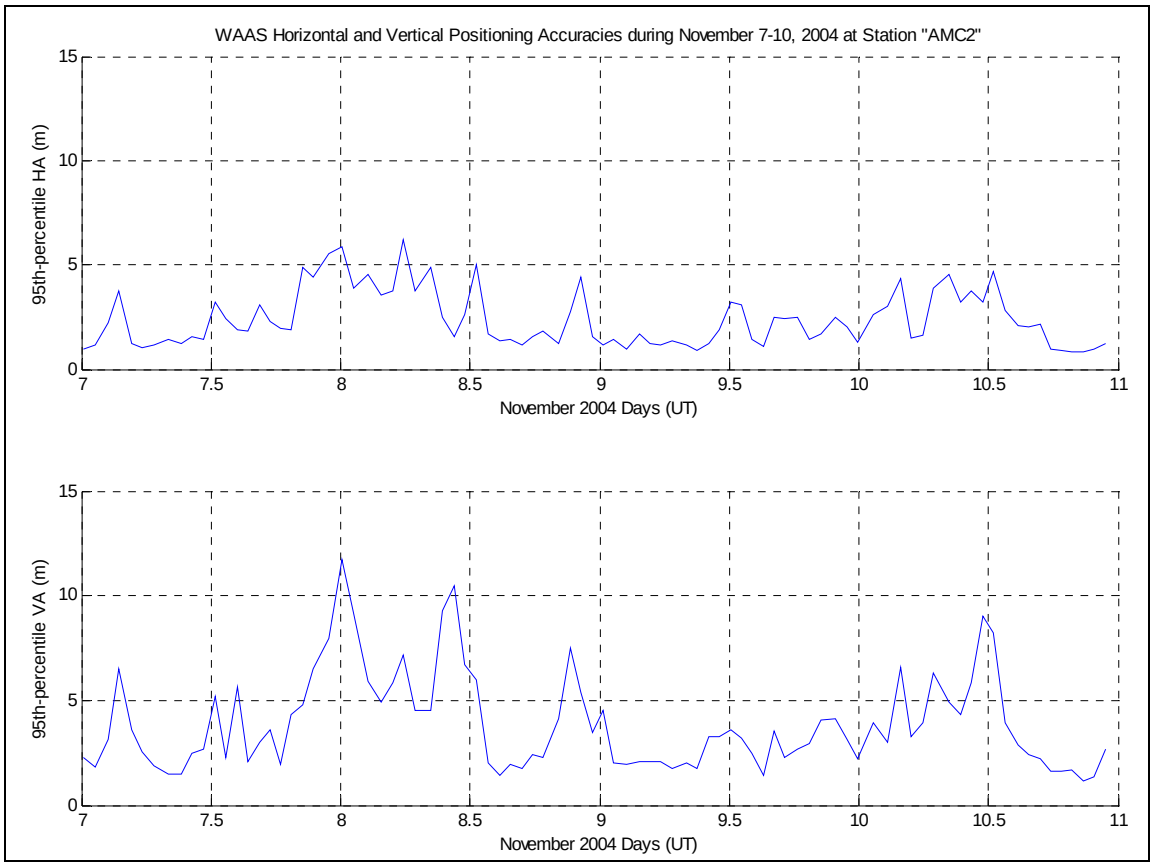

Figure 4.12: WAAS HA and VA during November 7-10, 2004 at Station "AMC2"

The spatial analysis will entail selecting a half-hour time interval where significant errors were seen in the time plots. For this storm event, the best candidate for the analysis would be near the end of the on November 7, and this timeframe would also correspond to the TEC maps shown in Chapter 3. Thus, the 2200-2230 UT time-period was again selected and the data for that were processed (review Subsection 4.1.1 for processing methodology) to compute the final positioning estimates across North America. Figure 4.13 presents the horizontal accuracies for the period. As can be seen from this plot, larger errors are concentrated in western/central regions, where these errors went up to 8

m in magnitude. In the remaining areas the errors were at the typical level of less than 5 m.

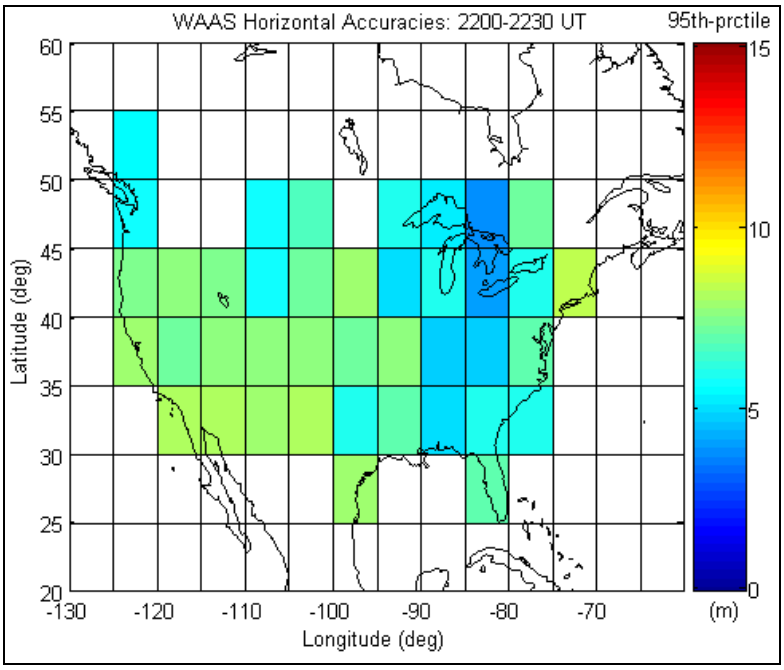

Figure 4.13: WAAS Horizontal Positioning Accuracies (2200-2230 UT, November 7, 2004)

Figures 4.14a and 4.14b are showing the vertical and 3D accuracies on November 7 during 2200-2230 UT, respectively. As expected, the vertical errors are larger than the horizontal ones but are distributed similarly across the CONUS region. These errors reached maximum of 10 m in some cases. Therefore, the 3D errors surpassed 14 m in areas, which is much less than for the earlier storm events where greater than 25 m 3D errors were seen at several places. The results in these plots are reasonably consistent with the WAAS ionosphere errors found in Chapter 3. Positioning accuracy degradations are correlated with the WAAS ionosphere error trends, and the error magnitudes also

agree with the positioning accuracies. The horizontal and vertical component accuracies also were consistent amongst them.

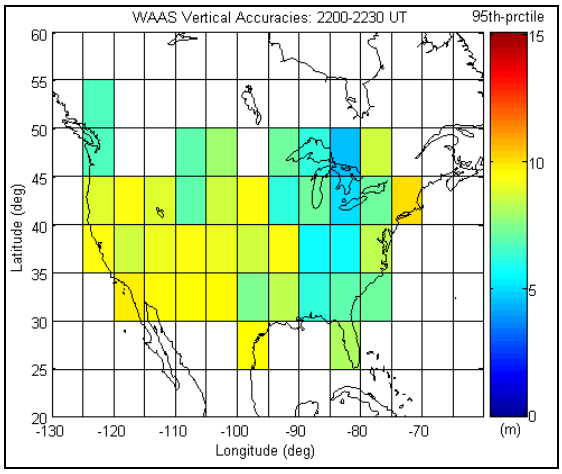

Figure 4.14a: WAAS Vertical Positioning Accuracies (2200-2230 UT, November 7, 2004)

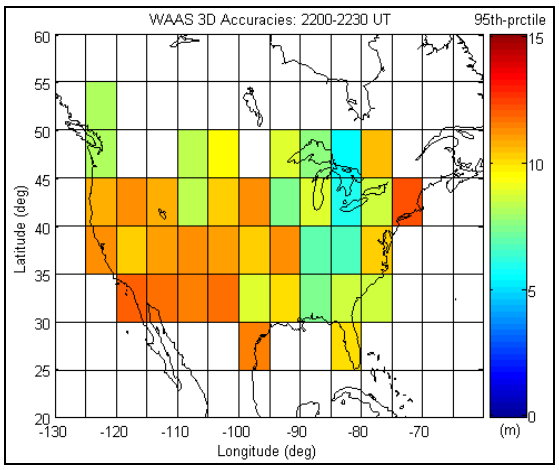

Figure 4.14b: WAAS 3D Positioning Accuracies (2200-2230 UT, November 7, 2004)

4.2.2 WAAS Positioning Reliability

In Subsection 2.10.4, post-correction error bounds were discussed; namely, the HPL and VPL that provide the users with positioning reliability in real-time were introduced. In this subsection, one of the ionospheric storm events seen earlier will be revisited, and the associated WAAS-provided error bounds will be observed to ensure that protection levels were maintained.

The October 2003 storm event presented the most difficult positioning conditions (in terms of accuracy) due to increased ionospheric activity. Thus, this event is of particular interest to observe if WAAS reliability is maintained in extreme conditions such as this.

Figure 4.15a shows WAAS horizontal accuracies for the most active time period (2200-2230 UT on October 30, 2003) during the storm event. Corresponding to that period and locations, Figure 4.15b shows the HPL values. Similarly, Figure 4.15c and 4.15d show the vertical accuracies and the VPL values, respectively. Clearly, the positioning errors are bounded for this period. However, this notion of over-protectiveness re-emerges through these plots. As seen in the case of GIVE values, WAAS tends to be over-protective estimating the ionospheric vertical error. In the same manner, the protection levels are significantly over-bound. There is a positive side to this, in that system reliability will be very rarely infringed, but the downside to this would that users would always expect considerably larger errors than the actual ones.

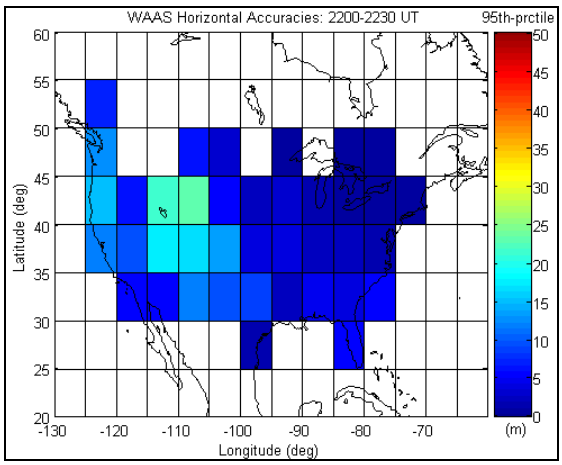

4.15a: WAAS Horizontal Positioning Accuracies (2200-2230 UT, October 30, 2003)

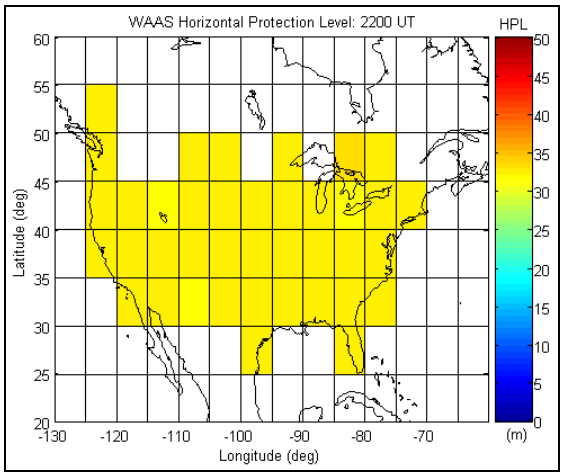

4.15b: WAAS Horizontal Protection Level (2200 UT, October 30, 2003)

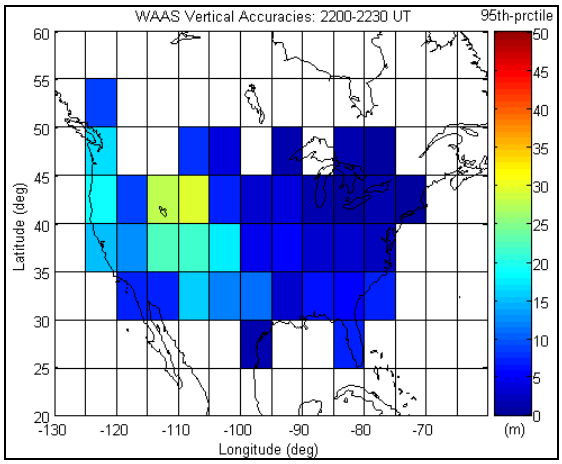

4.15c: WAAS Vertical Positioning Accuracies (2200-2230 UT, October 30, 2003)

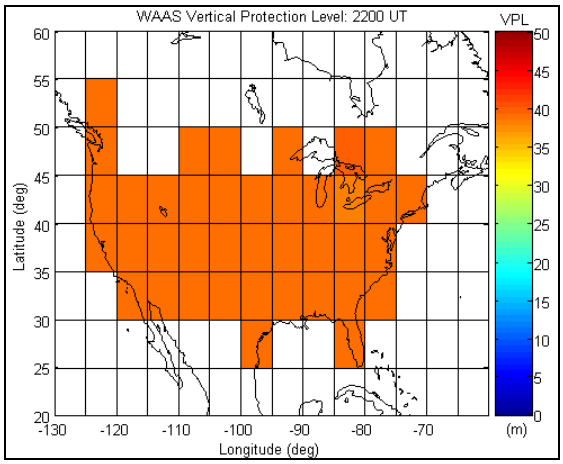

4.15d: WAAS Vertical Protection Level (2200 UT, October 30, 2003)

4.3 Comparison of Results with an Independent Study

A validity check of the study conducted herein would be to compare the results obtained here to a study done previously in this area of research. For this purpose, a comparable investigation from the past recent years was chosen. Namely, *Cannon et al.* [2002] evaluated Wide-Area GPS services, which included the WAAS. Therefore, a comparison in the positioning domain could be conducted using the results from that study in conjunction to the ones done here. For this purpose, a new set of data was obtained from the archives that would be parallel to this independent study. This newly acquired dataset was post-processed using the WADGPS processing methodology discussed in Subsection

4.1.1. The details of how consistency was maintained between the two studies are given below.

Cannon et al., 2002 Study

In this study, three different wide area services were assessed. Namely, the Global Surveyor, OmniSTAR, and WAAS positioning performances were evaluated. This was done in two different modes: real-time (receiver's internal solution) and post-processed (raw GPS data processed with RTCM corrections). The study-period for this evaluation was September 17-18, 2002. Two sets of 24-hour data were collected and processed. The tests took place on the roof of the Engineering Building at University of Calgary (UofC), where an array of antenna pillars (with known coordinates) was pre-existing. To preserve consistency amongst the three different types of WADGPS services, a single type of receiver (NovAtel OEM4) used to compute the final GPS positioning solution using the RTCM corrections, and the only difference for each case was the source of the WADGPS corrections (i.e. Global Surveyor, OmniSTAR, and WAAS) that were fed into the OEM4 receivers. The antenna receiving the GPS signal was a NovAtel 600 model, and the pillar ID for the antenna bearing the WAAS corrected position was S3. Figure 4.16 provides a schematic of the setup for this experiment [*Cannon et al.*, 2002].

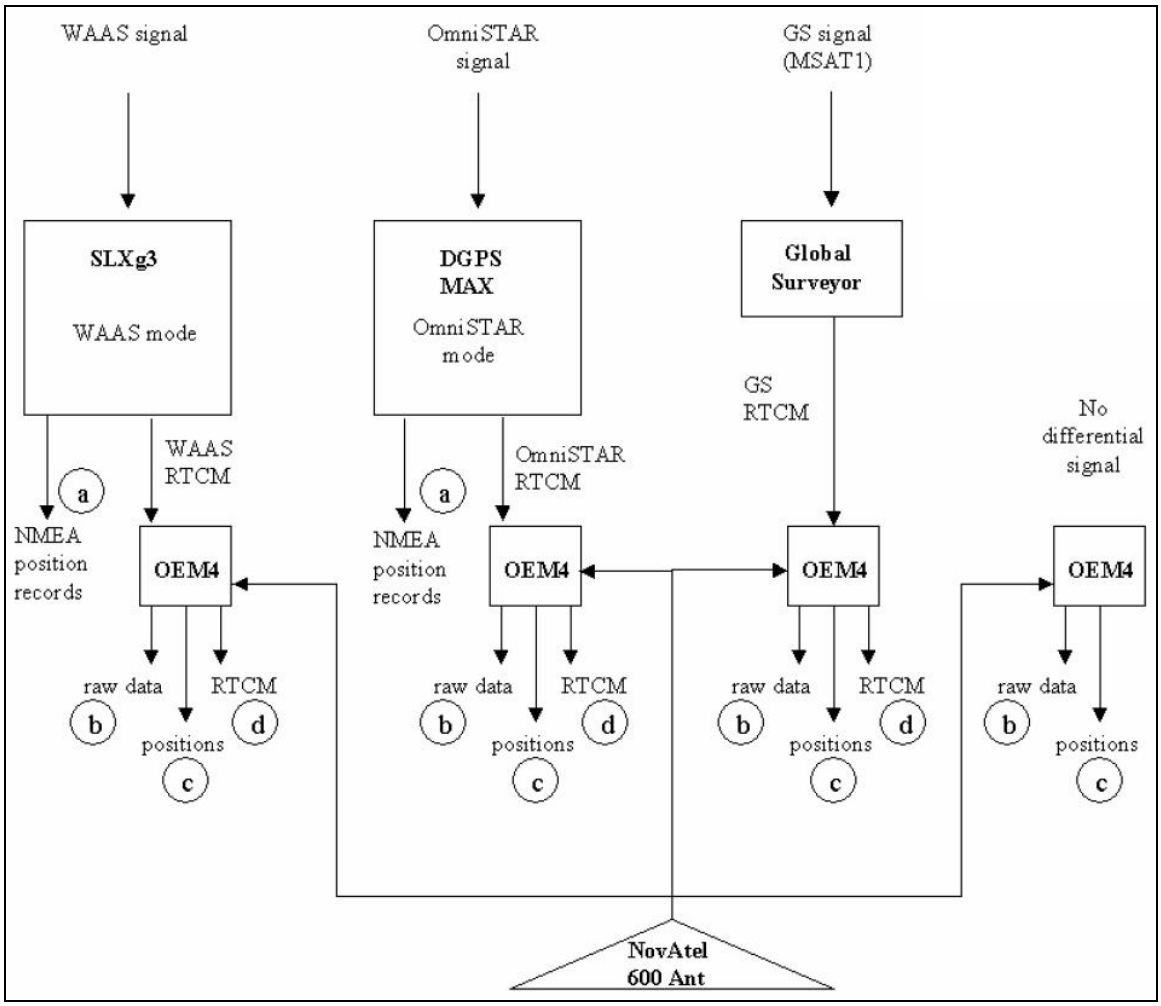

Figure 4.16: Test Setup for Three Different WADGPS Services [*Cannon et al.*, 2002]

Yousuf, 2005 Study

For this purpose, WAAS messages were obtained from the archives of a receiver that continuously logs GPS and WAAS data and is operated by the UofC. Figures 4.17a and 4.17b show the setup of the WAAS-capable receiver and GPS antenna, respectively, on the roof of the Engineering Building at UofC. The receiver was a NovAtel Modulated Precision Clock (MPC) with the OEM4 GPS engine, and the antenna was a NovAtel GPS-600-LB (antenna coordinates are given in Table 4.1).

Figure 4.17a: MPC Receiver Logging WAAS Messages

Figure 4.17b: GPS Antenna Receiving WAAS Downlink and GPS Signals

Table 4.1: Calgary Station Antenna Coordinates [*Henriksen*, 1997]

Pillar ID	X (m)	Y (m)	Z (m)
S3	-1641896.475	-3664879.647	4939966.917
	Latitude (dms)	Longitude (dms)	Height (m)
S3	51 04 45.80932	-114 07 57.99118	1116.867

As can be seen, consistency was maintained for the two studies: from the antenna type and pillar location to post-processing methods and receiver type. For analysis purposes, comparable positioning component accuracies and corresponding statistics were derived. The summary of the results is shown as positioning accuracy statistics given by Table 4.2. These statistics represent the performance levels observed during the September 17-18, 2002 period. By observing the general magnitude of the positioning accuracies, it could be said that typical WAAS positioning performance level was offered during this period. Moreover, the unusual accuracy degradations caused by a disturbed ionosphere was not

seen here, which is indicative of a relatively calm ionosphere during time when data were collected. In terms of comparison between the two studies, the results are similar in magnitude indicating accordance amongst the investigations. Accordingly, this validity check offers the assurance that the methodologies employed here to generate the results are reasonable.

Table 4.2: Accuracy Statistics Comparison with an Independent Study during September 17-18, 2002 at UofC

		Yousuf	*Cannon et al.*
Mean (m)	**N**	0.48	0.44
	E	-0.08	0.04
	U	0.58	1.13
RMS (m)	**N**	0.69	0.86
	E	0.55	0.63
	U	1.16	1.48
Max (m)	**N**	3.50	3.63
	E	2.26	1.94
	U	5.02	4.08
Min (m)	**N**	-2.05	-1.79
	E	-1.96	-1.62
	U	-2.23	-1.70

Chapter 5

Evaluation of WAAS Enhancements

This chapter is an important part of this thesis, as it will present the core research findings of this study. In particular, an investigation of a method to enhance the existing WAAS will be discussed and evaluated in various manners. Firstly, the fundamentals of the enhancement will be presented, which is the modelling of the ionosphere using a denser network covering the same area as the WAAS core network. The mathematical model behind the generation of the enhanced ionospheric grid will be described. Thereafter, a validation scheme will be implemented to verify that the model is within reasonable error bounds. Once the model is deemed adequate for the analysis, the discussion will move onto presenting the results obtained by processing the data from the storm events studied earlier but this time for simulated CWAAS and Enhanced WAAS. Similar to Chapter 4,

the spatial, temporal, and statistical analyses will be conducted for the October and November 2003 storm events. Comparisons in performance will be done between current WAAS, Enhanced WAAS, simulated CWAAS, and single point GPS. The investigation will also include an observability improvement test to illustrate the reason behind the performance improvements for Enhanced WAAS.

5.1 Description of the Ionospheric Model

In order to capture ionospheric features, it is necessary to make truth measurements of the ionosphere that evolve over time. Clearly, higher sampling density of the spatial manifold would mean more accurate representation of the features. The mathematical discretization of this continuous physical phenomenon forms the basis of ionospheric modelling.

The purpose here is to show that using a denser WAAS network and including stations near the proposed CWAAS sites, ionospheric features could be better resolved, especially during intensely disturbed periods. This task of computing a CWAAS approximate model requires modelling of the ionosphere using truth observations acquired from those reference stations (processed data obtained from MIT Haystack Observatory). This dataset was processed as follows. All satellites in view from each station intersect the ionosphere at IPPs (recall the IPP discussion from Subsection 2.11.2). The dataset was provided as single-station files containing the timely GPS observations. These station

measurements were then used as input observations to fit data onto a 2D surface. Basically, a 2D interpolation method at standard grid points was used: z = f(x,y) $\Rightarrow$|model| $\Rightarrow$ zi = f(xi,yi). In this expression, the function z = f(x,y) is considered to define the truth measurements (z being the VTEC value located at x,y representing longitude and latitude, respectively) and zi = f(xi,yi) is the function relating the interpolated values. The model between the two consisted of a 2D cubic function given by Equation 5.1.

$$z = f(x, y) = \sum_{j=0}^{3} \sum_{k=0}^{3} a_{jk} x^j y^k \tag{5.1}$$

where z is estimated using a 16-coefficient (a_{jk}) polynomial that is dependent on zeroth to the third degree of x and y. Note that this is a fit in geomagnetic latitude and solar local time and on an ionosphere shell at an altitude of 350 km above ground (same as in the WAAS standard ionospheric model). From this point forward, it will be referred to as the polynomial model.

It is to be noted that a standardized interpolation technique was adopted here, in that all data points were forced to interpolate at 5° x 5° grid points. This was done to be consistent with the WAAS ionospheric grid. Thus user station VTEC values would be computed from VTEC values at these surrounding standard grid points. A five-minute batch interval was used during the processing of this 2D model. This short time-interval produced effective time resolution yet enough observability existed because the ionosphere over North America could be observed at once by the network. After

generating the 2D model, it was fed into the WADGPS processing scheme given in Figure 5.1 to compute the final station coordinates. This scheme is very similar to the one discussed earlier in Subsection 4.1.1, except that the WAAS ionospheric model has been replaced by this simulated 2D model of the ionosphere that was discussed above.

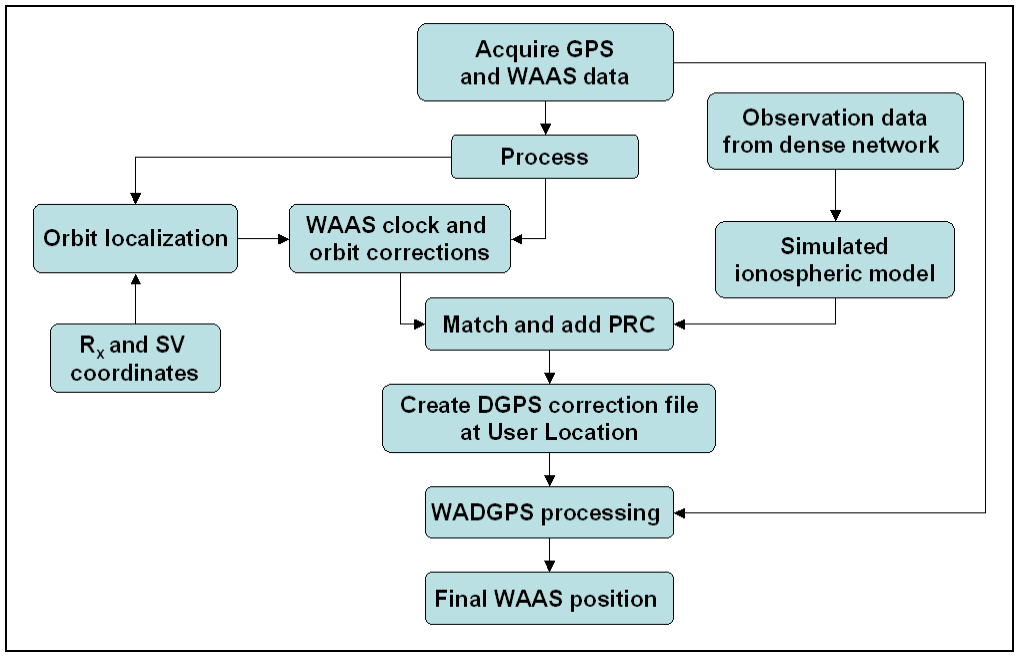

Figure 5.1: WADGPS Processing Flowchart with a Refined Ionospheric Model

5.1.1 Ionosphere Polynomial Model Validation

In order to validate the polynomial model (Equation 5.1), it is necessary to first simulate the current WAAS network by selecting available reference stations that are in close proximity to the existing WRS sites. In this manner, the observability taking place at each reference station will be very similar to the actual North American coverage for the WAAS network. As such, stations chosen as shown by the blue triangles are CORS stations that were used to create the model grid, and these stations were chosen to be

really close (less than 300 km) to the current WRSs so that spatial consistency is maintained, as shown in Figure 5.2. The average distance between the CORS simulation stations and corresponding WRSs is 55.4 km. This validation serves the purpose of showing that the polynomial model simulating the WAAS network is an adequate approximation of the WAAS model. This is why only the WRS model stations were shown below, and later when the enhanced network will be presented, more stations will be simulated, thus fully modelling a denser WAAS network. Consistency would not be preserved if data from actual WAAS WRSs were to be used because then the dense network would include both WAAS WRSs and CORS simulated stations, which would produce biases or systematic errors due to having data from entirely two different networks. This is why actual WAAS WRSs were not used in the simulation. Another point to be noted is the fact that WAAS Alaskan stations were not included in the simulation. This was done for the sake of simplicity/clarity (core network simulation/densification is the focus here), and it was found that those stations up in Alaska have very minimal affect on the WAAS network located in the CONUS region.

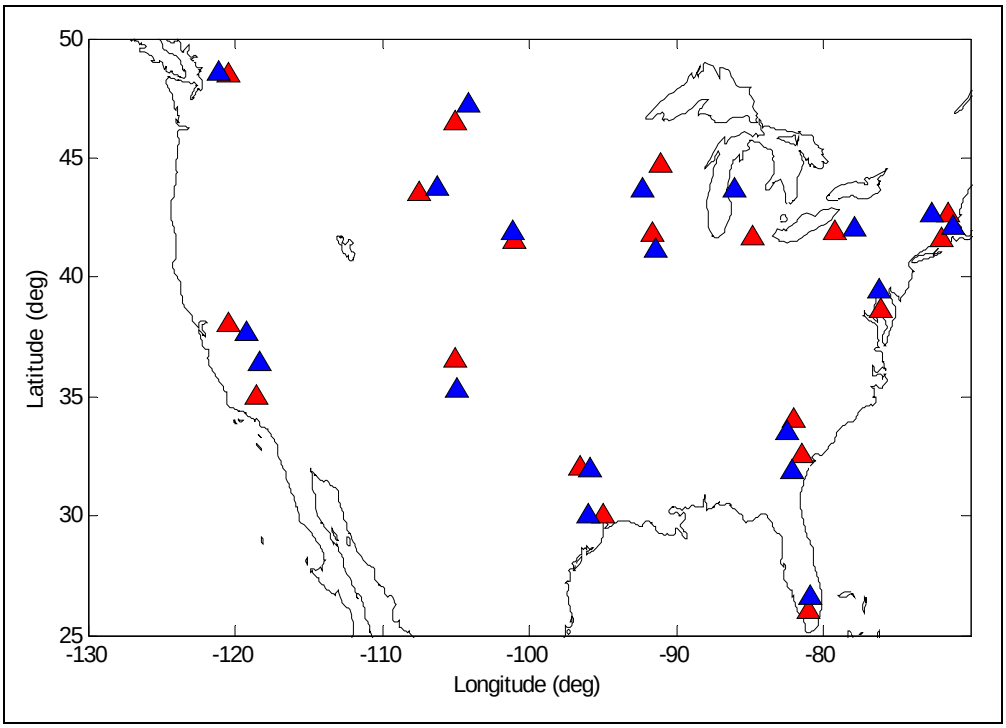

Figure 5.2: Existing WAAS WRS (Red) versus Simulated (Blue) WAAS Network

The validation of the constructed ionosphere model was twofold: 1) observe the difference in vertical ionospheric delay (expressed in VTEC) between WAAS and simulated model predictions at standard IGPs during ionospherically quiet time and 2) observe this vertical ionospheric delay during ionospherically disturbed time. Figure 5.3a and 5.3b respectively show the results of this analysis. The intent here is to show that the modelling technique used to simulate the generation of a WAAS ionospheric correction grid (Equation 5.1) for North America is consistent with the existing WAAS model implemented by the FAA. Improvements in ionosphere modeling can then be investigated for the addition of CWAAS stations or densification of the full North American WAAS network. It is intended that very minimal modelling errors should be introduced with the method implemented here, and that almost all of the noticeable

changes in positioning accuracy and ionosphere corrections are due to adding more reference stations to the WAAS network.

As can be seen from Figure 5.3a (average ionospheric condition was seen during this time period, as discussed in Chapter 3), across North America the difference in VTEC is less than half a metre. These plots were generated by computing the RMSE of the vertical delay during the given time-period for each of the two networks (Existing WAAS WRS versus Simulated WAAS Network) shown in Figure 5.2 and then taking the difference. It would be useful to also show the absolute plots for comparison of the two methods. Figure 5.3b (disturbed ionospheric condition was seen during this time period, as discussed in Chapter 3) shows the errors to be slightly higher than the former, still even during peak storm time the modelling errors are less than 0.5 m. Furthermore, Figure 5.4 is demonstrating that over time VTEC errors (at a single site – its location is shown by a black circle in Figure 5.3a) are consistently within the half-metre error bound. This plot was generated by computing the vertical delay at the given station during the October 2003 storm for each of the two networks (Existing WAAS WRS versus Simulated WAAS Network) shown in Figure 5.2 and then taking the difference. Therefore, it is safe to assume that the polynomial model errors are minimal and that any improvements observed from this simulation are very close to those expected from CWAAS or other enhancements to the WAAS network.

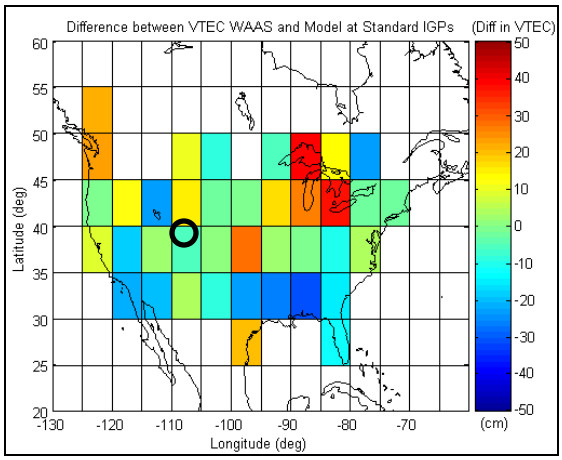

Figure 5.3a: Difference between VTEC for WAAS Ionosphere Model versus the Polynomial Model at Standard IGPs (0600-0630 UT, October 30, 2003)

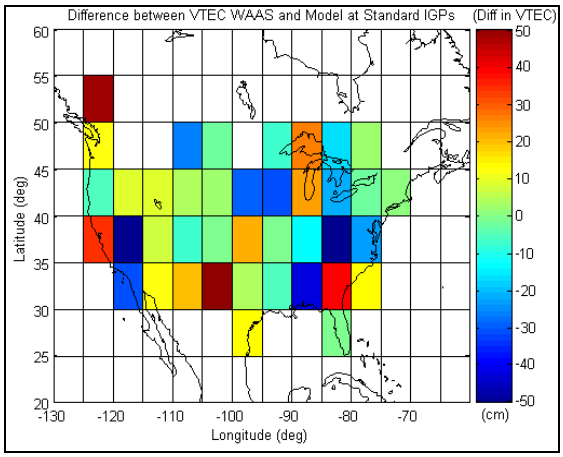

Figure 5.3b: Difference between VTEC for WAAS Ionosphere Model versus the Polynomial Model at Standard IGPs (2100-2130 UT, October 30, 2003)

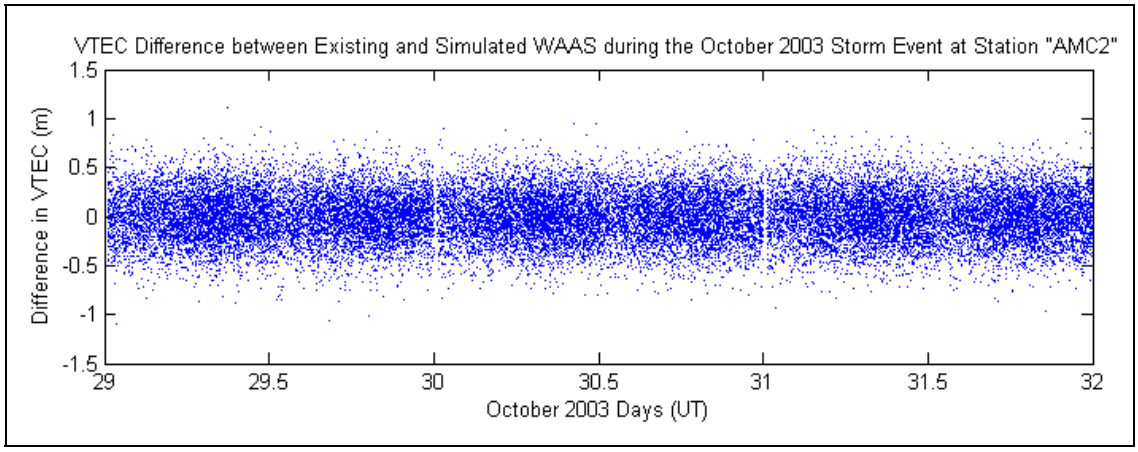

Figure 5.4: VTEC Difference between Existing and Simulated WAAS during the October 2003 Storm Event at Station "AMC2" for all Satellites in View

5.2 CWAAS Configuration Analysis

The discussion in this section involves studying the effects of adding the proposed CWAAS reference stations. In particular, a better-sampled ionosphere model is computed, one in which additional Canadian reference stations are used to derive the ionosphere estimates at WAAS IGPs. Positioning accuracies are then computed using this new model, as opposed to the current WAAS ionosphere model. WAAS clock and orbit corrections remain unchanged. Before reporting any results for this section, it will be shown that the ionosphere modelling technique used to simulate the proposed CWAAS configuration and grid interpolation is consistent with the WAAS current model. This will be accomplished by demonstrating that very minimal error exists due to the inadequacy of this simulated WAAS model. Once this is established, it is possible to spatially simulate the WAAS and/or CWAAS networks using CORS stations in the vicinity of existing and proposed WAAS WRSs. First, the November 2003 storm event will be used to observe how having the proposed CWAAS stations in Eastern Canada would strengthen the WAAS ionosphere model. A simulated “user” station located at the centre of the CWAAS network will be used to study the improvements during intense ionospheric activity. The last element of study in this regard will be to observe the improvements spatially and if the additional CWAAS stations would have any positive impact on performance in the west, especially during geomagnetic storm situations.

5.2.1 CWAAS Evaluation in Eastern Canada

The model network used for this purpose is given in Figure 5.5 and shows all the model stations used to simulate CWAAS and overlaid on top are the actual WAAS WRS locations and proposed CWAAS reference stations (refer to station locations given in Chapter 2 discussion of CWAAS). This is to show that the model stations were selected on the basis that spatially it resembles the WAAS + CWAAS network in Eastern Canada scheduled to be completed in 2006. The CORS site "VALD" (latitude: 48.80971° and latitude: -77.5642°), located in Val D'Or, Quebec, was chosen to be the "user" test station because its location would have the optimum effect from the proposed CWAAS network because it is at the centre of this network.

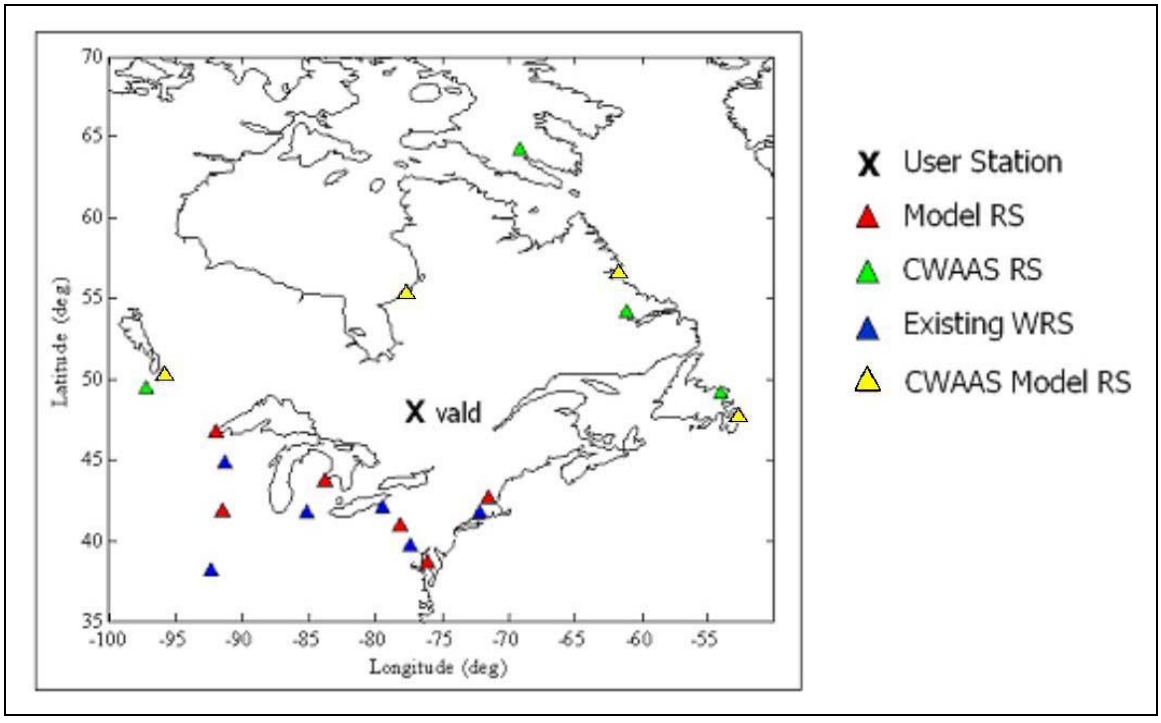

Figure 5.5: Model Network for CWAAS Assessment in Eastern Canada

Using this model network, it is possible to spatially model the ionospheric behaviour over time. An important difference between this model network and the current WAAS network is the fact that WAAS does not have existing WRSs in Eastern Canada, and so it has to apply a mathematical extrapolation; the simulation will enable the inclusion of observations from actual reference stations into the ionosphere model. The November 2003 storm event was used for these testing purposes, since a phenomenon of interest occurred in Eastern Canada during this event (see Chapter 3). Figure 5.6 presents the results obtained as a time-series plot during this event for the following four different methods (the numbers in the brackets in Figure 5.6 refer to the four positioning modes below):

1) Single Point

This is the most basic method of GPS positioning. It involves simply taking the raw L1 pseudorange observations and computing the best estimated solution. Standard atmospheric models were applied: the broadcast model for the ionosphere and the Hopfield model for the troposphere [*Hopfield*, 1969]. Additionally, no carrier phase smoothing was applied during processing.

2) WADGPS using Current WAAS Corrections

This is a WADGPS method that augments the single point solution in terms of accuracy with (existing current) WAAS provided corrections for clock, orbit and ionosphere. In theory, this solution should be better than single point. The ionospheric model was obtained from the WAAS grid, and the tropospheric model used was Hopfield.

3) WADGPS using Simulated WAAS Network

Basically this is the same as the method 2, except that the WAAS ionospheric model was replaced by the Simulated WAAS ionospheric model using reference stations approximating the current WRS configuration (red triangles in Figure 5.5). The WAAS clock and orbit corrections are used.

4) WADGPS using Simulated CWAAS Network

This is again similar to method 2, but this time the ionospheric model was generated from the Simulated CWAAS model network (yellow triangles in Figure 5.5). The WAAS clock and orbit correction sets are used.

Note: For all four methods the processing was done using a mask angle of 10°; HDOP filter was set to 2.3 and PDOP at 3.0.

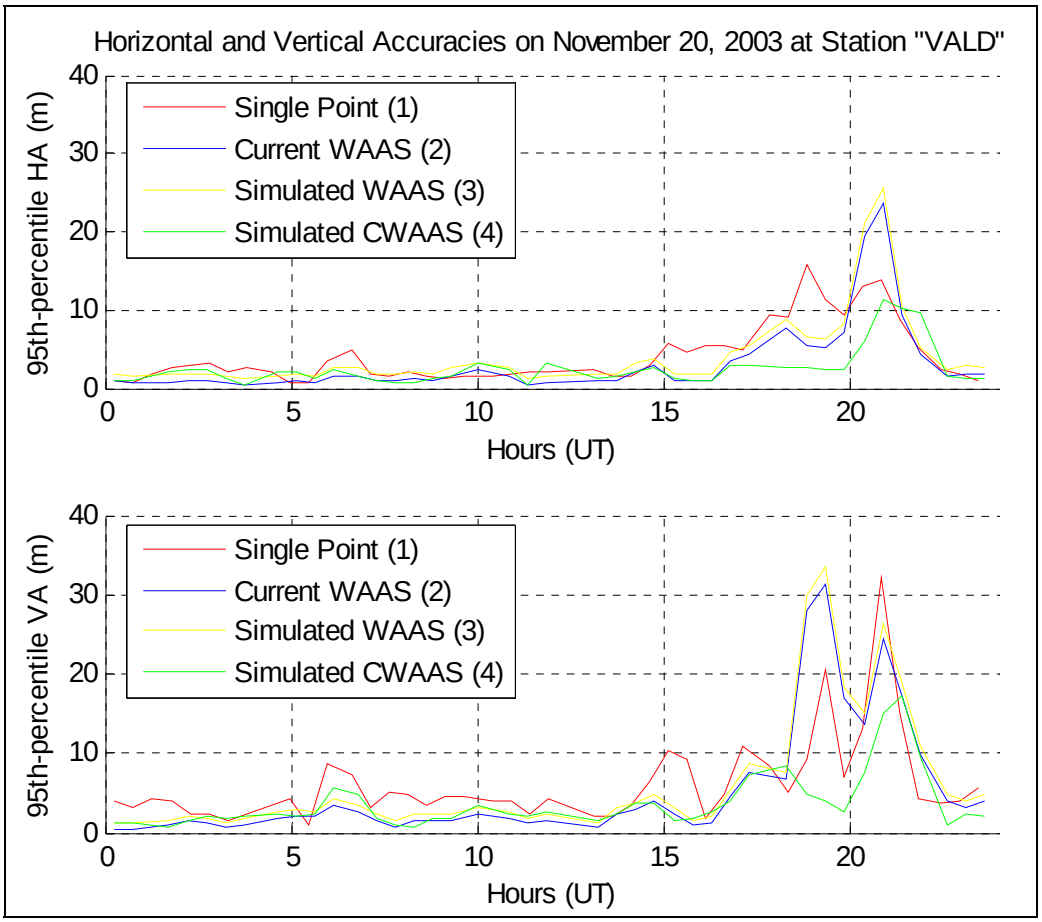

Figure 5.6: WAAS HA and VA on November 20, 2003 at Station "VALD"

Thus, a second purpose exists in showing this plot; that is to compare the different methods and observe how the current WAAS compares to the simulated WAAS in the positioning domain. Recall that the Simulated WAAS was devised by taking ionospheric truth observations from CORS stations and applying a 2D cubic function to interpolate the data at standard grid points. On the other hand, the current WAAS model entails using all observation data surrounding the WRS and applying a planar fit at every IGP to compute an ionospheric delay estimate.

The first comment to be made is about the sharp increase in error (for both HA and VA) around 2000 UT for all four methods. This sudden degradation in accuracy is due to SED because similar peaks were seen in time series plots for ionospheric delay at around the same time, and it has also been shown in numerous spatial plots earlier in Chapter 3. Typically the accuracies are better than 5 m (at the 95th-percentile), but SED causes the errors to increase to over 30 m in some cases. A summary of the statistics for this dataset is provided in Table 5.1. The statistics were separated into quiet and active ionospheric times to observe the level of degradation in positioning accuracy once the storm commenced. In general the RMSE went up about 100% during the disturbed periods.

Table 5.1: Overall HA and VA Positioning Statistics on November 20, 2003 at Station VALD for Quiet (0000-2000 UT) and Active (2000-2400 UT) Ionosphere

		Single Point		Current WAAS		Simulated WAAS		Simulated CWAAS	
		Quiet	Active	Quiet	Active	Quiet	Active	Quiet	Active
HA (m)	MEAN	2.53	5.34	1.29	4.32	1.43	4.41	1.02	3.12
	RMS	3.12	6.09	2.87	5.96	3.02	6.31	1.34	2.49
	STD	2.91	5.68	2.48	5.79	2.68	6.02	0.89	2.16
	95%	6.79	12.49	7.87	10.92	7.92	11.06	2.24	6.31
	MAX	5.13	30.46	4.96	23.75	5.23	24.32	4.98	10.42
	MIN	0.13	7.87	0.03	5.35	0.07	5.74	0.03	2.56
VA (m)	MEAN	3.46	6.45	3.12	5.64	3.42	5.75	1.56	2.89
	RMS	4.12	7.29	3.98	6.73	4.06	6.84	1.67	3.45
	STD	3.65	6.83	3.42	6.24	3.63	6.44	1.23	3.11
	95%	7.56	14.25	6.45	13.12	6.70	13.56	2.86	7.49
	MAX	6.23	54.63	5.87	26.61	5.96	28.01	5.23	12.07
	MIN	0.32	11.54	0.06	7.23	0.11	7.53	0.13	2.89

In terms of comparing between the methods, the most interesting point about this plot is how single point performs better horizontally than WAAS during 2000-2200 UT. One possible explanation for this is that since WAAS has no WRSs in Eastern Canada (thus no actual observations from there are input for the WAAS model), coverage is so minimal and only extrapolated model is available over that region, WAAS model is not as accurate as broadcast model for single point. This is especially the case during intense ionospheric times, but in general WAAS performs better than single point since typical accuracies (during ionospherically quiet times) are greater. The notion could be further investigated with the aid of ionospheric correction data. Thus, plots were generated showing the ionospheric delay accuracies for WAAS versus Broadcast (Figure 5.7). In both cases the vertical delays are being underestimated, and the differenced values are mostly negative. During the ionospherically quieter times, WAAS values are more accurate but during intense times the Broadcast delay values are closer to truth. This is sort of the scenario that was seen in the positioning plots above, where single point was doing more accurate WAAS during 2000-2200 UT.

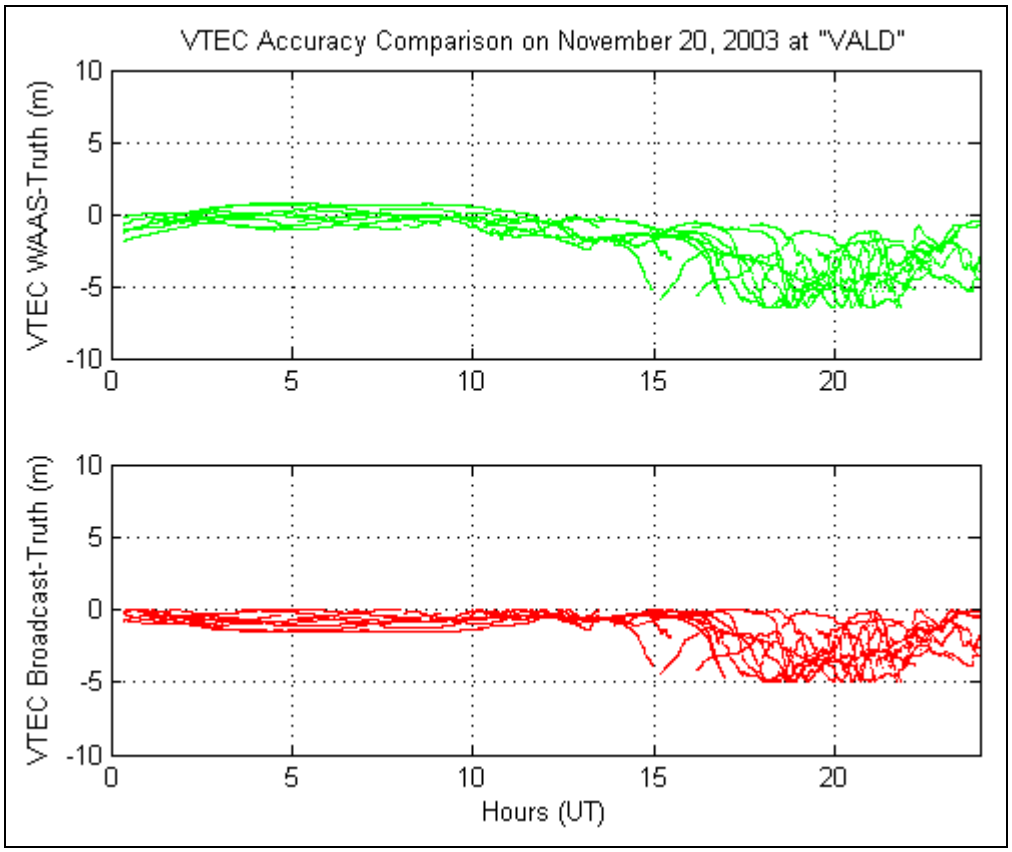

Figure 5.7: VTEC WAAS vs. Broadcast Accuracy on November 20, 2003 at Station "VALD"

Nonetheless, it is noticeable that the two variants of WAAS (simulated versus existing) are very similar in the positioning domain, which is indicative of the fact that the 2D interpolation used to simulate the WAAS ionosphere model is valid. This was also shown earlier in Subsection 5.1.1 using a VTEC-difference spatial map but in the correction domain.

Finally, simulated CWAAS has performed better than the other methods; this is mainly because in this case actual observations in the vicinity of "VALD" went into the model. In the other cases (current and simulated WAAS – methods 2 and 3), only a mathematical

extrapolation is used to spatially model that area in terms of ionosphere, and therefore does not adequately capture the true physical phenomenon.

5.2.2 WAAS/CWAAS Evaluation in North America

A broader model network was devised to assess the full WAAS/CWAAS station configuration. It included CORS stations that were near the existing WAAS reference stations and those that were near the proposed CWAAS stations. This model network is shown in Figure 5.8. This is what the full WAAS/CWAAS would look like in 2006 when all of the CWAAS stations would have been deployed. Previously, it was shown that CWAAS would offer better performance for the ionosphere model in Eastern Canada, but it would also be interesting to see if there are any benefits in other regions as a result of having the new sites in the east. Accordingly, the main intention in simulating this scenario is to observe the positive impact (if any) of CWAAS in Western Canada during ionospheric storm events.

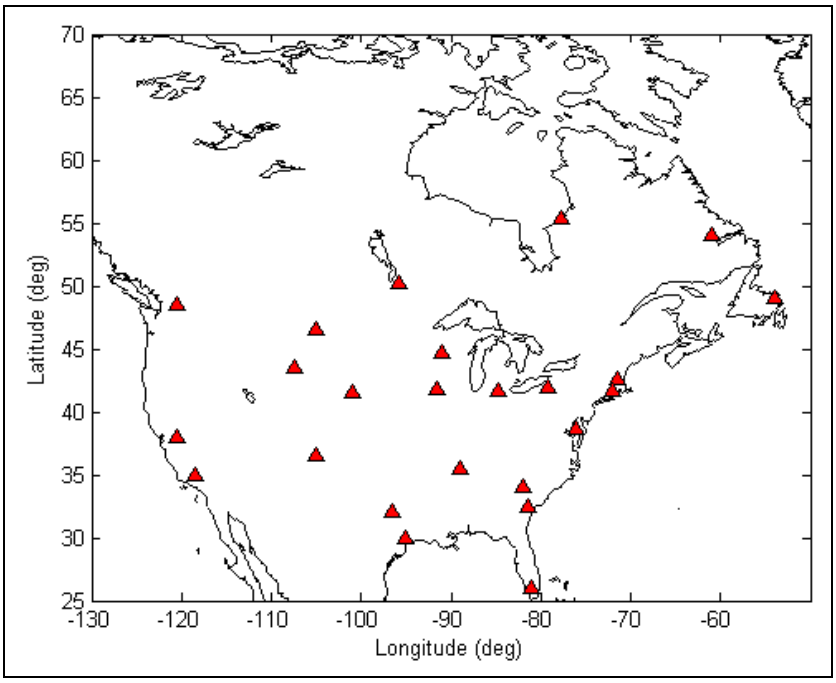

Figure 5.8: Full Configuration of WAAS + CWAAS Model Network

Using the truth data from the above network and applying a 2D cubic fit across North America, the ionospheric model for a given epoch was created. Even though the WAAS uses a local bi-linear fit at each IGP and a global 2D cubit fit is used here, the modelling errors due the dissimilar fits are insignificant, as was shown in Subsention 5.1.1. The following positioning spatial maps present the 95th-percentile positioning accuracies during 2200-2230 UT on October 30, 2003. As will be seen later in the time series plots, during this time-interval major error peaks were seen. The horizontal, vertical and 3D accuracies are respectively given by Figures 5.9, 5.10 and 5.11.

Clearly, CWAAS is not improving the horizontal positioning performance in Western Canada; the errors remained constant even after adding the additional reference stations. By observing the vertical and 3D errors, it could be said that slight degradation in

accuracy occurs after adding the CWAAS reference stations. It should not be assumed that the additional stations are having a negative impact on vertical accuracy. Rather, it is suspected that the slight degradation is caused by modelling errors that were discussed earlier and shown in Figures 5.3a, 5.3b and 5.4. Hence, if the modelling technique employed here and the one used by WAAS were exactly the same, there would be no degradation, as in the horizontal case; this discrepancy is only apparent in the vertical because height determination is more sensitive to ionosphere modelling errors than the horizontal components. In general, CWAAS would not improve performance for users in Western and central Canada. Thus, CWAAS development should include some reference stations in the west as well, to allow wide-area positioning benefits across Canada.

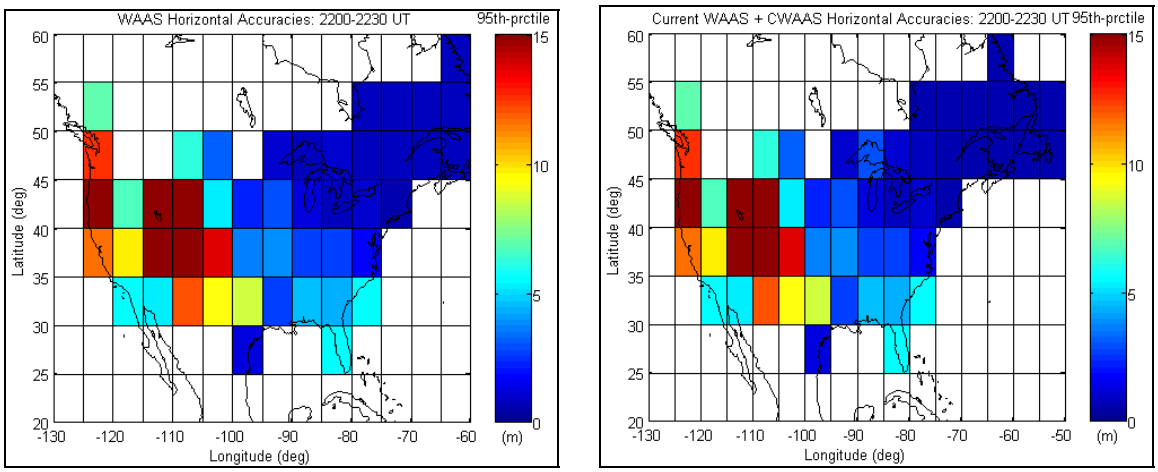

Figure 5.9: WAAS vs. WAAS + CWAAS Horizontal Positioning Accuracies (2200-2230 UT, October 30, 2003)

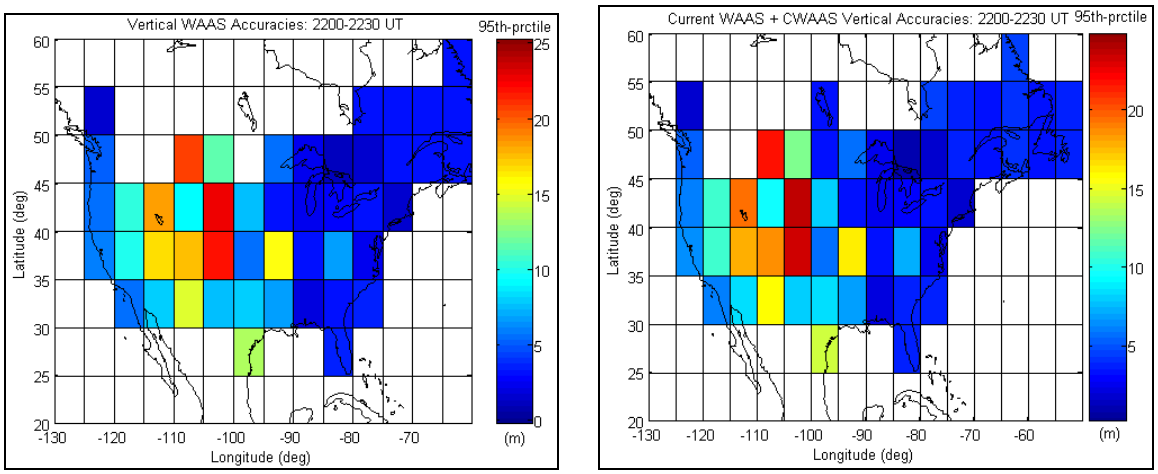

Figure 5.10: WAAS vs. WAAS + CWAAS Vertical Positioning Accuracies (2200-2230 UT, October 30, 2003)

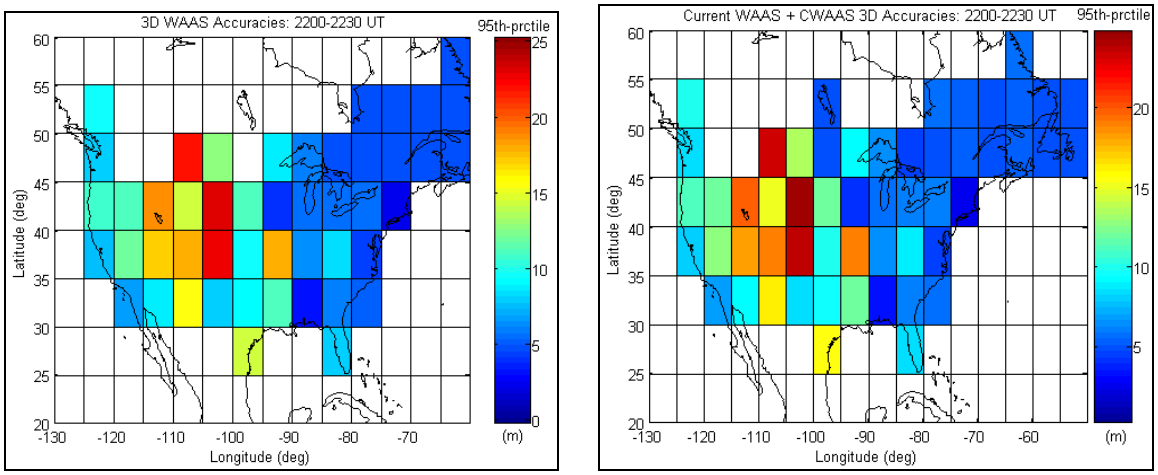

Figure 5.11: WAAS vs. WAAS + CWAAS 3D Positioning Accuracies (2200-2230 UT, October 30, 2003)

5.3 Assessment of the Enhanced WAAS

This final set of results will entail studying a hypothetical network that will model the ionosphere using more than 50 reference stations (Figure 5.12). It is to be noted that this network will include simulated WAAS and CWAAS stations (to approximately simulate the expected 2006 CWAAS infrastructure) as well as additional evenly distributed CORS stations to increase the station density throughout North America. The selection of the simulated stations was primarily based on proper spatial coverage and even distribution of sites throughout the network. However, it wasn't always possible to maintain these criteria because sometimes full datasets weren't available for the desired stations and time period; thus, the densified network couldn't be optimally distributed and some areas of the network possess uneven coverage.

The standard WAAS ionospheric model will be replaced by the polynomial ionosphere model (Equation 5.1) that was simulated using a denser network, similar to that computed in the previous section, and the clock/orbital error models will remain the same in the WAAS correction domain. The intent is to show how this refined ionospheric model would drastically improve WAAS performance in terms of accuracy due to its denser sample of the true physical process of the ionosphere. Thus, the so-called Enhanced WAAS will be put to the test during one of the storm events discussed throughout this research. This scenario is rather close to reality as future densification of the WAAS network is on the horizon and is being planned by the FAA and Raytheon. The current phase of the WAAS would incorporate four new stations in Alaska, four in Canada

(CWAAS), and five in Mexico. As well, additional reference stations may be included in the core CONUS region but this is not definite, and so the details have not been disclosed yet [*Cormier*, 2005].

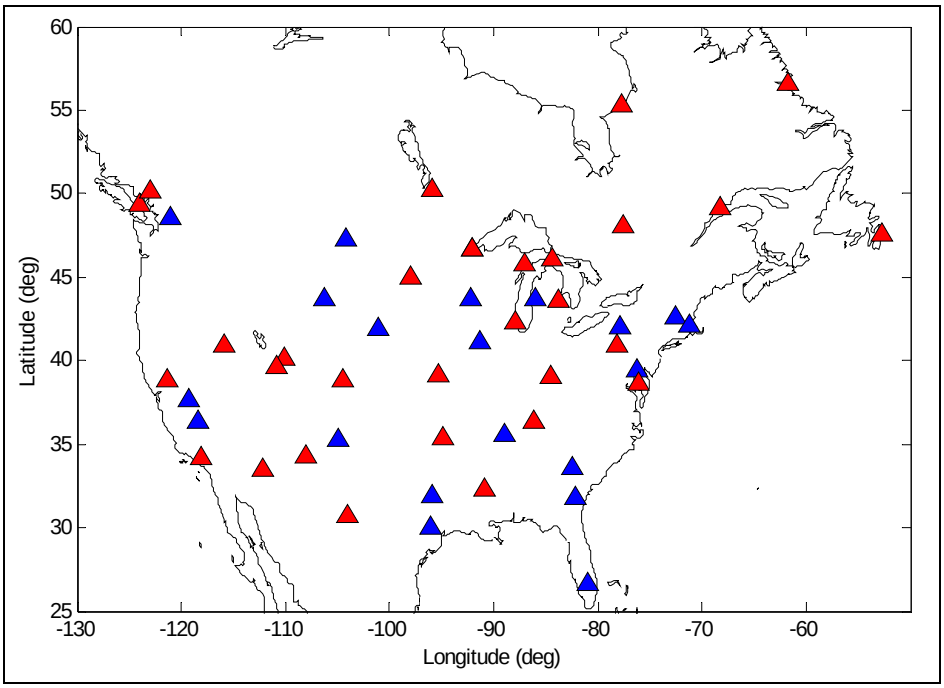

Figure 5.12: Enhanced WAAS Model Network Using 50+ Reference Stations (Blue Triangles are Stations Modelling Existing WAAS WRSs and Red Triangles are Additional Model Stations to Densify the Network and includes CWAAS RSs)

5.3.1 Observability Improvements for the Enhanced WAAS Network

An important aspect to investigate is the observability improvements to be gained via this densification. As such, a partial (for the sake of simplicity and clarity in the plots) area of this network in North America was chosen to study the increase in observability. Shown below in Figure 5.13 are five stations near the Great Lakes that are part of this Enhanced WAAS network. The four blue triangles represent the additional stations added to the

simulated network to further increase density and the red signifies a station that is approximating the location of one of the existing WAAS WRSs. The intent here is to provide an example of the observable redundancy that could be gained if WAAS were to possess more reference stations across North America.

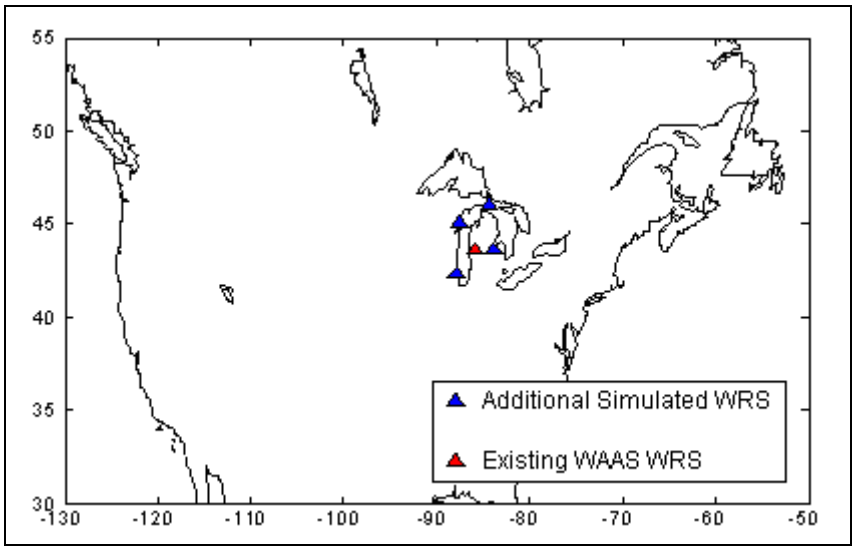

Figure 5.13: Partial Enhanced WAAS Network near the Great Lakes

One way to study measurement redundancy is to look at the IPPs for each station. And so, two plots were created: 1) the IPPs for the single WAAS WRS in the area are plotted (Figure 5.14) and 2) the IPPs for all five WRSs in the area are plotted (Figure 5.15). Note that the gridline intersections in these plots represent WAAS IGPs (5° x 5°). Clearly, the redundancy would increase by a factor of five (give or take a few coincident IPPs), and visually the second plot shows significantly more satellite observations than the first. Thus, it is easily conceivable that for the full network configurations significant observability improvements would exist. However, performance improvements are not solely dependent on network density. There is another aspect to obtaining benefits in the

positioning domain and that is the spacing of the IGPs. This issue will be further discussed later in the chapter.

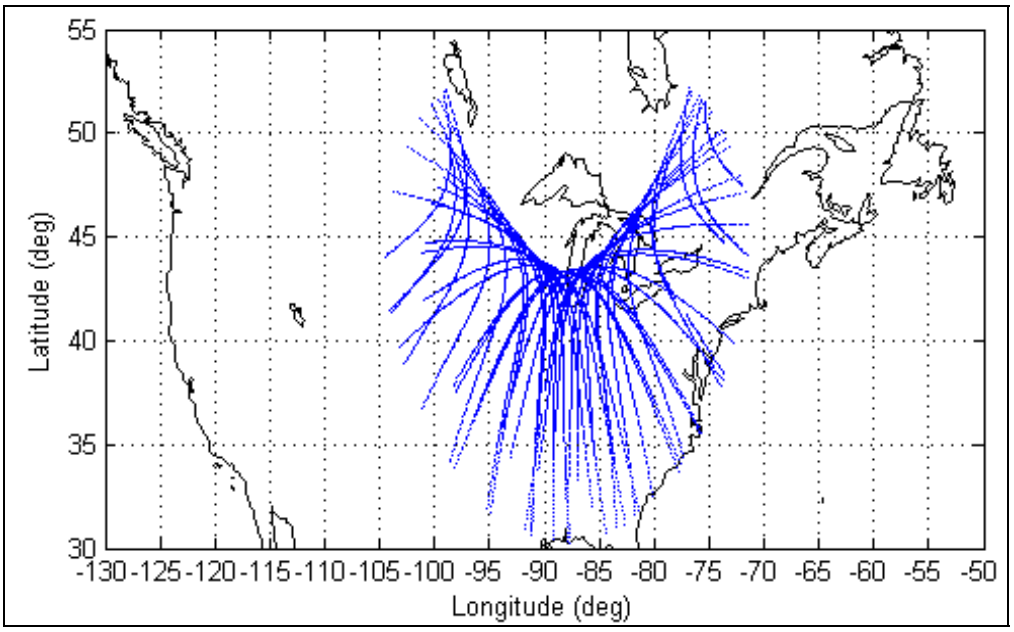

Figure 5.14: Single Station IPP Distribution Plot

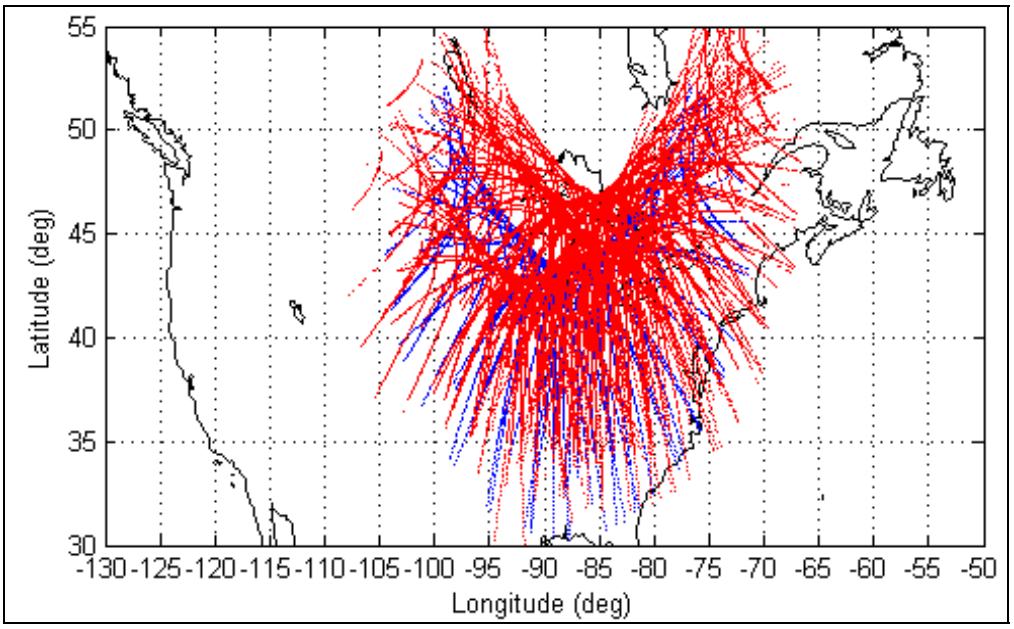

Figure 5.15: Multiple Station IPP Distribution Plot

A spatial analysis, similar to the ones in earlier sections, of the Enhanced WAAS will be conducted first. The analysis involves comparing the 95^{th}-percentile horizontal (Figure 5.16) and vertical (Figure 5.17) accuracies of the current WAAS against the Enhanced WAAS. This analysis was done by first creating model of the ionosphere for the given days using the polynomial model and ionospheric truth data as inputs. This provided an ionospheric grid (5° x 5°) similar to that of WAAS, except that this model was defined by many more observations (due to higher number of reference stations). Then at user "test" stations, both WAAS and Enhanced WAAS positioning were conducted. Figure 5.18 shows a map of the user "test" sites overlaid on top of the simulated reference stations. There is independence between the user "test" stations and the model stations, but sometimes the "test" stations had to be located fairy close to model stations because either data weren't available (data missing on archived web server) or better candidate stations did not exist. Nonetheless, in general the two sets of stations are reasonably spaced apart to provide independent solutions. As shown in the above two plots, the observability would improve significantly for the denser network, thus increasing redundancy and in turn strengthening the positioning solution. It wouldn't be practical to show the observability of the (full) dense network because the satellite traces would be so dense that the curves would overlap and no patterns would be visible. This is why only a portion of the network observability was presented to observe the improvements.

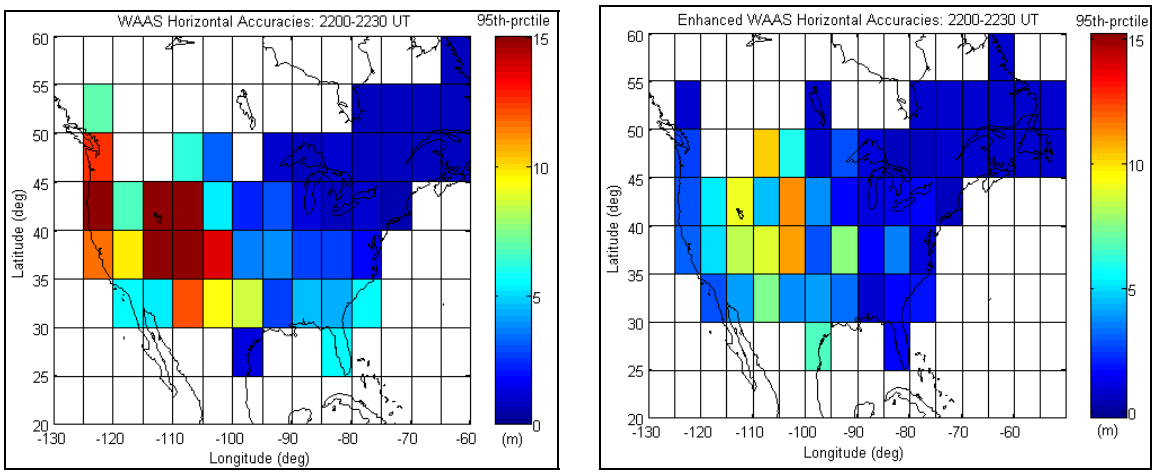

Figure 5.16: WAAS vs. Enhanced WAAS Horizontal Positioing Accuracies (2300-2330 UT, October 30, 2003)

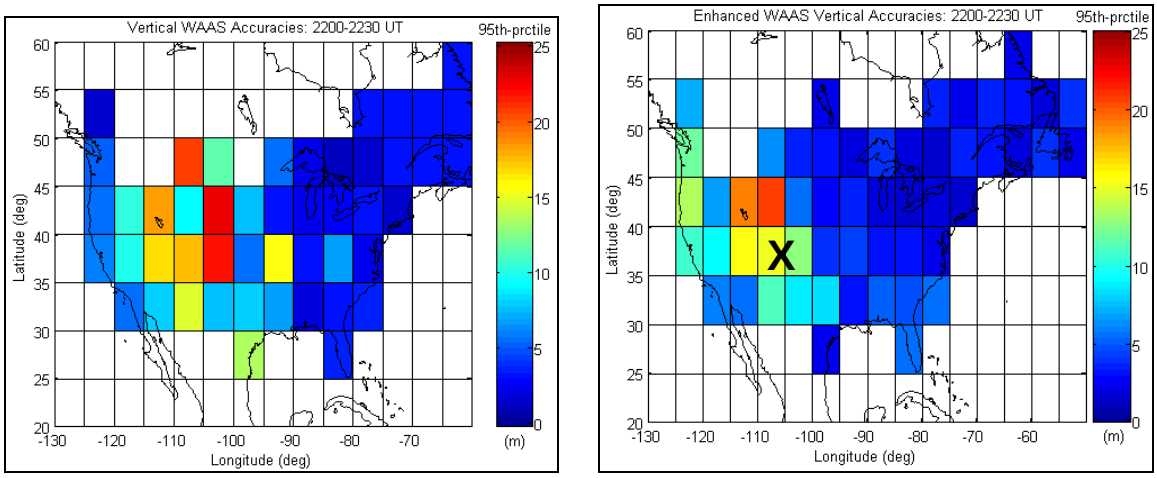

Figure 5.17: WAAS vs. Enhanced WAAS Vertical Positioing Accuracies (2300-2330 UT, October 30, 2003)

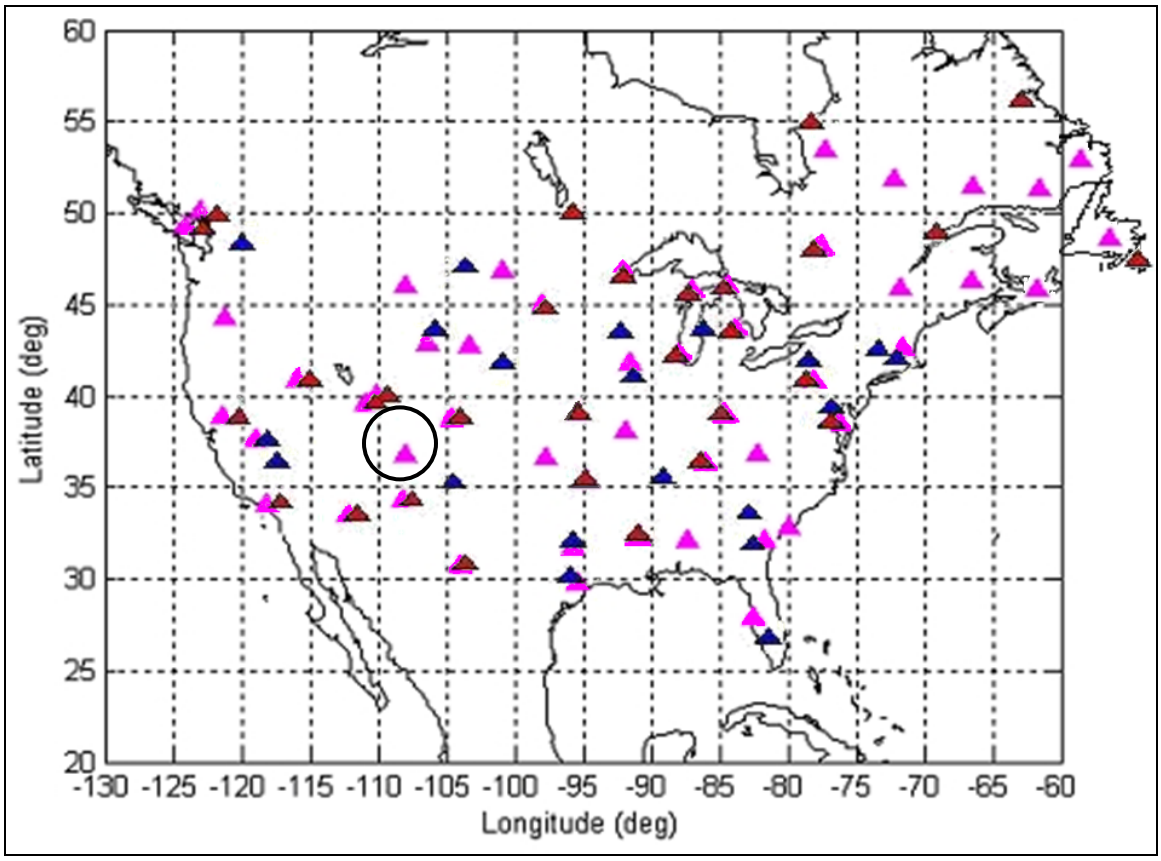

Figure 5.18: Map of User "Test" Sites (magenta triangles) Overlaid on top of the Simulated Reference Stations

Both in the horizontal and in the vertical, Enhanced WAAS offered much better performance levels as compared to current WAAS. For instance, at five stations the HA exceeds 15 m for current WAAS but this is true at only one station for the latter; also, the overall positioning errors are significantly reduced using the refined model of the ionosphere. Furthermore, maximum VA for current WAAS is about 23 m but its counterpart provided errors not exceeding 17 m across North America.

After this spatial analysis, it is interesting to study the benefits temporally. As such, a station ("AZCN" shown by a black cross Figure 5.17 and a black circle in Figure 5.18) was chosen directly beneath the SED. Once again the accuracies are plotted as a time series for this single station, over three days (the full October 2003 storm event). Accuracy plots of other time intervals for this event can be found in Appendix D.

Figure 5.19 shows the 95th-percentile HA and VA for single point, current WAAS and Enhanced WAAS over time during October 29-31, 2003. These plots are generated by computing the 95th-percentile over half hour periods for each of the three methods and representing them at the centres of those half hours. This helped in removing some of the noise components in the dataset. Note that for all positioning solutions were computed using a mask angle of 10°; HDOP filter was set to 2.3 and PDOP at 3.0. The results presented in the figure below are from a station ("AZCN", latitude: 36.8398° and longitude: -109.9251°) that was directly beneath the SED while it traveled through North America. As can be seen, both vertical and horizontal positioning accuracies (computed by taking the square root of the sum between errors in northing and easting) were poor near the end of October 29 and 30 (UT) in all three cases; the accuracy degradation periods in those instances were over 12 hours in length.

The peaks seen in VTEC plots are also present in the positioning plots, which is indicative of the fact that ionospheric error is the major driving force behind the positioning error. Near the end of the first and the second day of this event, the errors rose to ten times the typical level. As expected, single point would perform the poorest

compared to the rest; although, there is one instant (second VA peak) where it performs better than current WAAS. This irregularity has been explained in Subsection 5.2.1.

Evidently, there is considerable improvement offered by Enhanced WAAS in both the horizontal and vertical accuracy components (more than 100% improvement during SED). Refer to Table 5.2 for detailed statistics of these results. In addition, the typical values (during ionospherically quiet times) are also somewhat lower as compared to the levels offered by the current WAAS.

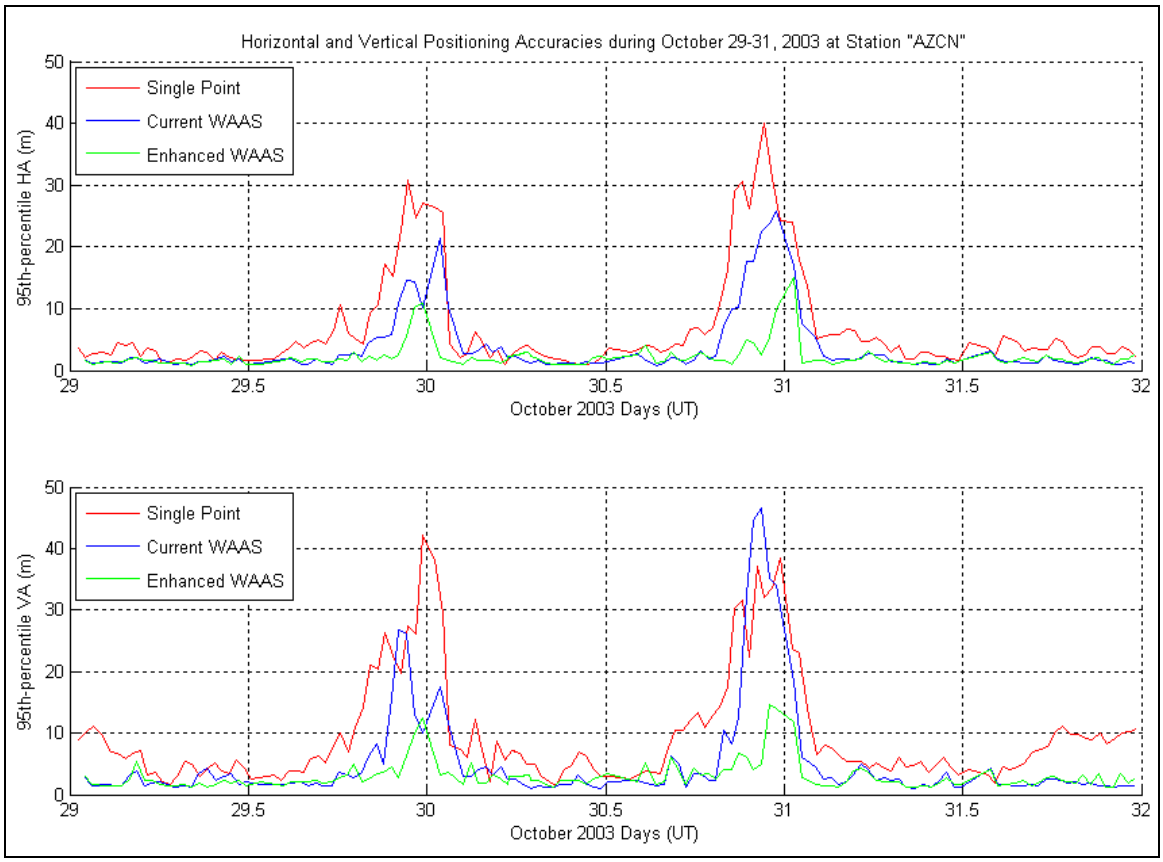

Figure 5.19: WAAS HA and VA during October 29-31, 2003 at Station "AZCN"

Table 5.2: Overall HA and VA Positioning Statistics for October 2003 Storm Event at Station "AZCN"

		Single Point	Current WAAS	Enhanced WAAS	Single Point	Current WAAS	Enhanced WAAS	Single Point	Current WAAS	Enhanced WAAS
		October 29			October 30			October 31		
HA (m)	MEAN	5.47	3.01	1.64	6.83	3.76	2.05	2.05	1.13	0.62
	RMS	9.16	5.22	2.30	11.45	6.53	2.88	3.43	1.96	0.86
	STD	7.35	4.27	2.10	9.19	5.34	2.63	2.76	1.60	0.79
	95%	23.08	13.43	7.18	28.85	16.78	8.98	8.66	5.03	2.69
	MAX	32.62	26.84	12.48	40.77	33.55	15.60	12.23	10.06	4.68
	MIN	0.07	0.06	0.02	0.09	0.08	0.02	0.03	0.02	0.01
VA (m)	MEAN	7.11	4.44	2.53	8.88	5.55	3.17	2.67	1.66	0.95
	RMS	10.11	8.82	5.59	12.64	11.03	6.98	3.79	3.31	2.10
	STD	7.19	7.63	4.04	8.99	9.53	5.05	2.70	2.86	1.52
	95%	24.25	26.20	13.96	30.31	32.76	17.45	9.09	9.83	5.24
	MAX	32.90	37.40	22.56	41.12	46.75	28.20	12.34	14.02	8.46
	MIN	0.39	0.05	0.08	0.48	0.06	0.10	0.14	0.02	0.03

Although the ionosphere is better captured, using a network that is twice as dense, these results may be misleading because the dense network observations are still reduced to a fixed set of IGP located no closer than 5 degrees apart. In this case it is usually expected that some spatial resolution to be lost. But the improvements seen herein are significant. In this context, improvements in the positioning domain depend upon two factors: the network density and grid spacing. There is a saturation point for improvements gained due to network densification. In other words, there is a point in the level of densification where addition of reference stations will cease to affect network performance. On the other hand, the grid spacing would have no such limit because the discretization would approach the continual spatial as the spacing between IGPs become infinitesimally small; this parameter would only be bound by practicality (e.g. computation load, data management, band width, etc.).

For the results obtained herein, it appears that this densification limit has not been reached since improvements are significant. Perhaps, the level of improvement is an indication of the fact that optimum balance between network density and spatial resolution has been reached. Having more reference stations is definitely helping to obtain more observation points near the IGPs (as shown earlier in IPP distribution plots show here as well), which is providing more accuracy. But, beyond a certain point IPPs will not approach IGPs and the measurements still will be reduced to the five-degree IGP spacing. Further study would be required to determine which densification level is required for optimal performance by the WAAS network. According to the results obtained here, decreasing the station spacing in the WAAS network would improve performance of the system. The level of densification that was studied herein showed significant improvement, but from this research it is not clear that this is the optimum level of densification, in that, if at this densification level the lowest cost/benefit ratio is obtained and if saturation of improvements has occurred or not. For instance, It could have been possible to test at IGPs for various station configurations and evaluate the accuracy at a given grid point for the ionospheric model; however these investigations fell outside the scope of this research, as the focus here was network densification but did not include reduced grid spacing. Based on the findings of this chapter, the following recommendations are made:

- WAAS reference network could include more closely–spaced WRSs to better model the ionosphere.

- The proposed CWAAS station locations in eastern Canada allowed significant performance improvements during a severe ionospheric storm event. Users in western Canada would not experience any performance improvement from this CWAAS development, however. As such, the CWAAS reference network would benefit from additional sites in the west.
- A study should be conducted to investigate the potential improvements that could be obtained from reducing the WAAS ionospheric grid spacing.

Chapter 6

Conclusions and Recommendations

6.1 Conclusions

The main objectives of this research were to evaluate the current WAAS (accuracy) performance in the correction domain, assess its positioning capabilities across North America under various ionospheric conditions, and finally to devise a better sampled ionospheric model using a denser/expanded network to study the potential future improvements in positioning performance for WAAS/CWAAS across North America, again under various ionospheric conditions. The major motivation for this was taken from

the fact that under the effects of SED, considerable accuracy degradation is experienced when trying to conduct positioning using a wide-area approach such as WAAS. The phenomenon is caused by enhanced ionospheric electric fields that are present near the mid- to high-latitudes during geomagnetically disturbed periods and are characterized by large TEC gradients, both spatially and temporally. SED causes positioning performance to deteriorate very rapidly, and even wide-area systems like the WAAS are unable to fully model the ionospheric behaviour during those times. This is even a bigger problem in Canada since very minimal WAAS coverage exists and no reference stations are actually located in Canada. Therefore, investigation of these issues is necessary.

This study has shown that typically WAAS clock and orbital errors are more accurate than broadcast clocks and orbits, but there could be some infrequent outliers due to satellites just coming into view or the age of correction being significantly large. Usually, these satellites are outside of network coverage but there are odd instances when satellites in view have large correction age. Because this is very infrequent, it has minimal impact in the positioning domain since it is one bad observation against hundreds of valid ones. Additionally, it is has been shown that the WAAS UDRE bounds all the errors, and in the positioning domain the protection levels (HPL and VPL) also bound the positioning errors; thus WAAS reliability was preserved during the course of the periods studied herein. In general, WAAS ionospheric corrections tend to be very smooth, and so the localized features are not captured well. This is due to having only 25 WRSs and 5° x 5° grid spacing. As it was shown in numerous TEC maps, the SED is a narrow plume of enhanced total electron content extending northerly through Canada which is not detect

by WAAS for the most part. This is of major concern for a user trying to position using WAAS when they are directly beneath the SED phenomenon, since the vertical ionospheric delay errors sometimes exceeded 15 m. It is not difficult to estimate the negative impact this will have in the positioning domain, but WAAS reliability was maintained in all instances by having the GIVE values bound the VTEC errors. As well, WAAS has proven to be at least much better than the broadcast (Klobuchar) model, in terms of accuracy of the ionospheric delay.

In the positioning domain, typical WAAS horizontal accuracies were well below the threshold levels set by regulating bodies for marine or land navigation, but during storm periods of SED WAAS accuracies degraded severely and far surpassed those safety thresholds (10 m HA at the 95^{th}-percentile). Since WAAS is a system that provides vertical guidance to aircrafts, it was essential to closely observe the height estimation. As is the case in any satellite-based navigation system, the vertical component is the hardest of the three to estimate. As such, it was seen that vertical errors were much more significant than the horizontal ones, and it raised the 3D errors to very high levels. Although the errors were large, the GIVE values provided the reliability necessary to offer adequate service, but during some storm events the vertical service was denied for all users in North America due to “unmonitored” GIVE predictions.

The study of the refined ionospheric model had two components to it: 1) to test the CWAAS candidate sites and 2) to assess the improvements of having a denser network of reference stations. For the CWAAS assessment, it was found that the proposed sites

would greatly aid in improving WAAS performance in Eastern Canada, but the benefits of CWAAS was virtually non-existent in Western Canada. As for the Enhanced WAAS, it was shown that if the WAAS were to have more than 50 stations in its network, the positioning errors would be reduced by a factor of two during SED and the typical error levels would also decrease.

The research led to conclusions about where challenges for WAAS exist and how it would be possible to strengthen those areas of the system. The major contributions of this research are:

- Identification of WAAS error behaviours for clock, orbit and ionosphere
- Comparison of WAAS corrections with those provided by broadcast
- Performance analysis of the WAAS in terms of accuracy, reliability and coverage in both spatial and temporal domains
- Quantification of positioning accuracies from different perspectives and various ionospheric conditions
- Simulation of WAAS/CWAAS networks to assess the validity of the proposed station locations and density
- Evaluation of the Enhanced WAAS in the positioning domain

6.2 Recommendations

The major problem with clock/orbital corrections has been the presence of outliers, which could cause positioning inabilities. Therefore, WAAS-enabled receivers should have a filtering mechanism to reject any observation that is deemed to be an outlier. As discussed earlier, a strong correlation exists between these outliers and when the satellite came into view and/or the age of correction, and there are instances when old corrections are available for satellites in view. Thus, the filtering method could be based on these two criteria in conjunction with the sheer magnitude of the outlier.

CWAAS evaluation was done to investigate if the candidate sites are optimal from positioning and practical perspectives; its benefits, however, were only seen in the east. Therefore, CWAAS development should also include a few reference stations in Western Canada, where the coverage is minimal and where the stations would best complement the existing WRSs.

The Enhanced WAAS has been shown to offer a great deal of benefits in all respects of positioning. Consequently, the FAA should consider adding more reference stations also to the core WAAS network, and there are talks that further development of the WAAS infrastructure is being envisioned by the FAA. However, adding more stations is just solving part of the problem; the other part is grid spacing, which will still be very coarse. One can have a sparse network and fine grid spacing or vice versa but still end up with poor results because both of these elements have to be appropriately dense or fine. In

practice, there are physical limits as to how dense a network or how fine the grid spacing could or should be. For instance, after a certain point no matter how many stations are added the accuracy will not improve further because the users will not necessarily be close enough to a given IGP. Nonetheless, in the results obtained here it has been shown that the model is definitely improved when more stations are added to the reference network. Thus, the method of improving the level of service would be also to lower the grid spacing, but this will entail reworking the message structure and upgrading to high bandwidth transmitters throughout the system – which is not likely. Thus, it becomes a question of cost versus benefit. Nonetheless, the options are there for future enhancements to the WAAS – it is a matter of implementing them if the feasibility exists.

In addition to SBAS, which was the focus of this research, nowadays other augmentation methods are being used to supplement GPS accuracy, reliability, integrity, continuity and availability. These include other GNSS, ground-based augmentations, pseudolites, GPS occultations, etc [*Shively*, 2004]. In addition to what was discussed in this study, the FAA should look into integrating some of these methods of positioning to further enhance WAAS services offered to its users. When making a modification of this scale, the main concern is reliability. If the additional supports could offer similar of higher levels of reliability at reasonable costs, then the integration would add value to the system in the long run.

Appendix A

Ionospheric TEC Plots on October 29, 2003

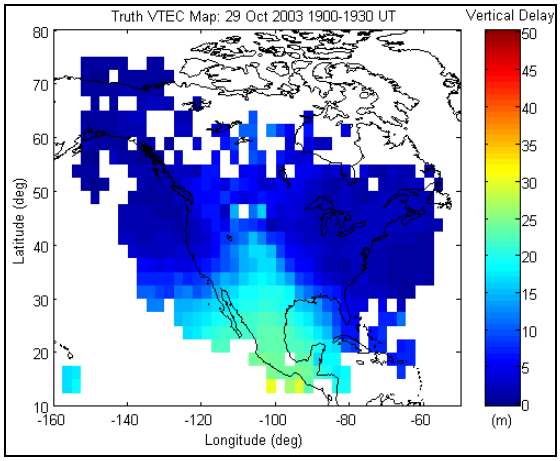

A1: Truth VTEC Map (1900-1930 UT, October 29, 2003)

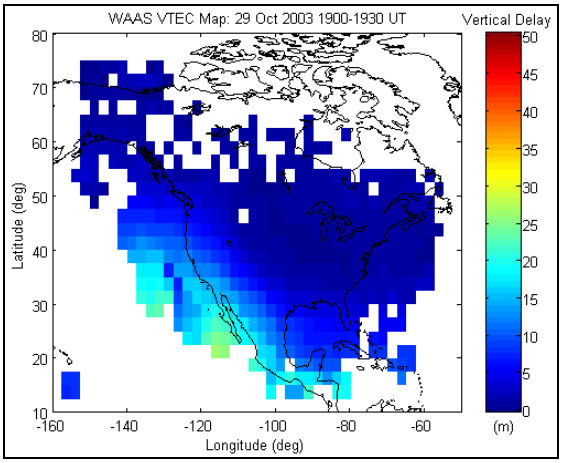

A2: WAAS VTEC Map (1900-1930 UT, October 29, 2003)

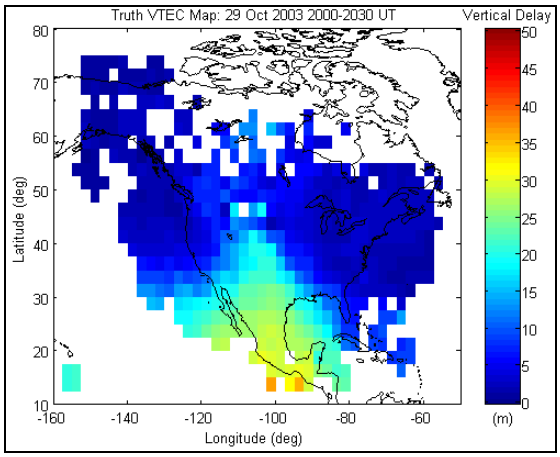

A3: Truth VTEC Map (2000-2030 UT, October 29, 2003)

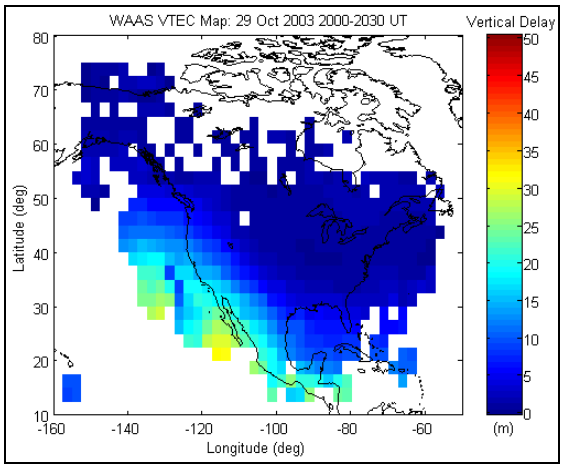

A4: WAAS VTEC Map (2000-2030 UT, October 29, 2003)

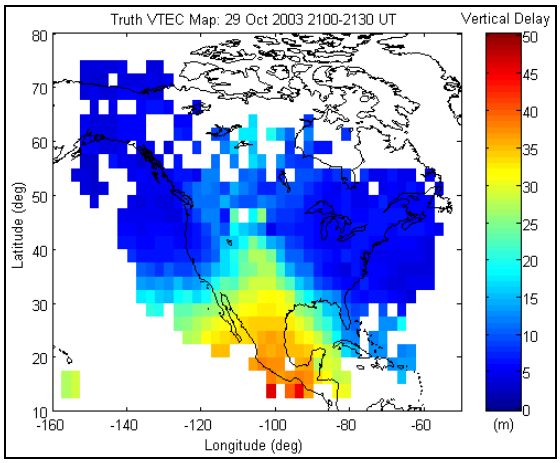

A5: Truth VTEC Map (2100-2130 UT, October 29, 2003)

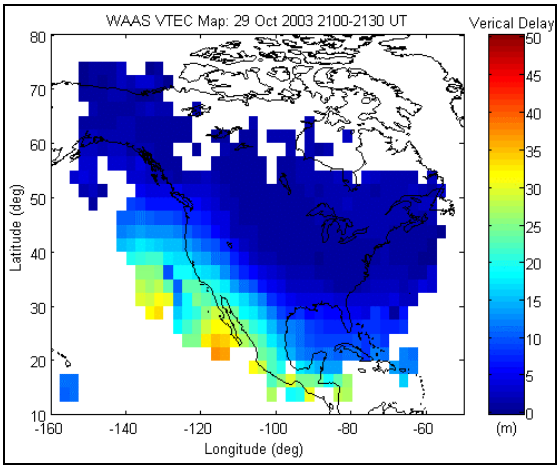

A6: WAAS VTEC Map (2100-2130 UT, October 29, 2003)

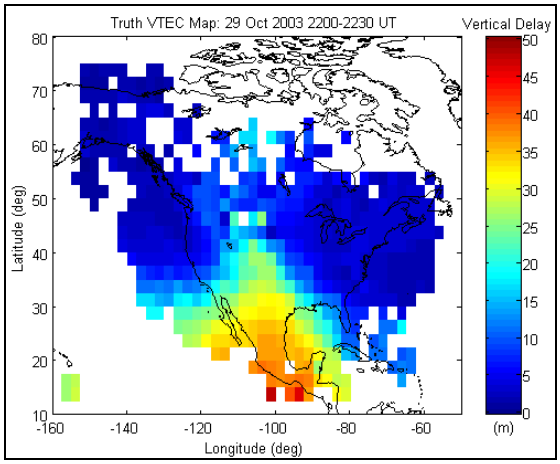

A7: Truth VTEC Map (2200-2230 UT, October 29, 2003)

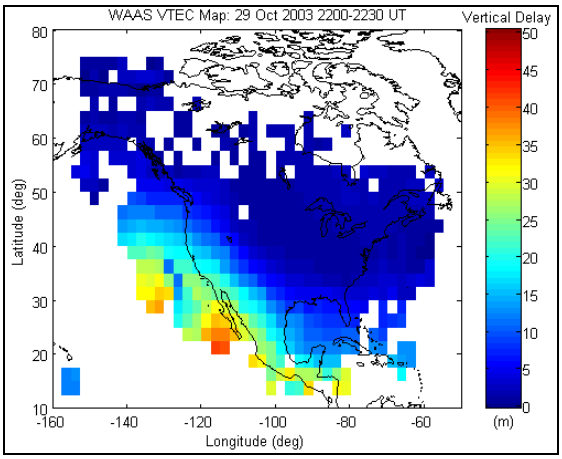

A8: WAAS VTEC Map (2200-2230 UT, October 29, 2003)

Ionospheric TEC Plots on October 30, 2003

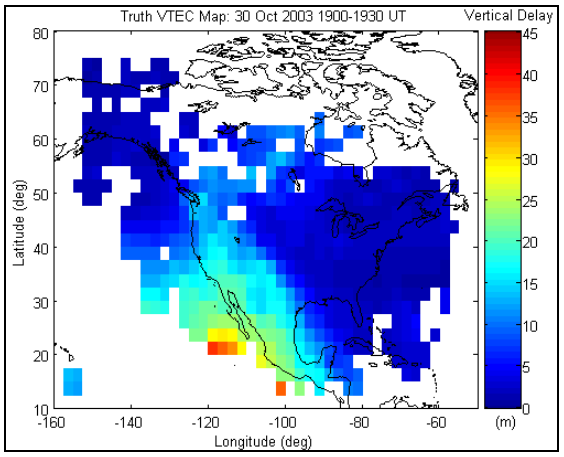

A9: Truth VTEC Map (1900-1930 UT, October 30, 2003)

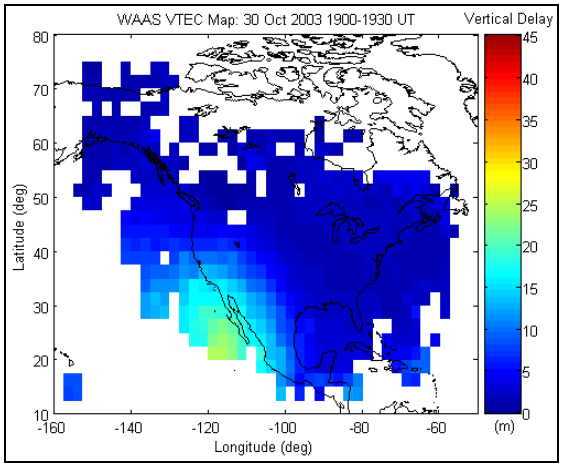

A10: WAAS VTEC Map (1900-1930 UT, October 30, 2003)

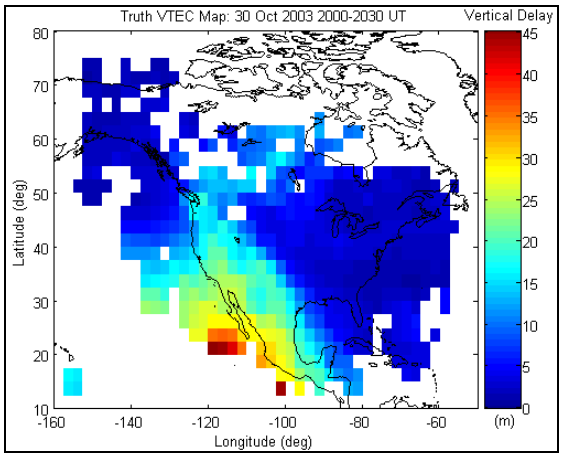

A11: Truth VTEC Map (2000-2030 UT, October 30, 2003)

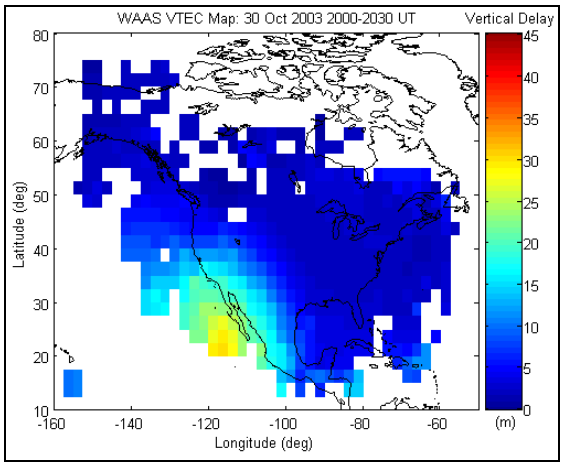

A12: WAAS VTEC Map (2000-2030 UT, October 30, 2003)

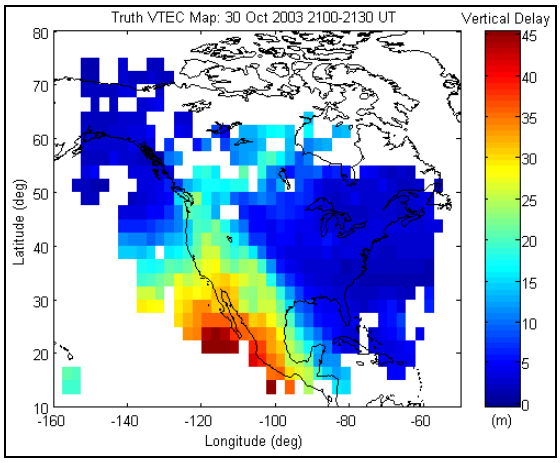

A13: Truth VTEC Map (2100-2130 UT, October 30, 2003)

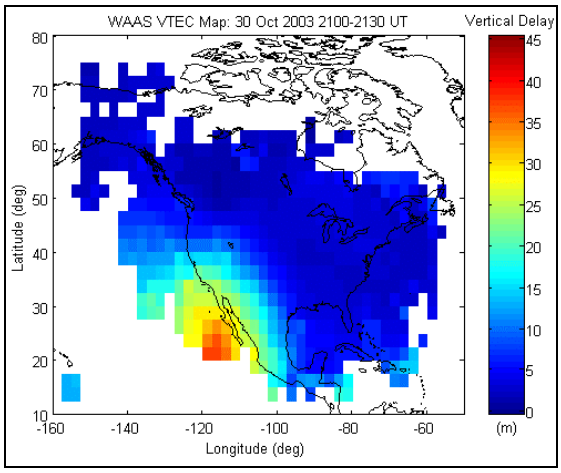

A14: WAAS VTEC Map (2100-2130 UT, October 30, 2003)

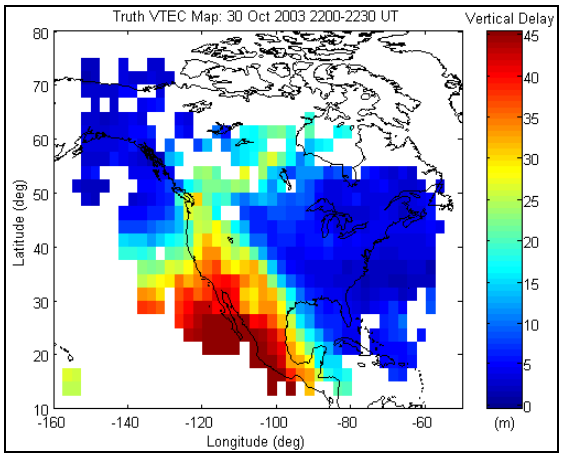

A15: Truth VTEC Map (2200-2230 UT, October 30, 2003)

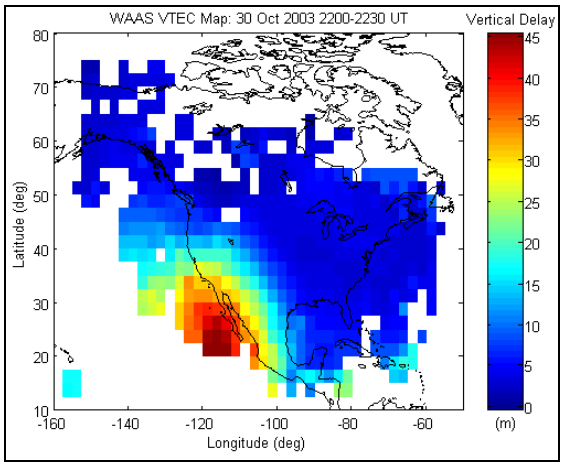

A16: WAAS VTEC Map (2200-2230 UT, October 30, 2003)

Appendix B

Ionospheric TEC Accuracy Plots on November 20, 2003

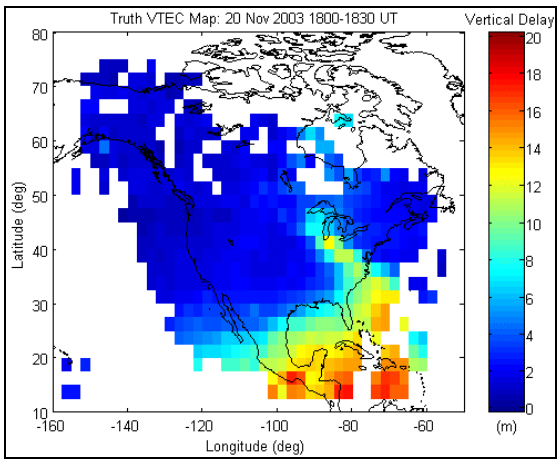

B1: Truth VTEC Map (1800-1830 UT, November 20, 2003)

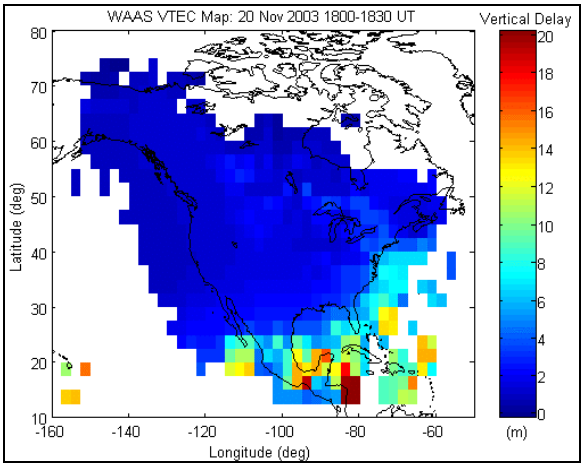

B2: WAAS VTEC Map (1800-1830 UT, November 20, 2003)

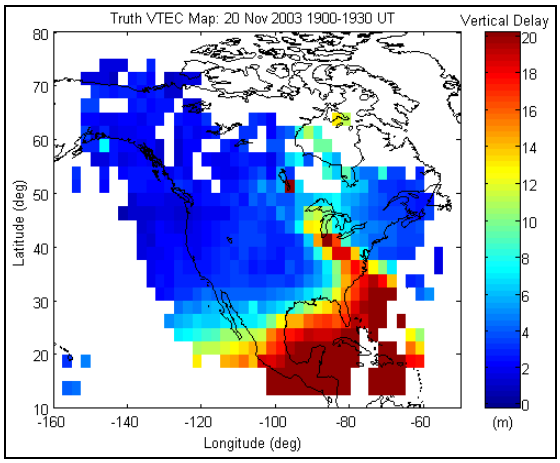

B3: Truth VTEC Map (1900-1930 UT, November 20, 2003)

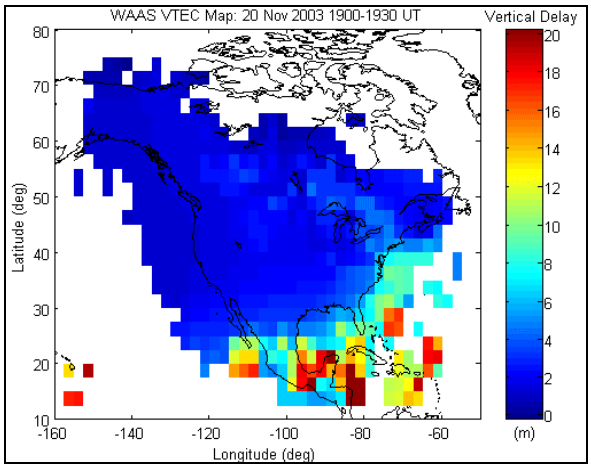

B4: WAAS VTEC Map (1900-1930 UT, November 20, 2003)

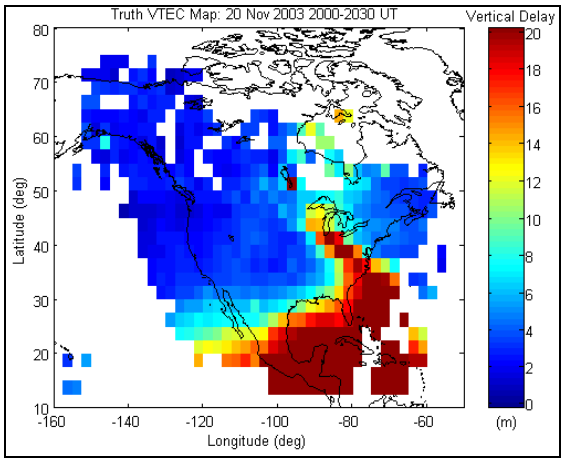

B5: Truth VTEC Map (2000-2030 UT, November 20, 2003)

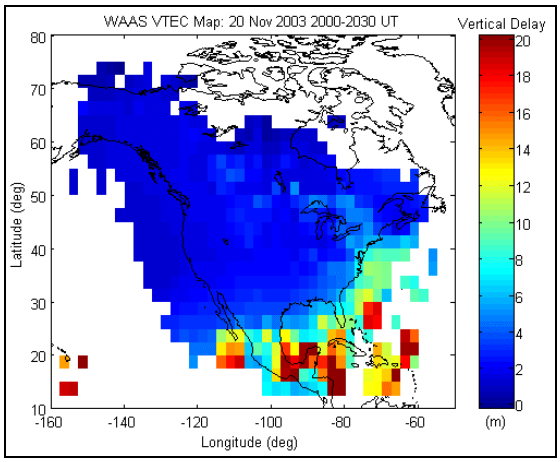

B6: WAAS VTEC Map (2000-2030 UT, November 20, 2003)

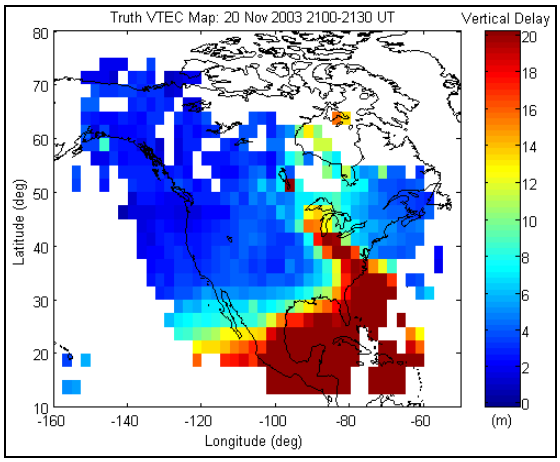

B7: Truth VTEC Map (2100-2130 UT, November 20, 2003)

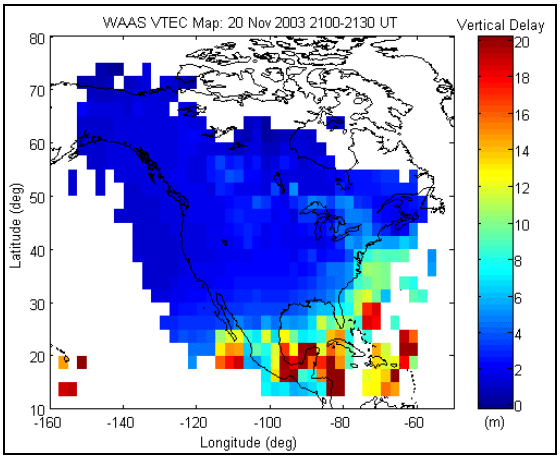

B8: WAAS VTEC Map (2100-2130 UT, November 20, 2003)

Appendix C

Positioning Accuracy Plots for Current WAAS on October 30, 2003

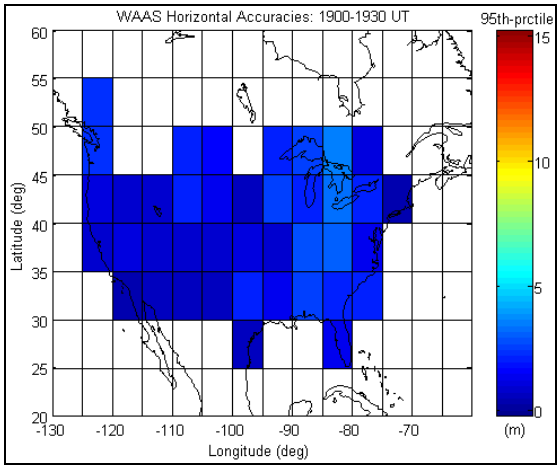

C1: WAAS Horizontal Accuracies (1900-1930 UT, October 30, 2003)

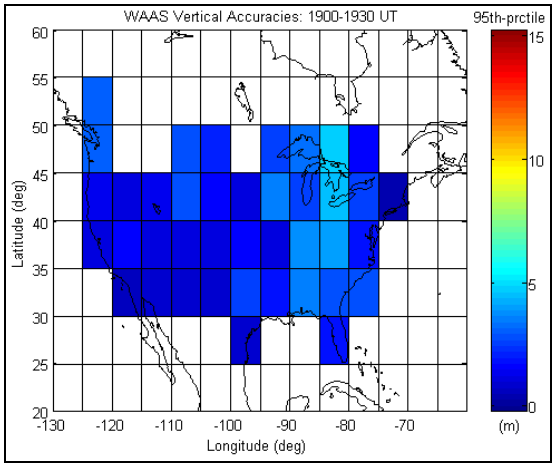

C2: WAAS Vertical Accuracies (1900-1930 UT, October 30, 2003)

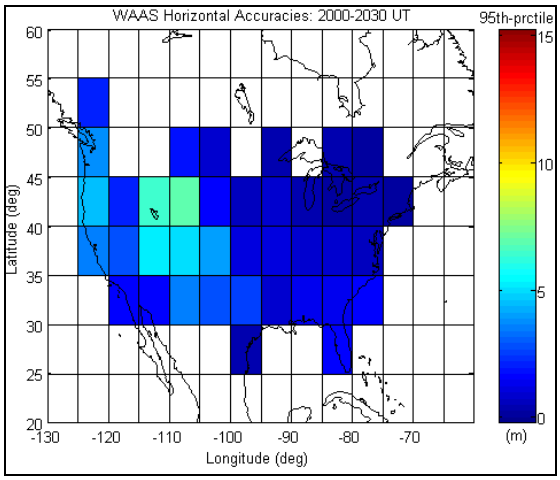

C3: WAAS Horizontal Accuracies

(2000-2030 UT, October 30, 2003)

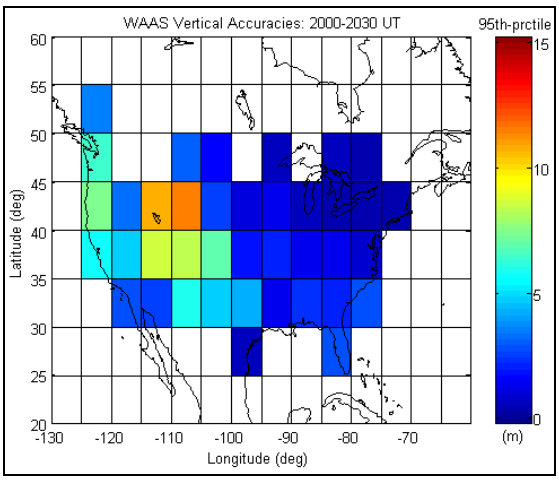

C4: WAAS Vertical Accuracies

(2000-2030 UT, October 30, 2003)

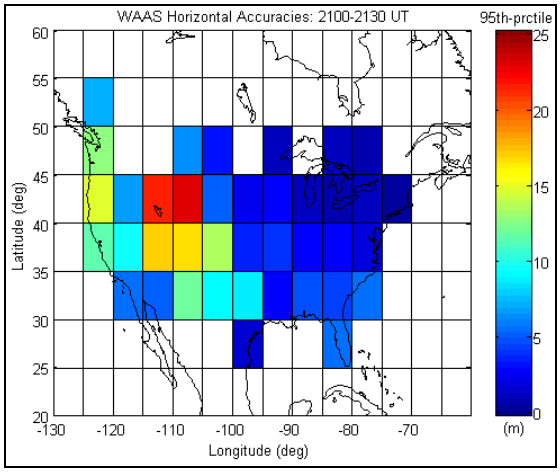

C5: WAAS Horizontal Accuracies

(2100-2130 UT, October 30, 2003)

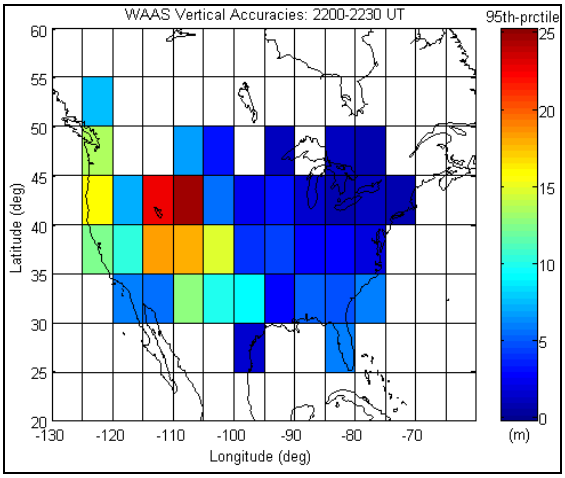

C6: WAAS Vertical Accuracies

(2100-2130 UT, October 30, 2003)

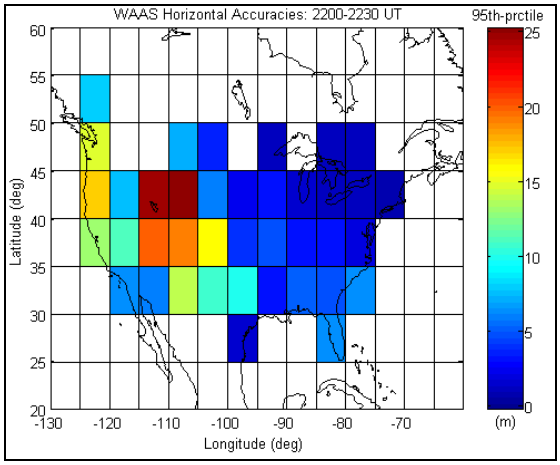

C7: WAAS Horizontal Accuracies

(2200-2230 UT, October 30, 2003)

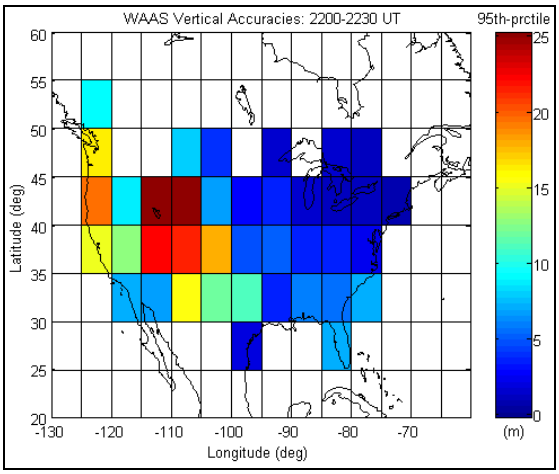

C8: WAAS Vertical Accuracies

(2200-2230 UT, October 30, 2003)

Appendix D

Positioning Accuracy Plots for Enhanced WAAS on October 30, 2003

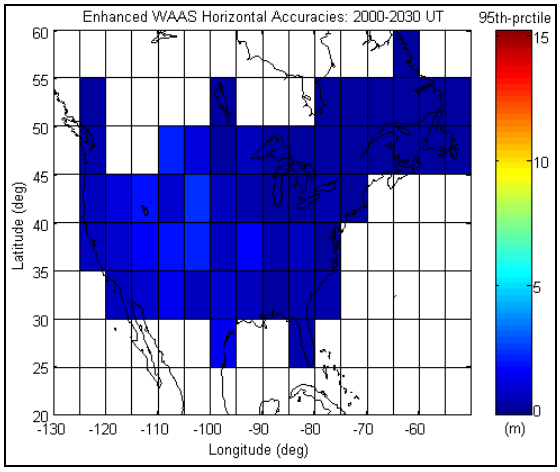

D1: EWAAS Horizontal Accuracies

(2000-2030 UT, October 30, 2003)

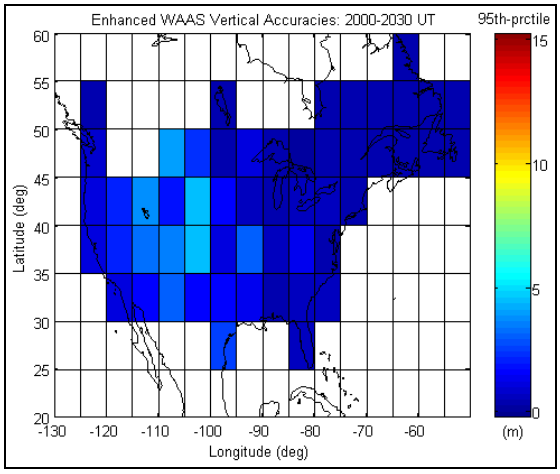

D2: EWAAS Vertical Accuracies

(2000-2030 UT, October 30, 2003)

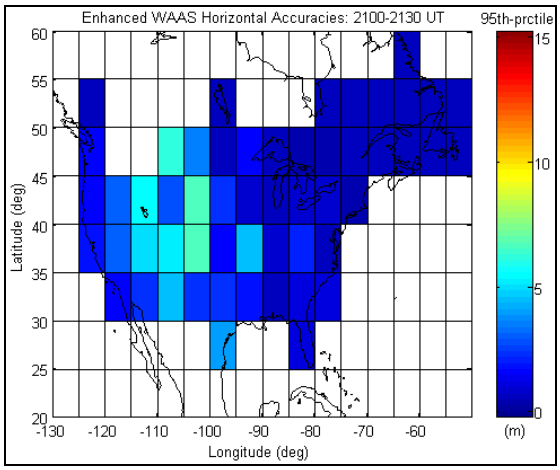

D3: EWAAS Horizontal Accuracies

(2100-2130 UT, October 30, 2003)

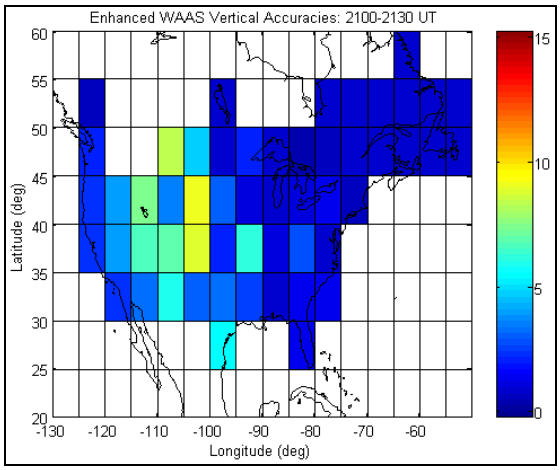

D4: EWAAS Vertical Accuracies

(2100-2130 UT, October 30, 2003)

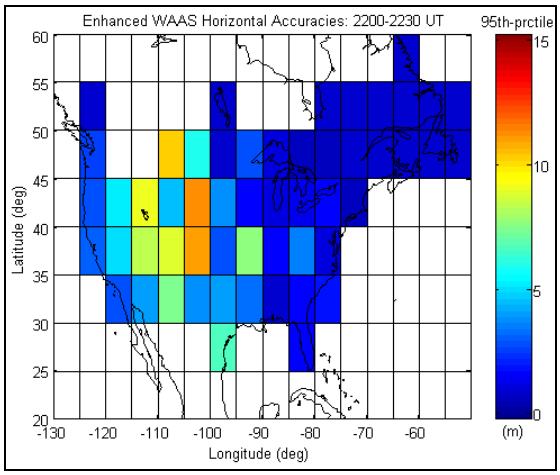

D5: EWAAS Horizontal Accuracies

(2200-2230 UT, October 30, 2003)

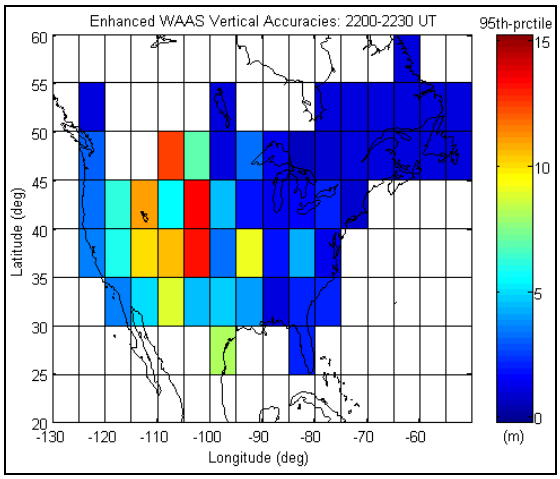

D6: EWAAS Vertical Accuracies

(2200-2230 UT, October 30, 2003)

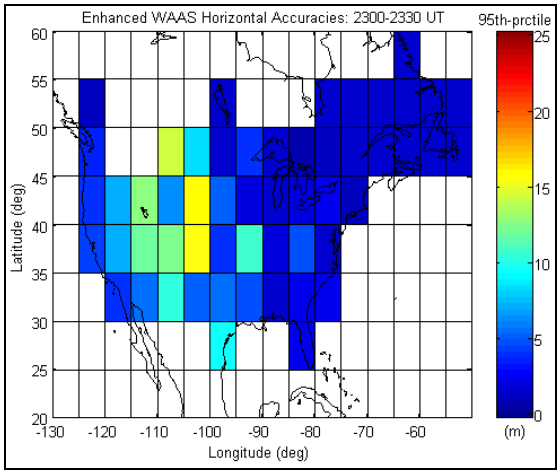

D7: EWAAS Horizontal Accuracies

(2300-2330 UT, October 30, 2003)

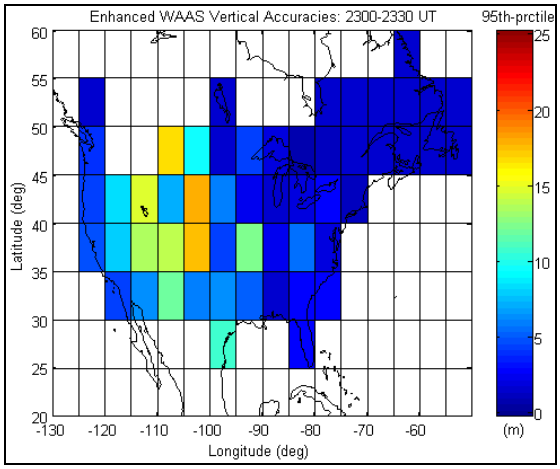

D8: EWAAS Vertical Accuracies

(2300-2330 UT, October 30, 2003)

References

Altshuler, E., D. Cormier and H. Go, Improvements to the WAAS ionospheric algorithms, Proceedings of the ION GPS 2002, Sept. 24-27, Portland, OR, pp. 2256-2261, 2002.

Bunce, D., Wide Area Augmentation System, Presentation Slides, WAAS Product Team, Federal Aviation Administration (FAA), July 2003.

Cannon, M.E. and Lachapelle, G., Analysis of a High-Performance C/A-Code GPS Receiver in Kinematic Mode", NAVIGATION: The Journal of the Institute of Navigation, Vol. 39, No. 3, Fall 1992, http://www.novatel.ca/Documents/Papers/File3.pdf.

Cannon, M.E., G. Lachapelle and W. Qui, C3NAV™ Operating Manual Version 2.0, The University of Calgary, Calgary, Alberta, 1995.

Cannon, M.E., Skone, S., Gao, Y., Moon, Y., Chen, K., Crawford, S. and G. Lachapelle, "Performance Evaluation of Several Wide-Area GPS Services", Conference Proceedings of ION GPS-02, Portland, September 24-27, 2002.

Conley, R., "Results of the GPS JOP's GPS Performance Baseline Analysis: The Gospar Project", NAVIGATION: The Journal of the Institute of Navigation, Vol. 45, No. 1, 1998.

Continuously Operating Reference Stations (CORS), http://www.ngs.noaa.gov/CORS/cors-data.html, January 2005.

Cormier, D., McKendree, T.L., Schempp, T.R., "Concept for New SBAS Message Types to Improve GIVE Resolution", ION NTM 2005, 24-26 January 2005, San Diego, CA.

Coster, A. J., J. C. Foster and P. J. Erickson, Monitoring the ionosphere with GPS, GPS World, pp. 40-45, May 2003.

Coster, A. J., J. C. Foster, P. Erickson, B. Sandel and F. Rich, Monitoring space weather with GPS mapping techniques, Proceedings of the ION National Technical Meeting 2003, Anaheim, CA, January 22-24, 2003.

Dai, D., Walter, T., Enge, P. and Powell, J.D., "Optimal Use of Ionospheric Corrections for Wide Area Augmentation System (WAAS) Users", Stanford University, IEEE, Volume 0-7803-4330-1/98, 1998.

El-Arini, M.B., Conker, R., Albertson, T., Reegan, J.K., Klobuchar, J.A., and Doherty, P., "Comparison of real-time ionospheric algorithms for a GPS wide-area augmentation system (WAAS)", NAVIGATION: Journal of the Institute of Navigation, vol. 41, no. 4, pp. 393-413, winter 1994-95.

El-Arini, M.B. and Lejeune, R.O., "Description of an Ionospheric Spatial Gradient Irregularity Detectors for WAAS" The MITRE Corporation, Center for Advanced Aviation System Development (CAASD) (Journal), 2001.

Enge, P.K. and Van Dierendonck, A.J., "Wide Area Augmentation System", Chapter 4 of Global Positioning System: Theory and Applications Volume II, American Institute of Aeronautics and Astronautics, Inc., Washington, DC, 1996.

Farah, F., "The Ionospheric Delay Effort for GPS Single-Frequency Users-Analysis Study for Simulation Purposes", The University of Nottingham, UK, August 2001.

Federal Aviation Administration (FAA), GPS Basics, http://gps.faa.gov/gpsbasics/index.htm, December 2004.

Federal Aviation Administration (FAA), http://gps.faa.gov/Programs/WAAS/waas.htm, February 2005.

Foster, J. C., P. J. Erickson, A. J. Coster, J. Goldstein and F. J. Rich, Ionospheric signatures of plasmaspheric tails, Geophys. Res. Lett., 29(13), 10.1029/2002GL015067, 2002.

Foster, J.C. and H. B. Vo, Average characteristics and activity dependence of the subauroral polarization stream, Journal of Geophysical Research, 0.1029/2002JA009409, 2002.

Hanlon, D. and K. Sandhoo, (1997) "FAA Satellite Navigation Program Overview", Proceedings of the ION Annual Meeting, The Institute of Navigation, Alexandria, VA., pp. 49-56.

Hopfield, H.S., "Two-quartic tropospheric refractivity profile for correction satellite data", Journal of Geophysical Research, 74, no. 18, 4487, 1969.

Hu, Z., Ning, L., Wang, Y. Li, C. and Yu, J., "The Quality of Service Evaluation Tool for WAAS", College of Electronic Science and Technology of China, University of Electronic Science and Technology of China, IEEE, (Journal) Volume 0-7803-7547-5/02, 2002.

International Reference Ionosphere (IRI), http://nssdc.gsfc.nasa.gov/space/model/models/iri.html, November 2003.

Jet Propulsion Laboratory (JPL), http://igscb.jpl.nasa.gov/, January 2005.

Kaplan, E.D., Understanding GPS Principles and Applications, Artec House, Norwood, Massachusetts, 1996.

Klobuchar, A.J., Doherty, P.H., El-Arini, M.B., “Potential Ionospheric Limitations to GPS Wide-Area Augmentation System (WAAS), NAVIGATION: The Journal of the Institute of Navigation, Vol. 42, No. 2, 1995.

Knight, M., M. Cervera and A. Finn, A comparison of predicted and measured GPS performance in an ionospheric scintillation environment, Proceedings of the ION GPS-99, September 14-17, Nashville, Tennessee, 1437-1450, 1999.

Komjathy, A., Sparks, L., Mannucci, A.J. and Pi, X., “An Assessment of the Current WAAS Ionospheric Correction Algorithm in the South American Region”, NAVIGATION: Journal of The Institute of Navigation, Vol. 50, No. 3, Fall 2003.

Komjathy, A., Sparks, L., Mannucci, A.J. and Pi, X., “On the Ionospheric Impact of Recent Storm Events on Satellite-Based Augmentation Systems in Middle and Low-Latitude Sectors”, Conference Proceedings of ION GPS/GNSS 2003, 9-12 September 2003, Portland, OR.

Krankowski, A., Sergeenko, N.P., Baran, L.W., Shagimuratov, I.I., Rogova, M.V. “The Short-Term Forecasting of the Total Electron Content” Artificial Satellites, Vol.40, No.2, 2005.

Lachapelle, G., “ENGO 625 NAVSTAR GPS: Theory and Applications”, Department of Geomatics Engineering, University of Calgary, September 2003.

Liu, Z. and Gao, Y., "Development and evaluation of a 3-D Ionospheric Modeling Method", NAVIGATION: Journal of The Institute of Navigation Vol. 51, No. 4, Winter 2004.

Loh, R., Wullschileger, V., Elrod, B., Lage, M. and Haas, F., "The U.S. Wide-Area Augmentation System (WAAS)", NAVIGATION: Journal of The Institute of Navigation Vol. 42, No. 3, Fall 1995.

McCaskill, T., Buisson, J. and Buonaguro, A., "A Sequential Range Navigation Algorithm of Projected DGPS for High-Accuracy DGPS-Based System", NAVIGATION: Journal of The Institute of Navigation Vol. 23, No. 2, 1976.

Misra P. and Enge, P.K., "GPS Measurements and Error Sources", Chapter 4 of Global Positioning System: Signals, Measurements, and Performance, Ganga-Jamuna Press, Lincon, Massachusetts, 2001.

Nationwide Differential Global Positioning System (NDGPS), http://www.tfhrc.gov/its/ndgps/, July, 2003.

NOAA website http://www.sec.noaa.gov/ftpdir//plots/kp/ , December 2003.

NOAA website http://www.sec.noaa.gov/ftpdir//plots/kp/ , January 2005.

NAV CANANDA, http://www.navcanada.ca, January 2005.

Parkinson, B.W. and J.J. Spilker, Global Positioning System: Theory and Applications Volume I, American Institute of Aeronautics and Astronautics, Washington, D.C., 1996.

Peterson, E.R., Walter, T., Hansen, A., Comp, C. and Enge, P., "The Application of a 3-D Empirical Ionosphere Model to WAAS Simulation", Department of Aeronautics and Astronautics, Stanford University, IEEE, (Journal) Volume 0-7803-4330-1/98, 1998.

Pullen, P.S., Chao, Y.C., Enge, P.K. and Parkinson, B.W., "Effects of Local Ionospheric Anomalies on Navigation Performance and Integrity using WAAS", Department of Aeronautics and Astronautics, Stanford University, IEEE, (Journal) Volume 0-7803-3085-4/96, 1996.

Rho, H., Langley R. and Kassam, A, "The Canada-Wide Differential GPS Service: Initial Performance", Conference Proceedings of ION GPS/GNSS 2003, 9-12 September 2003, Portland, OR.

Radio Technical Commission for Aviation Services (RTCA) Inc., "Minimum Operational Performance Standards for Global Positioning System/Wide Area Augmentation System Airborne Equipement",DO-229C, 2001.

Rodrigues, F.S., Aquino, M. H. O., Danson, A., Moore, T. and Waugh, S., "Statistical Analysis of GPS Ionospheric Scintillation and Short-Time TEC Variations over Northern Europe", NAVIGATION: Journal of The Institute of Navigation Vol. 51, No. 1, Spring 2004.

Shively, C. A. and Hsiao, T. T., "Availability Enhancements for CAT IIIB LAAS", NAVIGATION: Journal of The Institute of Navigation Vol. 51, No. 1, Spring 2004.

Skone, S., "TECANALYS Operating Manual", Department of Geomatics Engineering, University of Calgary, September 2002.

Skone, S., Coster, A., Hoyle, V. and Laurin, C., "WAAS Availability and Performance at High Latitudes", Conference Proceedings of ION GPS/GNSS 2003, 9-12 September 2003, Portland, OR.

SPARG website http://www.shef.ac.uk/~sparc/tutorial.html#3.0, October 2003.

The Canadian Coast Guard (CCG) website http://www.ccg-gcc.gc.ca/dgps/main_e.htm, June 2005

The GPS Store website http://www.thegpsstore.com/Detail-Furuno-GP32-GPS-WAAS-receiver.asp, July 2005.

Till, R.D., Wanner, W. and Evangelos, J.R., “Wide Area Augmentation System (WAAS) Test and Evaluation Concepts”, IEEE, (Journal) CH35797-95/0000-0169, 1995.

U.S. Department of Transportation, “FAA Specification: Wide Area Augmentation System (WAAS)”, FAA-E- 2892B, 1999.

Van Dierendonck, A.J., P. Fenton and T. Ford, “Theory and performance of narrow correlator spacing in a GPS receiver”, NAVIGATION: The Journal of the Institute of Navigation, Vol. 39, No. 3, 283, Fall, 1992, http://www.novatel.ca/Documents/Papers/File2.pdf.

Walter, T., Course 730: Wide Area Augmentation System (WAAS), ION GPS-2003 Tutorial, Navtech Seminars & GPS Supply, Inc., Alexendria, VA, 2003.

Yousuf, R., Skone, S. and Coster, A., “Evaluation of DGPS and WADGPS Methods for Land and Marine Applications”, Conference Proceedings of ION NTM 2005, 24-26 January 2005, San Diego, CA.

Zhang, J. and Bartone, C., “A General Concept and Algorithm of Projected DGPS for High-Accuracy DGPS-Based Systems”, NAVIGATION: Journal of The Institute of Navigation Vol. 51, No. 4, Winter 2004.